Effect of Multiple Nanofiltration Layers of γ-Al_2O_3 and Fe-SiO_2 on Salt Removal Properties of Ceramic Membranes

By

Jennifer Joy Jackowski

A dissertation submitted in partial fulfillment of

the requirements for the degree of

Doctor of Philosophy

(Environmental Chemistry and Technology)

at the

UNIVERSITY OF WISCONSIN-MADISON

2015

Date of final oral examination: 6/4/2015

The dissertation is approved by the following members of the Final Oral Committee:
Marc A. Anderson, Professor, Environmental Chemistry and Technology
M. Isabel Tejedor-Tejedor, Senior Scientist, Environmental Chemistry and Technology
James J. Schauer, Professor, Environmental Chemistry and Technology
Linda K. Graham, Professor, Botany
John L. Rudolph, Professor, Curriculum and Instruction

Abstract

Single and bilayer ceramic membranes with deposited γ-Al_2O_3 and Fe-SiO_2 nanofiltration (NF) layers were fabricated and evaluated with respect to physical characteristics and salt removal properties. The fabrication method proved to be generally reproducible, and would be further improved controlling relative humidity during the coating process. The thickness of the individual NF layers was found to be dependent on the slipcasting of the γ-Al_2O_3 and Fe-SiO_2 materials, regulated by the amount of water in the pores at the time of coating. Layer thickness was determined by scanning electron microscopy and measurements were compared with calculated values from nitrogen gas permeation experiments. The γ-Al_2O_3 material had an average pore diameter of 39Å or 43Å, depending on the firing temperature (400 or 500°C, respectively) used to sinter the NF layer to the support; the average pore diameter for Fe-SiO_2 was 21Å. Porosity of the two materials was found to be 31% for Fe-SiO_2 and 51% (400°C) or 42% (500°C) for γ-Al_2O_3. The MWCOs for rejection of polyethylene glycol were 300 g mol^{-1} and 700 g mol^{-1} for Fe-SiO_2 and γ-Al_2O_3, respectively.

Rejection of charged solutes with the membranes was correlated, in a semi-quantitative manner, with the value for potential in the center of the pore, as calculated from zeta potential measurements of the two materials exposed to various electrolytes and solution conditions. Comparisons between single layer membranes with either Fe-SiO_2 or γ-Al_2O_3 NF layers and bilayer membranes composed of both materials showed that rejection of salts is highly dependent on solution conditions and the type of electrolyte. For NaCl, a Fe-SiO_2 single layer membrane provides the largest rejection in the range of pH 5.0 to 9.0. A bilayer membrane with the γ-Al_2O_3 layer facing the feed solution shows superior performance for rejection of $MgCl_2$ in the same pH

range. In general, results demonstrate that the order in which NF layers are deposited on a porous ceramic support affects rejection; the layer facing the feed solution primarily controls salt removal properties. Bilayer membranes excel in salt separation, with a Cl^-/SO_4^{2-} selectivity four times greater than that obtained with a single layer membrane.

Marc A. Anderson, Thesis Advisor

10 June 10, 2015

Date

Acknowledgements

The completion of this dissertation would not have been possible without my advisors, Dr. Marc Anderson and Dr. Isabel Tejedor. Dr. Anderson served as a source of continual encouragement and support as a developed my skills as a scientific researcher. Dr. Anderson inspired me as a teacher as well, through my experience as a student in his classroom. Although Dr. Anderson was my official thesis advisor, Dr. Tejedor was my primary mentor in both scientific research and many other aspects of life! Dr. Tejedor is rigorous in her pursuit of scientific knowledge and is the most thorough researcher I have ever known. Dr. Tejedor's wisdom extends well beyond the scientific realm; without her as a role model, I doubt this effort would have been successful.

I would also like to thank Dr. Ken Walz, another important role model in my life, first as a teacher, then as a research mentor and now, as a colleague. Dr. Walz encouraged me to further my education in science and was instrumental in providing me with opportunities for advancement throughout my academic career. I am extremely grateful for his support and guidance over the years. The many additional friends, family members and fellow graduate students who deserve my appreciation are too numerous to mention. Thank you all for believing in me and for celebrating my success!

Finally, I would like to thank my mom, Carla Berndt, who passed on during my doctoral process. My mom was the strongest person I have ever met, and she taught me everything I know about struggle. When finishing my degree seemed impossible, it was her strength that I drew on to keep moving forward. My only regret is that she is not here to see the completion of this work. This thesis is dedicated to my mom.

Table of Contents

List of Tables

List of Figures

Symbol Definitions

C	concentration (mol L^{-1})
C_F	concentration of feed solution (mol L^{-1})
C_P	concentration of permeate solution (mol L^{-1})
CF	concentration factor
D_1	counter-ion diffusion coefficient (cm^2 s^{-1})
D_2	co-ion diffusion coefficient (cm^2 s^{-1})
d_p	pore diameter (m)
ε_0	permittivity of free space (F m^{-1})
ε	membrane porosity
	dielectric constant of water (F m^{-1})
F	Faraday constant (C mol^{-1})
I	ionic strength
J_v	volume flux (L m^{-2} h^{-1})
κ^{-1}	Debye length (m)
L_m	membrane thickness (m)
M	molecular weight (g mol^{-1})
ξ	normalized charge density, (X/C)
ΔP	pressure difference across membrane (N m^{-2})
q_w	surface charge density of membrane (mol m^{-2})
Q	Knudsen permeance (mol m^{-2} s^{-1} Pa^{-1})
r_p	pore radius (m)
R	rejection
	ideal gas constant (8.314 J mol^{-1} K^{-1})
σ^s	reflection coefficient of membrane
τ	tortuosity
X	fixed charge density of membrane (mol m^{-3})
ψ_0	surface potential (V)
ψ_ζ	zeta potential (V)
$\psi_{dp/2}$	potential in the center of the pore (V)

1. Introduction

1.1. Global water resources

Freshwater constitutes only 2.5% of the global water supply[1]. Furthermore, 70% of this freshwater supply is fixed in glaciers and icecaps, making it unavailable for withdrawal and use. The other 30% is mostly groundwater, with only 0.3% of freshwater resources being easily accessible as surface waters. Considering that over 1.2 billion people in the world have inadequate potable water supplies[2], access to clean water is one of the most critical global environmental (and sociopolitical) challenges we must confront. One avenue for conserving our freshwater resources is to develop new technologies to reclaim water currently used in agricultural and industrial processes. In perspective, the global volume of water used in the industrial and agricultural sectors in 2007 was estimated at 716 $Gm^3\ yr^{-1}$ and 6390 $Gm^3\ yr^{-1}$, respectively[3]. The data is based on the concept of the "water footprint," which was introduced in 2002 as a way to quantify and compare water consumption among nations and for various agricultural and industrial products. In 2005, the water footprint was linked to the concept of "virtual water" [4], defined as the volume of water required to produce a commodity or service. With much effort being dedicated to quantifying water consumption and availability, it is clear that the issue of freshwater resources is of utmost importance. As human population increases, so too does the stress on our freshwater supply. Therefore, the development and implementation of novel newer water treatment technologies, as well as the improvement of current technologies, will allow for the renewal and reuse of wastewater streams to prevent further withdrawal of the limited natural sources of freshwater.

1.2. Water Treatment Technology

The scarcity of freshwater resources has resulted in much research and development in the field of water treatment. Water treatment is the process of removing undesirable chemicals, biological contaminants, suspended solids or gases from contaminated water. The goal is to produce water fit for a specific purpose. In general, methods of water treatment can be classified as physical, biological, or chemical processes. Physical processes for treating water include filtration, sedimentation and distillation. Examples of biological methods for water treatment are secondary wastewater treatment and anaerobic digestion. Water treatment can also occur via chemical means such as flocculation, chlorination and advanced oxidation processes. The technology chosen for treating a contaminated water stream is dependent on the nature of the water source (e.g. seawater, municipal wastewater, industrial waters, etc.) and the required quality of the treated water (potable water for drinking, deionized, industrial reuse, etc.). Often, water treatment requires the use of multiple techniques in order to ensure the purification process is effective and efficient.

1.3. Membrane Technology for Water Treatment

A membrane acts as a very specific filter that allows water to flow through, while preventing suspended solids and/or dissolved substances from passing. In general, there are three different mechanisms by which membranes filter substances from water. The first is by applying pressure across the membrane, referred to as transmembrane pressure. The pressure is the driving force by which small water molecules are forced through the semipermeable membrane while larger species are excluded. The second method is the use of a concentration gradient, known as membrane dialysis, which operates on the principle that substances will move from a region of high concentration to a region of lower concentration until equilibrium is reached. The final

mechanism for treating water with membrane technology is the introduction of an electric potential across the membrane, known as electrodialysis. This electric potential controls the transport of charged substances from one side of the membrane to the other.

1.3.1 Pressure-driven membrane filtration processes

The membrane technology in this work utilizes transmembrane pressure to clean water. There are several types of pressure-driven membrane filtration processes. These are normally defined by the pore size of the material comprising the membrane and the size range of the substances they are capable of removing. Microfiltration (MF) and ultrafiltration (UF) are useful for removing particles from solution. Typically, MF is used to remove suspended solids and colloids larger than 0.05 μm, while UF is capable of removing biological organisms, such as bacteria, and soluble macromolecules, such as proteins, that are 2 -100 nm in size. For the removal of dissolved substances, such as salts, nanofiltration (NF) or reverse osmosis (RO) is required. NF and RO can be distinguished based on the size of the pores of the materials utilized in these types of membrane water treatment. RO membranes have pore sizes ranging from 1 – 10 Å, while NF membranes typically have pore sizes in the 10 – 40 Å range[5]. Due to these differences in pore size, the above membrane technologies have distinct pressure requirements for effective water treatment. Operating pressures for the different types of membrane technologies are given in Table 1.1.

Pressure-driven membrane filtration is desirable because it works without the addition of any chemicals, is easily scalable from a research setting to an industrial application, has a relatively small operating plant footprint and requires no phase change for water treatment (as opposed to

distillation, for example). However, there are limitations to the use of membrane technology in water treatment. One such concern is the occurrence of membrane fouling, where the membrane becomes contaminated with biological organisms, salts, etc. Methods to prevent membrane fouling, as well as fabricating anti-fouling membrane materials, are current research topics of interest in the membrane science community. As this type of filtration requires transmembrane pressure, there is work to be done to reduce the costs associated with pumping the water across the membrane and the intrinsic costs of pump maintenance. Finally, improvements can be made with respect to the rate of water flow in current membrane processes.

The effectiveness of the membrane filtration process is typically measured with two parameters that serve as criteria for evaluating membrane performance. The first is selectivity, which is given by the rejection (R) of a specific solute according to:

$$R = 1 - \frac{C_P}{C_F} \qquad \text{Equation 1.1}$$

where C_P refers to the concentration of the solute in the permeate solution ("clean" water) and C_F is the concentration in the feed solution (contaminated feed stream). Membrane performance is also measured by the productivity, given by the volume flux (J_v) according to:

$$J_V = \frac{\Delta P}{\eta R_{tot}} \qquad \text{Equation 1.2}$$

where ΔP is the effective transmembrane pressure, η is solute viscosity and R_{tot} is the resistance to solvent flow. J_v is typically expressed as a flux per unit time.

1.4 Nanofiltration

In general, nanofiltration (NF) membranes are defined as a membrane filtration process falling somewhere between ultrafiltration (UF) and reverse osmosis (RO). NF membranes are characterized as having pore diameters ranging from one to several nanometers and molecular weight cut-off (MWCO) values of approximately 1000 Daltons or less[6,7].

1.4.1 Nanofiltration and reverse osmosis

NF is a relatively new technology for water purification compared to competing processes such as reverse osmosis (RO). Unlike RO membranes, both polymeric and ceramic NF membranes have physical pores[8]. Therefore, while diffusion is responsible for the separation of solutes from solution in RO filtration[9], both diffusion and pore flow contribute to separation in NF. Although RO yields very high rejection of salts in solution (99.5% for 35,000 mg/L NaCl)[10], the high operating pressures and relatively low water fluxes in these systems make reverse osmosis an extremely energy-intensive process for water desalination. This has been the motivation behind the increase in nanofiltration research over the last 20 years; NF membrane systems are much more energy-efficient[11,12]. For example, an RO system capable of almost complete removal of NaCl operates at a pressure of 800 psi with a water flux of 1.2 m^3 m^{-2} day^{-1} [10]. State-of-the-art organic NF membranes show moderate rejection of NaCl (50.9 ± 5.1% for 2000 mg/L NaCl) and similar flux (1.2 ±0.1 m^3 m^{-2} day^{-1}) at a fraction of the operating pressure (200 psi) of RO systems[13].

1.4.2 Polymeric NF membranes

The majority of current studies in NF focus on developing and characterizing polymeric membranes, especially polyelectrolyte multilayer (PEM) membranes[14–16]. In fact, almost all commercially available NF membranes are made of organic materials. These membranes consist of multiple, alternating layers of positively and negatively charged polymers. The most common materials used in the production of these membranes are polysulfones and polyamides. Synthesis of multilayered, polyelectrolyte membranes begins with immersion of a porous, charged substrate into a solution containing a polyelectrolyte. A second immersion in a solution containing an oppositely charged polyelectrolyte results in an additional layer on the surface, and repetition of the process produces multilayer films. Terminating these polymers with polycations leads to positively charged membranes whereas termination with polyanions gives a negatively charged membrane[17,18].

1.4.3 Ceramic NF membranes

Ceramic NF membranes, which are the focus of this study, are composed of nanoporous layers of amphoteric metal oxides. While very few studies have focused on preparing ceramic NF membranes[19–22], there are numerous advantages to ceramic nanofilters such as greater chemical, thermal and mechanical stability. Ceramic NF membranes are composed of inorganic materials with pores that range from 1 nm to a few nanometers in size. These membranes develop charge, and therefore electric potential, on the pore surface when brought into contact with aqueous solutions. Most of the ceramic membranes are made of chemically stable metal oxides as TiO_2, ZrO_2, and SiO_2, which in the colloidal chemistry field are regarded as constant surface potential materials. This means that the magnitude and sign of the surface charge / potential acquired upon

immersion in a solution is determined by surface adsorption / desorption reactions of ions present in the solution. In the absence of ions that could specifically adsorb, other than H^+, the surface charge / potential will be controlled only by the solution pH. Many of these materials exhibit this amphoteric behavior in the pH range of interest for NF applications (pH 3 to 11). This implies that at a certain value of pH between 3 and 11 the surface charge / potential will be zero, and the magnitude will increase as distance from the pH of zero charge increases. The sign of the surface charge / potential will be different on each side of the pH of zero charge. Thus, when the solution contains only indifferent electrolytes, the membrane charge and sign can be controlled by solution pH alone.

1.5 Ceramic NF Membranes for Salt Removal

Ceramic NF membranes are most highly charged at pH values far from the isoelectric pH (pH_{iep}). Under these conditions, the surface charge leads to an electrostatic double layer of ions near the pore wall surface, which results in a decaying electrochemical potential across the pore diameter[23–25]. This potential prevents ions of the same charge (co-ions) from passing through the porous membrane. Ions of opposite charge (counter-ions) are rejected as well in order to maintain electroneutrality in solution.

1.5.1 Electrical double layer (EDL) in charged pores

The EDL phenomenon describes the potential distribution at the interface between a charged surface and a solution containing charged species, such as salt ions. A schematic of the EDL is provided in Figure 1.1. In the figure, a positively charged surface is the y-axis; this is analogous to a positively charged pore wall in a ceramic NF membrane. As distance from the surface

increases, so does the electric potential. Also defined in Figure 1.1 are the distances from the surface at which different potentials are defined. Of particular importance to this research is the zeta potential (ψ_ζ), the measurement of which is used as a surrogate to approximate surface potential (ψ_0). The amount of EDL overlap from one pore wall to another determines the potential distribution across the pore, which ultimately controls whether or not ions will be transported through the pores or rejected. The distance the EDL extends from the surface is known as the Debye length (κ^{-1}) and is given by:

$$\kappa = \left(\frac{2F^2 I \times 10^3}{\varepsilon\varepsilon_0 RT}\right)^{1/2} \qquad \text{Equation 1.3}$$

κ is dependent only on ionic strength (I) of the solution; F, ε, ε_0 and R are constants having their usual meaning. In addition to ionic strength, the potential distribution across the pore is affected by solution pH (which determines ψ_ζ of the membrane material) and pore diameter of membrane material (through the amount of EDL overlap required to extend across the entire diameter of the pore). As an example, a schematic of this concept is provided in Figure 2. The absolute value of the potential is plotted as a function of distance, measured from zero at one pore wall to the pore diameter at the other wall. The solid line indicates conditions where the potential remains relatively constant across the entire pore diameter. The dashed line represents an environment where there is a decrease in the potential at the center of the pore, resulting from incomplete overlap of the EDLs from opposing pore walls. This drop in potential is expected with large pore sizes, high ionic strength solutions, or when solution pH is close to the pH_{iep} of the membrane material.

1.5.2 Donnan potential

Due to the electrochemical potential in pores, a distribution of co-ions and counter-ions occurs at the membrane / solution interface (Figure 1.1). This results in a space-charge separation and, consequently, an uneven distribution of electrical charges. The potential that develops across the membrane as a result of this uneven distribution is known as the Donnan potential. This potential acts to hinder the diffusion of ions having the same sign as that of the Donnan potential. Due to electroneutrality requirements, ions of opposite charge to the Donnan potential are also rejected, leading to salt retention and separation[26,27]. Thus, fabrication of ceramic nanofilters can be tailored to specific applications based on pH and ionic strength of the feed solution.

1.5.3 Ion Transport

Rejection of salts in ceramic nanofiltration is influenced not only by properties of the membrane and the solution, but also the nature of the solute[28]. In this research, we are concerned with treating water containing salt solutions, so the solutes are ions. The extended Nernst-Planck equation is commonly used as the basis for modeling the rejection performance of charged ions by nanofiltration membranes[19,20,27,29]. This equation provides a quantitative description of the interaction between ions and a membrane through the calculation of ion flux (J_i):

$$J_i = -D_{i,p}\frac{dc_i}{dx} - \frac{z_i c_i D_{i,p}}{RT} F \frac{d\psi}{dx} + K_{i,c} c_i J_v \qquad \text{Equation 1.4}$$

where:

J_i = ion flux, mol m^{-2} s^{-1}
$D_{i,p}$ = hindrance factor for diffusion, m^2 s^{-1}
c_i = ion concentration, mol m^{-3}
F = Faraday constant, 96487 C mol^{-1}
ψ = electric potential, V
T = temperature, K

$K_{i,c}$ = hindrance factor for convection
z_i = ion valence
J_v = volume flux, $m^3\ m^{-2}\ s^{-1}$
R = ideal gas constant, 8.314 J mol^{-1} K^{-1}

This equation describes the transport of ions through the pores of charged membranes as a result of diffusion, convection, and electromigration caused by gradients in concentration, pressure, and electric potential, respectively. Equation 1.4 is not directly employed in this research, as our aim is not to model the transport of electrolytes for varying solution compositions and membranes. Rather, our objective is to determine which of these variables are most useful in predicting the rejection performance of our membranes.

1.6 Bilayer Ceramic Membranes

Almost all ceramic NF membranes are composed of a single filtration layer that is either positively or negatively charged for a given solution composition; the sign of membrane charge determines whether the cation or the anion behaves as the co-ion. Ions with higher valence states are more readily rejected than monovalent ions due to increased charge density. Therefore, currently available ceramic NF membranes are best suited for applications where removal of divalent ions is important and pH of feed solution is far from the pH_{iep} of the nanofiltration layer. The overall objective of this research is to fabricate, characterize and evaluate bilayer, ceramic nanofiltration (NF) membranes that limit the transport of ions through the membranes without hindering water flux. Our hypothesis is that by preparing membranes made of layers having two different nanoparticulate metal oxide materials, with distinct charging properties as a function of pH, we will be able to "reject" ions in a wider range of solution conditions than is possible with current ceramic membrane technology. In addition to verifying this hypothesis, we attempt to elucidate the major variables affecting ion transport in our bilayer membranes (i.e. solution pH,

salt concentration, ionic strength of solution, pore size of membrane materials) in order to provide an experimental set useful for evaluating modeling efforts in the field of nanofiltration. Our goal is to fabricate ceramic membranes that exhibit high rejection values in a variety of salt solutions and throughout a range of pH levels without significantly affecting the flux of water through the membranes in order to improve the competitiveness of ceramic membranes for water treatment processes requiring the removal of charged ions.

Three major objectives need to be satisfied to meet our overall goal.

1. Synthesize and characterize metal oxide materials that have significantly different pH_{iep} values. To accomplish this goal, we chose iron-doped silica (Fe-SiO_2) and γ-Al_2O_3 as the materials that comprise the nanofiltration layers in our membranes. For purposes of comparison, we prepared bilayer membranes according to the schematic provided in Figure 1.3 as well as single layer membranes of the same materials,.
2. Characterize nanofiltration membranes to determine physical membrane parameters that affect rejection of ions.
3. Determine solution properties that control rejection in single and bilayer membranes.

The final goal of this dissertation is to relate the concepts and principles of bilayer ceramic nanofiltration discovered in the above objectives to practical applications in current water treatment technology.

1.7 References

1. Gleick, P. H. *Water in crisis: a guide to the world's fresh water resources.* (Oxford University Press, Inc., 1993).

2. Black, M. *The no-nonsense guide to water*. (Verso Books, 2004).

3. Hoekstra, A. Y. & Chapagain, A. K. Water footprints of nations: Water use by people as a function of their consumption pattern. *Water Resour. Manag.* **21,** 35–48 (2007).

4. Hoekstra, A. Y. & Hung, P. Q. Globalisation of water resources: international virtual water flows in relation to crop trade. *Glob. Environ. Change* **15,** 45–56 (2005).

5. Schafer, A. I., Fane, A. G. & Waite, T. D. *Nanofiltration - Principles and Applications*. (Elvesier, 2005).

6. Burggraaf, A. J. & Cot, L. *Fundamentals of inorganic membrane science and technology*. (Elsevier Science, 1996).

7. Sarrade, S., Rios, G. M. & Carlès, M. Dynamic characterization and transport mechanisms of two inorganic membranes for nanofiltration. *J. Membr. Sci.* **97,** 155–166 (1994).

8. Bowen, W. R. & Sharif, A. O. Prediction of optimum membrane design: pore entrance shape and surface potential. *Colloids Surf. Physicochem. Eng. Asp.* **201,** 207–217 (2002).

9. Amjad, Z. *Reverse osmosis: membrane technology, water chemistry & industrial applications*. (Chapman & Hall, 1993).

10. Baker, R. W. *Membrane technology and applications*. (Wiley, 2004).

11. Christy, C. & Vermant, S. The state-of-the-art of filtration in recovery processes for biopharmaceutical production* 1. *Desalination* **147,** 1–4 (2002).

12. Yaroshchuk, A. & Staude, E. Charged membranes for low pressure reverse osmosis properties and applications. *Desalination* **86,** 115–133 (1992).

13. Ba, C. Design of advanced reverse osmosis and nanofiltration membranes for water purification. (University of Illinois, 2010).

14. Sanyal, O., Sommerfeld, A. N. & Lee, I. Design of ultrathin nanostructured polyelectrolyte-based membranes with high perchlorate rejection and high permeability. *Sep. Purif. Technol.* **145,** 113–119 (2015).

15. Dirir, Y. I., Hanafi, Y., Ghoufi, A. & Szymczyk, A. Theoretical Investigation of the Ionic Selectivity of Polyelectrolyte Multilayer Membranes in Nanofiltration. *Langmuir* **31,** 451–457 (2015).

16. De Grooth, J., Oborný, R., Potreck, J., Nijmeijer, K. & de Vos, W. M. The role of ionic strength and odd–even effects on the properties of polyelectrolyte multilayer nanofiltration membranes. *J. Membr. Sci.* **475,** 311–319 (2015).

17. Ouyang, L., Malaisamy, R. & Bruening, M. L. Multilayer polyelectrolyte films as nanofiltration membranes for separating monovalent and divalent cations. *J. Membr. Sci.* **310,** 76–84 (2008).

18. Hadj Lajimi, R., Ferjani, E., Roudesli, M. S. & Deratani, A. Effect of LbL surface modification on characteristics and performances of cellulose acetate nanofiltration membranes. *Desalination* **266,** 78–86 (2011).

19. Palmeri, J., Blanc, P., Larbot, A. & David, P. Theory of pressure-driven transport of neutral solutes and ions in porous ceramic nanofiltration membranes. *J. Membr. Sci.* **160,** 141–170 (1999).

20. Palmeri, J., Blanc, P., Larbot, A. & David, P. Hafnia ceramic nanofiltration membranes:: Part II. Modeling of pressure-driven transport of neutral solutes and ions. *J. Membr. Sci.* **179,** 243–266 (2000).

21. Tsuru, T., Miyawaki, M., Yoshioka, T. & Asaeda, M. Reverse osmosis of nonaqueous solutions through porous silica zirconia membranes. *AIChE J.* **52,** 522–531 (2006).

22. Tsuru, T., Ogawa, K., Kanezashi, M. & Yoshioka, T. Permeation Characteristics of Electrolytes and Neutral Solutes through Titania Nanofiltration Membranes at High Temperatures. *Langmuir* (2010).

23. Farsi, A. *et al.* Modeling water flux and salt rejection of mesoporous γ-alumina and microporous organosilica membranes. *J. Membr. Sci.* **470,** 307–315 (2014).

24. Fievet, P., Szymczyk, A., Aoubiza, B. & Pagetti, J. Evaluation of three methods for the characterisation of the membrane-solution interface: streaming potential, membrane potential and electrolyte conductivity inside pores. *J. Membr. Sci.* **168,** 87–100 (2000).

25. Kukizaki, M. Relation between salt rejection and electrokinetic properties on Shirasu porous glass (SPG) membranes with nano-order uniform pores. *Sep. Purif. Technol.* **69,** 87–96 (2009).

26. Schaep, J., Van der Bruggen, B., Vandecasteele, C. & Wilms, D. Influence of ion size and charge in nanofiltration. *Sep. Purif. Technol.* **14,** 155–162 (1998).

27. Schaep, J., Vandecasteele, C., Mohammad, A. W. & Bowen, W. R. Analysis of the salt retention of nanofiltration membranes using the Donnan–Steric partitioning pore model. *Sep. Sci. Technol.* **34,** 3009–3030 (1999).

28. Labbez, C. *et al.* Analysis of the Salt Retention of a Titania Membrane using the. *J. Membr. Sci.* **208,** 315–329 (2002).

29. Donnan, F. G. The theory of membrane equilibria. *Chem. Rev.* **1,** 73–90 (1924).

Membrane Process	*Operating Pressure (psi)*
microfiltration	< 30
ultrafiltration	15 – 150
nanofiltration	45 – 300
reverse osmosis	200 – 1200

Table 1.1: Typical operating pressures for different types of pressure-driven membrane filtration processes.

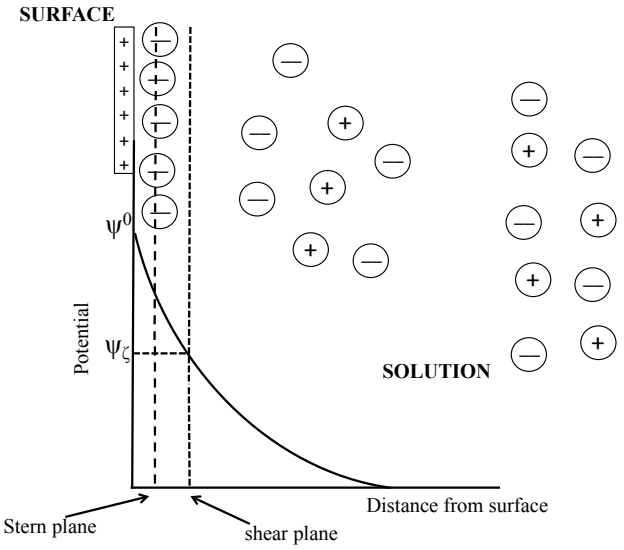

Figure 1.1: Schematic of the electrical double layer and resulting charge distribution at the interface between a charged solid and a solution containing charged ions. In the drawing, the surface is represented as being positively charged.

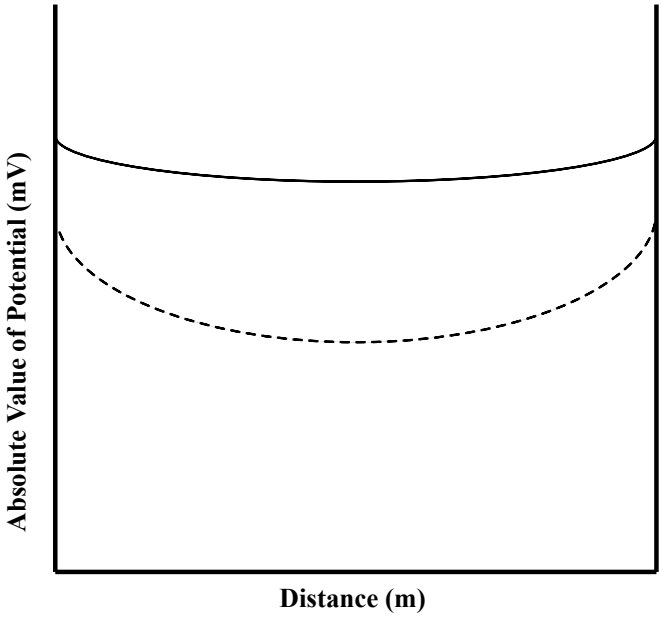

Figure 1.2: Schematic of absolute value of the pore potential as a function of distance from the pore wall.

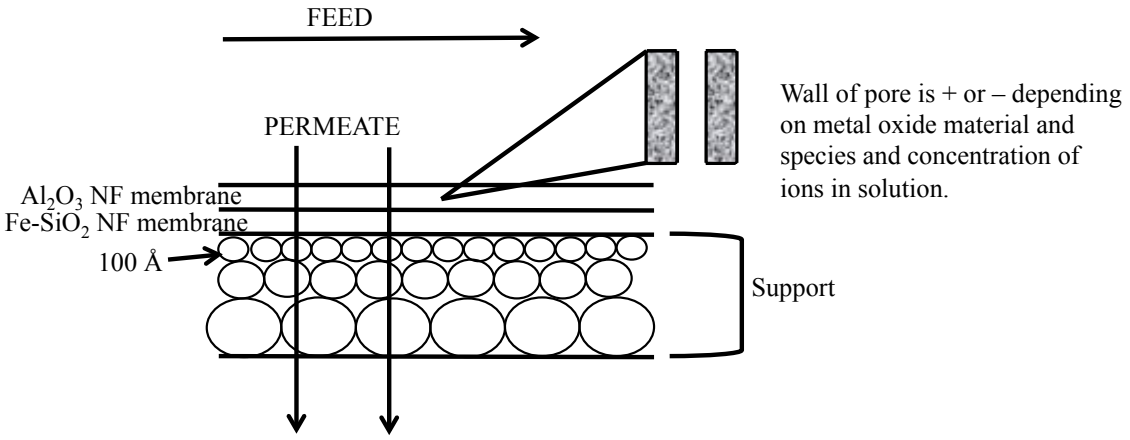

Figure 1.3: Diagram of proposed inorganic, bilayer NF membranes. Magnified portion of membrane represents a pore with charged pore walls. *Note: sequence of the metal oxide layers can be reversed.*

2. Preparation and Physical Characterization of Single and Bilayer γ-Al_2O_3 and Fe-SiO_2 Nanofiltration Membranes

2.1. Introduction

Nanofiltration is the most recently developed of all membrane separation techniques. The technology has attracted the attention of researchers for a number of applications, including but not limited to: treatment of wastewaters in the textile[1,2], dairy[3,4], as well as the food and beverage[5,6] industries. It has also been employed in the treatment of production water resulting from manufacturing of fuels such as gas and oil[7,8]. In addition, nanofiltration is currently being investigated as a mechanism for the aqueous phase removal of organic contaminants, such as personal care products, endocrine-disrupting compounds, and bisphenyl-A[9,10]. Nanofiltration is a promising technology for recycling wastewater streams in order to reduce overall consumption of freshwater and for recovery of useful by-products in these industrial processes. At a time when the limited supply of freshwater is becoming an ever-increasing global concern, nanofiltration has the potential to excel as a water purification technique for a wide range of feed streams containing molecular and/or ionic solutes.

In general, nanofiltration (NF) membranes are defined as a membrane filtration process falling somewhere between ultrafiltration (UF) and reverse osmosis (RO). NF membranes are characterized as having pore diameters ranging from one to several nanometers and molecular weight cut-off (MWCO) values of approximately 1000 Da or less[11,12]. NF membranes are further classified as organic (polymeric) or inorganic (ceramic). Unlike RO membranes, both polymeric and ceramic NF membranes have physical pores[13]. Therefore, while diffusion is responsible for the separation of solutes from solution in RO filtration[14], both diffusion and pore flow contribute to separation in NF. The majority of current studies in NF focus on developing and characterizing organic membranes, especially polyelectrolyte multilayer (PEM) membranes[15–17].

In fact, almost all commercially available NF membranes are made of organic materials. While very few studies have focused on preparing ceramic NF membranes[18–21], there are numerous advantages to ceramic nanofilters such as greater chemical, thermal and mechanical stability. Ceramic NF membranes are composed of inorganic materials with pores that range from 1 nm to a few nanometers in size. These membranes develop charge, and therefore electric potential, on the pore surface when brought into contact with aqueous solutions. Most of the ceramic membranes are made of chemically stable metal oxides as TiO_2, ZrO_2, and SiO_2, which in the colloidal chemistry field are regarded as constant surface potential materials. This means that the magnitude and sign of the surface charge/potential acquired upon immersion in a solution is determined by surface adsorption /desorption reactions of ions present in the solution. In the absence of ions that could specifically adsorb, other than H^+, the surface charge/potential will be controlled only by the solution pH. Many of these materials exhibit amphoteric behavior in the pH range of interest for NF applications (pH 3 to 11). This implies that at a certain value of pH between 3 and 11 the surface charge/potential will be zero, and the magnitude will increase as distance from the pH of zero charge increases. The sign of the surface charge/potential will be different on each side of the pH of zero charge. Thus, when the solution contains only indifferent electrolytes, the membrane charge and sign can be controlled by solution pH alone.

Solution flux (J_v) through NF membranes has been described by the widely accepted Donnan-Steric Partitioning Pore Model (DSPM), which only takes into account electrostatic and steric /hydrodynamic interactions of the ions with the membrane[16,22,23]. In this model, solute transfer through the membrane is the result of a distribution of charged species at the membrane/solution interface and transport occurs via a combination of convection, diffusion and electro-migration

of the charged species across the membrane. The rejection of an ion will be determined by ion properties (ion feed concentration, valence, radius and bulk ion diffusion coefficient) and membrane parameters. The membrane is characterized according to three parameters:

1. pore characteristics (average diameter, d_p and porosity, ε)
2. membrane thickness, L_m
3. surface charge density, q_w.

This present study describes the fabrication of nanofiltration membranes composed of Fe-doped silica and γ-alumina nanofiltration layers deposited on 100 Å commercially available ceramic UF membranes. The resulting single layer and bi-layer membranes are evaluated to determine the above mentioned physical membrane parameters that influence transport and removal of charged solutes in aqueous nanofiltration. The pore radius (r_p) and porosity (ε) are measured by N_2 adsorption isotherms of the materials used to fabricated the nanofiltration layers, subjected to the same heating processes as the supported membranes. Effective thickness is extracted from ultra-high purity N_2 gas permeation as a function of transmembrane pressure. Also the thickness of the nanofiltration membranes layers (L_m) is determined using SEM imaging. The value of q_w can be approximated or surrogately inferred from zeta potential maesurements for a given solution composition. However, this paper will only provide zeta potential data of the nanofiltration layers immersed in NaCl to illustrate the different charging properties of the γ-alumina and Fe-silica materials in the range of pH 4 to 10.

2.2. Experimental Methods

2.2.1 Preparation of nanoporous materials

Four different nanofiltration membranes, using two different materials, were fabricated for use in these studies (Table 2.1). The materials used to construct the nanofiltration layers on the ceramic supports are derived from suspensions of metal oxide nanoparticles synthesized using sol-gel techniques.

2.2.1.1 Synthesis of Fe-doped SiO_2 sol

The first material used to prepare our membranes was an iron-modified silica sol, the synthesis of which is similar to that described previously by this research group.[24] Briefly, a basic SiO_2 (silica) sol was prepared by hydrolysis of tetraethylorthosilicate (TEOS, Aldrich, 98%) precursor in the presence of ammonium hydroxide (Fisher Scientific, Certified ACS). The TEOS was added to a 2.0 M solution of NH_4OH and stirred for 1 hour. The SiO_2 sol was transferred to 3500 MWCO dialysis membranes, and allowed to dialyze for 2 h with slow stirring in ultra high purity (Milli-Q) water. The dialysis water was changed and this process was repeated three times. After completing dialysis , the silica sol was collected and the pH was measured at 8.5. The SiO_2 sol was allowed to settle for 24 h and was decanted to eliminate any larger-sized particles that had formed during preparation. 19.1 mL of a 0.1M iron (III) nitrate nonahydrate (Fisher Scientific, Certified ACS) solution was then added to 80.0 mL of the silica sol to adsorb iron onto the surface of the silica particles. The final pH of the Fe-doped silica sol after equilibration was measured at pH 2.6. The final concentration of Fe-silica in the sol was approximately 20 g/L.

2.2.1.2 Synthesis of γ-AlOOH sol

Nanofiltration layers were also fabricated from alumina sol prepared by the hydrolysis of aluminum tri-sec-butoxide (ATSB, Acros Organics); the synthesis of this material was first described by Schultz and Anderson[25] and was modified for this application as reported by Wouters et al.[26] ATSB was diluted with 2-butanol and added to 85°C ultra high purity (Milli Q) water. The mixture was stirred vigorously for 2 h. Nitric acid (Fisher Scientific, Certified ACS) was added to the mixture in a 12.9:1 ATSB:HNO_3 ratio and stirring continued for an additional 2 h. Boiling stones were then added to the flask and the mixture was allowed to stir for 4 h. Finally, stirring was stopped and the resulting mixture was allowed to reflux overnight. The alumina suspension was passed through a 0.45μm filter to remove any large particles. The final concentration of γ-AlOOH in the sol was approximately 40 g/L.

2.2.2 Characterization of the microstructure of nanofiltration layers

As surrogates for the actual membranes, unsupported samples of the Fe-silica and alumina materials were dried by evaporation to create xerogels, then heated at 400 or 500°C for characterization. The size distribution and average pore size of the xerogels was determined by nitrogen adsorption using a Micromeritics ASAP 200 instrument. The total pore volume and pore size distribution in both materials was calculated using the DFT model. Using this method, the shape of pores must be assumed; for both the alumina and iron-silica materials, the cylindrical pore model provided the better fit. The porosity of the materials was calculated from the pore volume and the crystallographic density of the solid phase.

2.2.3 Charging properties of the nanofiltration layers

The unsupported xerogels were also used to examine the charging properties of the two materials. Zeta potential, in the presence of sodium chloride in solution, throughout the pH range 2-10 was measured using a Malvern (3000 HS) ZetaSizer. Xerogels were ground to a fine powder and suspended in solutions of 0.01M NaCl (Fisher Scientific, Certified ACS). pH was adjusted using sodium hydroxide or hydrochloric acid (Fisher Scientific, Certified ACS chemicals) to obtain zeta potential values for the xerogels as a function of solution pH.

2.2.4 Fabrication of nanofiltration membranes

The nanofiltration membrane layers were deposited onto commercially available tubular ceramic membranes with a 100Å top layer (U.S. Filter) using a dip-coating technique. The support membranes have an inner diameter of 7 mm, outer diameter of 10 mm, and were cut to 5 cm lengths. Using a peristaltic pump, the Fe-silica or alumina sol was drawn into contact with the interior of the tube and held for 10 min. The coated membranes were then dried over a period of 4 days at room temperature in a controlled environment where relative humidity was gradually decreased from 85% to 30%. The nanofiltration layers were sintered by heating at 400 or 500°C for 3 h (5°C min^{-1} ramp rate). This coating, drying, and firing procedure was repeated three or four times for each deposited nanofiltration layer. In total, four types of membranes were created, with duplicate versions of each, for a sum of eight ceramic nanofiltration membranes utilized in this study, as described in Table 2.1.

2.2.5 Nitrogen gas permeation

The permeation flux (mol s^{-1} m^{-2}) of ultra-high purity nitrogen (N_2) gas was measured as a function of varying transmembrane pressure through both the uncoated support and the eight

membranes containing the deposited nanofiltration layers. Experiments were performed at room temperature. In nanofiltration membranes, if there is no involvement of adsorption, the predominant mechanism of transport in the gas phase is Knudsen diffusion[27]. Knudsen permeance (Q) is given by:

$$Q = \frac{\varepsilon d_p}{\tau L_m}\left(\frac{8}{9\pi \mathrm{M} RT}\right)^{\frac{1}{2}} \qquad \text{Equation 2.1}$$

where M is the molecular weight of the diffusing gas, R is the gas constant, and T is temperature. The permeation also depends on the following properties of the membrane: ε is the porosity of the membrane, d_p is the pore diameter, τ is the tortuosity, and L_m is the membrane thickness. Our ceramic membranes consist of both a 100Å support layer and either one or two types of nanofiltration layers. To separate the permeation through the nanofiltration layer from that of the total membrane, we model nitrogen gas flow (F) as a series of resistances where:

$$\frac{1}{\mathrm{F}_{\mathrm{total}}} = \frac{1}{\mathrm{F}_{\mathrm{support}}} + \frac{1}{\mathrm{F}_{\mathrm{layer}}} \qquad \text{Equation 2.2}$$

and

$$Q = \frac{\mathrm{F}}{\Delta P} \qquad \text{Equation 2.3}$$

where ΔP is the pressure difference across each region of the membrane. The pressure difference for the total membrane is determined experimentally by controlling P_{Low} and measuring a corresponding P_{High} value. The permeation of N_2 through the support plus nanofiltration layers falls in the transition between Knudsen and Poiseuille diffusion; thus, the relation between permeation (Q) and average pressure can be described as follows:

$$Q = a_{\text{total}} + b_{\text{total}}\left(\frac{P_{\text{High}} + P_{\text{Low}}}{2}\right) \qquad \text{Equation 2.4}$$

In this equation, a_{total} represents the Knudsen contribution while the remainder of the left-hand side of the equation describes the Poiseuille contribution to gas flow. If the flow through the total membrane is constant, then P_{Int} (pressure at the interphase) can be calculated as:

$$\left[a_{\text{total}} + b_{\text{total}}\left(\frac{P_{\text{High}} + P_{\text{Low}}}{2}\right)\right]\left[P_{\text{High}} - P_{\text{Low}}\right] = \left[a_{\text{support}} + b_{\text{support}}\left(\frac{P_{\text{Int}} + P_{\text{Low}}}{2}\right)\right]\left[P_{\text{Int}} - P_{\text{Low}}\right]$$

Equation 2.5

Where *a* and *b* are the y-intercept and slope, respectively, from the experimentally determined linear regression equations for nitrogen permeation through the membrane. For single layer membranes, the "support" is the commercial tubular membrane with 100 Å top layer (Figure 2.1a). In bi-layer membranes, both the 100 Å support and the bottom nanofiltration layer are considered as the new "support" (Figure 2.1b) to calculate nitrogen permeation through the layer facing the feed solution exclusively.

2.2.6 Scanning electron microscopy

Scanning electron microscopy (SEM) was performed using a Zeiss 1540XB CrossBeam Focused Ion Beam FE SEM. Membrane modules were broken in order to obtain both edge and surface views of the nanofiltration layers. Segments of the membranes were sputter coated with gold at 20 mA for 60 seconds prior to SEM imaging.

2.2.7 Liquid filtration of neutral species

A schematic of the apparatus used to test the filtration properties of the membrane is provided in Figure 2.2. The system utilized SS 316 tubing, a LEWA positive displacement pump, and the pressure was adjusted using manual valves and monitored by a pressure gauge just downstream of the membrane compartment. The feed solution was continuously circulated throughout the system while the permeate solution was collected in a glass vessel. Both solutions were at room temperature and atmospheric pressure. The operating pressure for the filtration system was 250 psi for all experiments and samples were simultaneously collected from both the feed and permeate solutions after 30 and 45 min of circulation. Between each experiment, ultra-high purity water was flushed through the filtration line and the membrane for 30 min to prevent contamination and to ensure complete removal of any solute remaining in the pores, respectively. Polyethylene glycol (PEG, Alfa Aesar) rejection was investigated to determine the molecular weight cut-off values for these nanofiltration membranes. Solutions were prepared containing several sizes of PEG: 200 D, 400 D, 600 D, 1000 D, 2000 D, and 4000 D to reach a total PEG concentration of 0.2% w/v. The concentration of PEG in feed and permeate samples was analyzed by gel permeation chromatography (GPC, Shodex OHpak SB-802.5 HQ column) to obtain molecular weight distribution curves. This was performed for single layer membranes

only, as bi-layer membranes are fabricated from the same materials with constant pore size and are therefore assumed to behave similar to their single layer counterparts in size exclusion experiments.

2.2.8 Membrane durability

As a measure of durability of the membrane module, permeation of N_2 gas through the Al_2O_3/Fe-SiO_2 membrane was measured after all liquid filtration experiments were completed. The data is compared with nitrogen permeation through the membrane before experimental use. This specific membrane is represented as it was most widely used, therefore had the largest volume of liquid passed, 2600 L m^{-2} of membrane.

2.3. Results and Discussion

2.3.1 Pore structure of unsupported xerogels

The average pore diameter for Fe-SiO_2 heated to 500°C is 2.1 nm. The average pore sizes for γ-Al_2O_3 heated to 400 and 500°C are 3.9 nm and 4.3 nm, respectively (Figure 2.3). The data show a much wider distribution of pore size in the γ-Al_2O_3 material compared to the Fe-SiO_2 material. By determining the pore radius (r_p) of the materials used in the construction of our nanofiltration layers, we should be able to better understand the mechanism for rejection of ions in solution. For comparison, values for radii (in units nm) of common ions in solution are: 0.097-0.47 (Na^+), 0.070-0.78 (Mg^{2+}), 0.164-0.39 (Cl^-), 0.242-0.55 (SO_4^{2-}), 0.177-0.335 (NO_3^-), 0.241-0.35 (ClO_4^-).[28–32] The large variation in the published values is partially due to the different types of radii calculated by each author and the method used in determining the radius. However, it is clear that the diameter of each ion is an order of magnitude smaller than the diameter of the pores in

either Fe-SiO_2 or γ-Al_2O_3. Therefore, we can assume that the primary mechanism for rejection of ions in these membranes is electrostatic, as opposed to steric, in nature.

When fired to 400°C, there is a decrease in average pore diameter of γ-Al_2O_3 as compared to the higher 500°C firing temperature. A smaller pore size is ideal for the nanofiltration of salts in solution, as an increase in pore diameter leads to a decrease in the electric potential at the center of the pore for the same surface charge. It has been shown in the literature that the rejection of ions associated with these type of membranes for a given salt depends largely on the value of the potential at the center of the pore[33], rather than on the potential at the shear plane (zeta potential). This finding means that decay in potential (and, consequently, charge) across the radius of the pore is something to consider for these type of membranes. Therefore, the preferred firing temperature for the γ-Al_2O_3 material following deposition onto the support is 400°C. In all single and bi-layer membranes prepared, the γ-Al_2O_3 layers are heated at 400°C, with the exception of the bi-layer membranes with the Fe-SiO_2 layer facing the feed solution. In the $FeSiO_2/Al_2O_3$ bi-layer membranes (reference Table 2.1), the γ-Al_2O_3 is heated to 500°C during the firing process of the Fe-SiO_2 layers.

Another property that affects solute transport according to the DSPM model for nanofiltration membranes is membrane porosity (ε). The γ-Al_2O_3 and Fe-SiO_2 materials were compared with respect to porosity, calculated from total pore volume and density of the materials. The Fe-SiO_2 material fired to 500°C is less porous (31.3%) than the γ-Al_2O_3 heated at either 400°C or 500°C, with porosity values of 50.8% and and 42.2%, respectively. Although the γ-Al_2O_3 at 400°C has a smaller average pore size, it is a more porous material than its 500°C counterpart.

2.3.2 Charging properties of unsupported fired xerogels

The rationale for doping the silica sol with iron is evident as shown in a comparison of the charging properties of these two materials (see Figure 2.4a). While SiO_2 has a greater magnitude of zeta potential at increasingly basic pH values, it is less charged at lower pH. Upon addition of Fe, the zeta potential is practically constant throughout the measured pH range. The Fe-SiO_2 should perform well as a negatively charged NF membrane independent of pH. The zeta potential titration curves for both Fe-SiO_2 and γ-Al_2O_3 xerogels exposed to 0.01M NaCl solution are displayed in Figure 2.4b. Fe-SiO_2 has a large negative zeta potential at all pH values studied. It is not possible to determine the isoelectric pH (pH_{iep}) of this material from the data. However, it is assumed to be below pH 3.0 and probably near pH 2.0. Conversely, γ-Al_2O_3 has a positive zeta potential at pH ≤ 8.5, with a pH_{iep} near 8.7. As pH increases in the basic region, the zeta potential of γ-Al_2O_3 becomes more negative. Figure 2.4b also shows that the zeta potential/pH curves are practically overlapping for γ-Al_2O_3 heated at 400°C and 500°C and the pH_{iep} has the exact same value; thus, the charging properties of these two porous materials should be similar. In the literature, surface charge density (q_w) of NF membranes has been determined in several ways; extraction as a fitting parameter from nanofiltration transport models and determination of streaming potential are the most common methods for polymeric membranes. However, zeta potential is the preferred technique for ceramic nanofiltration membranes[34]. While the calculation of q_w is beyond the scope of the present study, it is certainly reasonable to assume that membrane materials will have a greater charge density when zeta potential values are largest. While the magnitude of q_w is certainly important for the rejection of charged solutes in nanofiltration, our materials (Fe-SiO_2 and γ-Al_2O_3) were chosen based on the difference in the

sign (positive or negative) of q_w. As Figure 2.4b clearly demonstrates, the two materials are oppositely charged from pH 5.0 to pH 8.5, a relevant pH range for many salt removal applications, including those in naturally occurring aquatic systems. Our objective here has been to fabricate bilayer membranes that behave as bipolar membranes in this pH range. Bipolar membranes, consisting of two oppositely charged nanofiltration layers, make rejection of ions in solution possible through either the cation or anion as being the co-ion.

2.3.3 Nitrogen gas permeation through single and bilayer γ-Al_2O_3 and Fe-SiO_2 membranes

The flux (mol m^{-2} s^{-1}) of N_2 gas through both our single (Fe-SiO_2 and Al_2O_3) and bilayer (Al_2O3/Fe-SiO_2 and Fe-SiO_2/Al_2O_3) membranes was measured after layers of the iron-silica and alumina sols were coated onto ceramic supports. Table 2.1 is provided as a reference for the specific composition of each membrane type. The permeance, Q, (mol m^{-2} s^{-1} Pa^{-1}) of nitrogen gas through all eight membranes prepared and the ceramic support alone is plotted as a function of average pressure (psi) between the two sides of the membrane in Figure 2.5. The data show a decrease in N_2 permeation through the porous membranes with deposited nanofiltration layers as compared to the support. This is to be expected with the decreased pore size of the materials (21 and 43 Å) as compared to the 100 Å layer of the support. Replicates of each membrane type have practically overlapping regression lines, indicating that the fabrication process used to create these membranes is reproducible.

Knudsen diffusion as the primary mechanism for gas transport in our membranes is confirmed in Table 2.2 by examining the values of slope for the linear regression equations. All membrane slopes are in the range of 10^{-8} (or smaller) mol m^{-2} s^{-2} Pa^{-1} per psi of increased pressure,

indicating that nitrogen permeation through the membrane (support + nanofiltration layer) or through the nanofiltration layer alone is mostly independent of pressure across the membrane. The data for nitrogen permeation through each deposited layer is useful for comparing the thickness of layers of the same composition (when equal porosity and tortuosity are assumed) in different membranes, as gas permeation varies inversely to membrane thickness (L_m) . The permeation of nitrogen gas through γ-Al_2O_3 nanofiltration layers deposited on the different membranes is shown in Figure 2.6a. Permeation is lowest in single layer γ-Al_2O_3 membranes and therefore the thickness of the nanofiltration layer is greater than in either of the bilayer membranes. This is expected as four layers of the alumina sol were deposited on the single layer membranes as compared to three layers in the bilayer membranes. In the bilayer membranes, an equal number of layers of alumina sol were deposited; the variable is the order in which the layers were applied. It is clear from Figure 2.6a that L_m for γ-Al_2O_3 layer is greater when applied on top of an Fe-SiO_2 layer as compared to when this layer is deposited directly onto the 100 Å support. This difference is most likely a result of the different heating temperatures applied to the alumina layer when it is the A or B nanofiltration layer. As thickness of the membrane layer (L_m) is a physical property of nanofiltration membranes affecting ion transport, we expect the order that layers are deposited on the support to influence rejection of ions in our bilayer membranes. The values for *a* (y-intercept) and *b* (slope) from the linear regression of permeation through the γ-Al_2O_3 NF layers are provided in Table 2.3a. The same comparison is provided for single and bi-layer membranes with respect to permeation through the Fe-SiO_2 nanofiltration layers in Figure 2.6b. The *a* and *b* values for permeation through the Fe-SiO_2 NF layers are listed in Table 2.3b. The larger values of slope for the single-layer Fe-SiO_2 membranes may provide evidence of physical defects in the nanofiltration layers that could affect solution phase transport. It was not

possible to compare the data for the two bilayer membranes with oppositely configured layers due to the increased heating temperature of γ-Al_2O_3 when the top Fe-SiO_2 layer is heated to 500°C. This is due to the fact that there are changes in porosity and pore size in the alumina layer the transport properties in the new "support". The data imply that L_m for Fe-SiO_2 layer is greater on a bilayer membrane with the Fe-SiO_2 layer facing the feed solution as compared to a single layer membrane.

2.3.4 Determining L_m for single and bilayer γ-Al_2O_3 and Fe-SiO_2 membranes

SEM imaging was used to determine the thickness (L_m) of Fe-SiO_2 and γ-Al_2O_3 NF layers in both single and bilayer membranes. The micrographs shown in Figure 2.7 (a-d) are images of the two single layer membranes and a bilayer NF membrane having an Fe-SiO_2 "A" layer. In Figure 2.7a, the structure of the Al_2O_3 A membrane is shown with the asymmetric support, containing increasingly smaller pore sizes with the dense, upper border representing a combination of the 100Å layer and the γ-Al_2O_3 NF layer. Unfortunately, as the composition of the two materials is quite similar, there is not enough contrast in the image to differentiate the border between the two layers.

2.3.4.1 L_m of γ-Al_2O_3 NF layers

From Figure 2.7b, thickness of the γ-Al_2O_3 NF layer was determined by subtracting the 100Å support layer. This supporting layer was measured at 1.8 μm in previous work by Skluzacek et al. with the same tubular supports[33]. The total of the 100Å and NF layer was measured as 3.9 μm, resulting in a γ-Al_2O_3 layer with L_m = 2.1 μm. This measurement was used to calculate both τ and L_m for layers in other membranes according to Equation 2.1; the results are displayed in

Table 2.3a. It is clear from the values of L_m that the γ-Al_2O_3 layer is thicker for the single layer compared to bilayer membranes. In comparing the two bilayer membranes, the γ-Al_2O_3 layer is more reproducible and has a smaller value of L_m when it is deposited as the bottom layer of our membranes.

2.3.4.2 L_m of Fe-SiO_2 NF layers

Thickness of the Fe-SiO_2 layer was determined from the micrograph of the Fe-SiO_2 B membrane (Figure 2.7c) and found to be 0.5 μm. This measurement was used to calculate τ and L_m values for Fe-SiO_2 NF layers on other membranes with Equation 2.1; the results are displayed in Table 2.3b. The thickness of the Fe-SiO_2 layer was also determined from the micrograph of the FeSiO_2 A membrane shown in Figure 7d; L_m for the Fe-SiO_2 layer on this membrane was similar at 0.4 μm. Comparing the values for L_m from Table 3b, the Fe-SiO_2 layer is similar in thickness for the single layer and bilayer membranes having Fe-SiO_2 as the top layer. However, in a bilayer membrane where the Fe-SiO_2 is deposited as the bottom NF layer, L_m is almost three times larger. All data for Fe-SiO_2 NF layers indicate that replicate membranes yield reproducible results.

The differences in layer thickness for the four types of membranes prepared in this study are likely the result of inconsistencies in depositing the layers during the coating process. The NF layers are believed to form by a process of slipcasting the sol onto the porous support. In this process, the thickness of the deposited layer is largely influenced by the capillary suction capability of the support, which is, in turn, affected by the water content of the pores before deposition of the γ-Al_2O_3 or Fe-SiO_2 materials. The amount of water in 100Å pores layer seems

to be largely determined by the relative humidity of the surrounding atmosphere; this is not controlled during the coating process as layers are deposited in an open system. The observed high degree of reproducibility for the thickness of a given layer in replicate membranes may be due to the fact that a given layer of the two membranes was deposited on the same day, thus under equal relative humidity conditions.

2.3.5 Liquid filtration of neutral solutes

A schematic is provided in Figure 2.8 to clarify the liquid phase membrane filtration process. J_V indicates the direction of solution volume flux as water and ions are transported from the feed solution (C_F), through the membrane, and into the permeate solution (C_P). One important physical property useful for defining nanofiltration membranes is the molecular weight cut off (MWCO) for uncharged solutes. Typically, nanofiltration occurs in materials where removal of neutral species with molecular weight 1000 g mol^{-1} is greater than or equal to 90% of the initial concentration.[35] The results for the rejection of polyethylene glycol using single layer Fe-SiO_2 and γ-Al_2O_3 membranes are provided in Figure 2.9. In the case of both materials, the layers coated onto the support are acting as nanofiltration membranes. The 90% MWCOs for the Fe-SiO_2 and γ-Al_2O_3 membranes are 700 and 300 g mol^{-1}, respectively, indicating that membranes composed of these materials fall well within the nanofiltration range. In fact, 100% of neutral species will be rejected at the 1000 g mol^{-1} MWCO. Values for MWCO have been proposed as a technique for approximating pore diameter in NF membranes[36]. However, the accuracy of this method has not yet been described and the calculation is unnecessary for this study as pore diameter was obtained from nitrogen adsorption isotherms.

2.3.6 Membrane durability

The permeation of N_2 gas through the Al_2O_3/Fe-SiO_2 A membrane before and after liquid filtration experiments is displayed in in Figure 2.10. A total of 2600 L m^{-2} of solution was passed through the membrane and there is very little change in nitrogen permeation. From the linear regression equations, there is only a 24% increase in Knudsen diffusion of the gas through the membrane. This result predicts a relatively long lifetime for our ceramic NF membranes. Furthermore, there is likely very little membrane fouling, as any biological or chemical contamination would cause pore blockage and the permeation of gas through the membrane would be decreased.

2.4. Conclusions

The sol-gel method provides a useful technique for preparing ceramic membranes. In this study, both single and bilayer γ-Al_2O_3 and Fe-SiO_2 nanofiltration membranes were fabricated and characterized. Zeta potential titration curves show that the two materials are oppositely charged from pH 3.0 to pH 9.0. The MWCOs for γ-Al_2O_3 and Fe-SiO_2 membranes are 700 and 300 g mol^{-1}, respectively, clearly showing that these membranes fall well within the NF classification range.

Microstructural parameters, relevant for the membrane performance in nanofiltration, including pore size distribution, average pore size, porosity, layer thickness and tortuosity, can be experimentally determined. In comparison, for the case of polymeric membranes, many of these parameters are obtained from nanofiltration models.

Gas permeation experiments indicate that the mechanism for gas flow in these membranes is primarily Knudsen diffusion, which is in agreement with the expected result in nanoporous systems. In general, the physical characteristics of the membranes show good reproducibility for identically prepared membranes. The results of this study show that the thickness of the nanofiltration layers depends more on when the layer is deposited (atmospheric relative humidity conditions) than on the actual substrate (100Å layer or nanofiltration layer). The outcome for the measurement of L_m for identical layers was unexpected, as equivalent amounts and concentrations of the materials were deposited onto the supports, regardless of the order in which they were configured. Therefore, it is clear that a variation in atmospheric conditions, and specifically relative humidity, can affect the degree to which a sol-gel coating is slipcast onto a ceramic support. In order to allow for maximum capillary motion, and therefore perfectly reproducible coatings, the pores must be completely free of water. This can only be accomplished in a controlled relative humidity environment.

We believe that the experimentally measured properties of these ceramic nanofiltration layers reported in this study should provide a valuable tool for interpreting salt removal performance of inorganic NF membranes in general. This would be particularly useful for the modeling community and therefore represents a practical future focus of research in the nanofiltration field.

2.5 References

1. Lin, J. *et al.* Fractionation of direct dyes and salts in aqueous solution using loose nanofiltration membranes. *J. Membr. Sci.* **477,** 183–193 (2015).

2. Varol, C., Uzal, N., Dilek, F. B., Kitis, M. & Yetis, U. Recovery of caustic from mercerizing wastewaters of a denim textile mill. *Desalination Water Treat.* **53,** 3418–3426 (2014).

3. Kyrychuk, I., Zmievskii, Y. & Myronchuk, V. Treatment of dairy effluent model solutions by nanofiltration and reverse osmosis. *Ukr. Food J.* **3,** 281–288 (2014).

4. Zmievskii, Y. G., Kirichuk, I. I. & Mironchuk, V. G. Membrane treatment of wastewater obtained after the whey processing. *J. Water Chem. Technol.* **36,** 309–316 (2014).

5. Malik, A. A., Harleen Kour, Anju Bhat & Nirjeet Kour. Membrane separation technology in food and allied industry. *Int. J. Process. Post Harvest Technol.* **5,** 92–98 (2014).

6. Blöcher, C. *et al.* Recycling of spent process water in the food industry by an integrated process of biological treatment and membrane separation. *Desalination* **144,** 143–150 (2002).

7. Gamal Khedr, M. Nanofiltration of oil field-produced water for reinjection and optimum protection of oil formation. *Desalination Water Treat.* 1–9 (2014).

8. Ebrahimi, M. *et al.* Investigations on the use of different ceramic membranes for efficient oil-field produced water treatment. *Desalination* **250,** 991–996 (2010).

9. Cincinelli, A., Martellini, T., Coppini, E., Fibbi, D. & Katsoyiannis, A. Nanotechnologies for Removal of Pharmaceuticals and Personal Care Products from Water and Wastewater. A Review. *J. Nanosci. Nanotechnol.* **15,** 3333–3347 (2015).

10. Escalona, I. *et al.* Fenton coupled with nanofiltration for elimination of Bisphenol A. *Desalination* **345,** 77–84 (2014).

11. Burggraaf, A. J. & Cot, L. *Fundamentals of inorganic membrane science and technology*. (Elsevier Science, 1996).

12. Sarrade, S., Rios, G. M. & Carlès, M. Dynamic characterization and transport mechanisms of two inorganic membranes for nanofiltration. *J. Membr. Sci.* **97,** 155–166 (1994).

13. Bowen, W. R. & Sharif, A. O. Prediction of optimum membrane design: pore entrance shape and surface potential. *Colloids Surf. Physicochem. Eng. Asp.* **201,** 207–217 (2002).

14. Amjad, Z. *Reverse osmosis: membrane technology, water chemistry & industrial applications*. (Chapman & Hall, 1993).

15. Sanyal, O., Sommerfeld, A. N. & Lee, I. Design of ultrathin nanostructured polyelectrolyte-based membranes with high perchlorate rejection and high permeability. *Sep. Purif. Technol.* **145,** 113–119 (2015).

16. Dirir, Y. I., Hanafi, Y., Ghoufi, A. & Szymczyk, A. Theoretical Investigation of the Ionic Selectivity of Polyelectrolyte Multilayer Membranes in Nanofiltration. *Langmuir* **31,** 451–457 (2015).

17. De Grooth, J., Oborný, R., Potreck, J., Nijmeijer, K. & de Vos, W. M. The role of ionic strength and odd–even effects on the properties of polyelectrolyte multilayer nanofiltration membranes. *J. Membr. Sci.* **475,** 311–319 (2015).

18. Palmeri, J., Blanc, P., Larbot, A. & David, P. Theory of pressure-driven transport of neutral solutes and ions in porous ceramic nanofiltration membranes. *J. Membr. Sci.* **160,** 141–170 (1999).

19. Palmeri, J., Blanc, P., Larbot, A. & David, P. Hafnia ceramic nanofiltration membranes:: Part II. Modeling of pressure-driven transport of neutral solutes and ions. *J. Membr. Sci.* **179,** 243–266 (2000).

20. Tsuru, T., Miyawaki, M., Yoshioka, T. & Asaeda, M. Reverse osmosis of nonaqueous solutions through porous silica zirconia membranes. *AIChE J.* **52,** 522–531 (2006).

21. Tsuru, T., Ogawa, K., Kanezashi, M. & Yoshioka, T. Permeation Characteristics of Electrolytes and Neutral Solutes through Titania Nanofiltration Membranes at High Temperatures. *Langmuir* (2010).

22. Schaep, J., Vandecasteele, C., Mohammad, A. W. & Bowen, W. R. Analysis of the salt retention of nanofiltration membranes using the Donnan–Steric partitioning pore model. *Sep. Sci. Technol.* **34,** 3009–3030 (1999).

23. Schaep, J. & Vandecasteele, C. Evaluating the charge of nanofiltration membranes. *J. Membr. Sci.* **188,** 129–136 (2001).

24. Skluzacek, J. M., Isabel Tejedor, M. & Anderson, M. A. An iron-modified silica nanofiltration membrane: Effect of solution composition on salt rejection. *Microporous Mesoporous Mater.* **94,** 288–294 (2006).

25. Schultz, F. S. & Anderson, M. A. Effects of Surface Adsorption and Confinement on the Photochemical Selectivity of Previtamin D3 Adsorbed within Porous Sol−Gel Derived Alumina. *J. Am. Chem. Soc.* **121,** 4933–4940 (1999).

26. Wouters, J. J., Lado, J. J., Tejedor-Tejedor, M. I. & Anderson, M. A. Low Surface Area Carbon Fiber Electrodes Coated with Nanoporous Thin-Films of γ–Al2O3 and SiO2: Relationship between Coating Conditions, Microstructure and Double Layer Capacitance. *J. Electrochem. Soc.* **159,** A1374–A1382 (2012).

27. Peterson, R. A., Anderson, M. A. & Hill Jr., C. G. Development of TiO2 membranes for gas phase nanofiltration. *J. Membr. Sci.* **94,** 103–109 (1994).

28. Kielland, J. Individual activity coefficients of ions in aqueous solutions. *J. Am. Chem. Soc.* **59,** 1675–1678 (1937).

29. Nightingale Jr, E. R. Phenomenological theory of ion solvation. Effective radii of hydrated ions. *J. Phys. Chem.* **63,** 1381–1387 (1959).

30. Marcus, Y. Ionic radii in aqueous solutions. *Chem. Rev.* **88,** 1475–1498 (1988).

31. Marcus, Y. Thermodynamics of solvation of ions. Part 5.-Gibbs free energy of hydration at 298.15 K. *J. Chem. Soc. Faraday Trans.* **87,** 2995–2999 (1991).

32. Volkov, A. G., Paula, S. & Deamer, D. W. Two mechanisms of permeation of small neutral molecules and hydrated ions across phospholipid bilayers* 1. *Bioelectrochem. Bioenerg.* **42,** 153–160 (1997).

33. Skluzacek, J. M., Tejedor, M. I. & Anderson, M. A. NaCl rejection by an inorganic nanofiltration membrane in relation to its central pore potential. *J. Membr. Sci.* **289,** 32–39 (2007).

34. Oatley, D. L. *et al.* Review of the dielectric properties of nanofiltration membranes and verification of the single oriented layer approximation. *Adv. Colloid Interface Sci.* **173,** 1–11 (2012).

35. Cleveland, C., Seacord, T. & Zander, A. Standardized Membrane Pore Size Characterization by Polyethylene Glycol Rejection. *J. Environ. Eng.* **128,** 399–407 (2002).

36. Puhlfür, P., Voigt, A., Weber, R. & Morbé, M. Microporous TiO2 membranes with a cut off <500 Da. *J. Membr. Sci.* **174,** 123–133 (2000).

Membrane ID	**Composition of "A"**	**Composition of "B"**
Fe-SiO_2	4 layers Fe-doped SiO_2	*N/A*
γ-Al_2O_3	4 layers γ-Al_2O_3	*N/A*
Al_2O_3/Fe-SiO_2	3 layers γ-Al_2O_3	3 layers Fe-doped SiO_2
Fe-SiO_2/Al_2O_3	3 layers Fe-doped SiO_2	3 layers γ-Al_2O_3

Table 2.1: Four types of nanofiltration membranes used in this study. Bilayer membranes are described with layer "A" facing feed solution in liquid filtration experiments and layer "B" facing permeate solution.

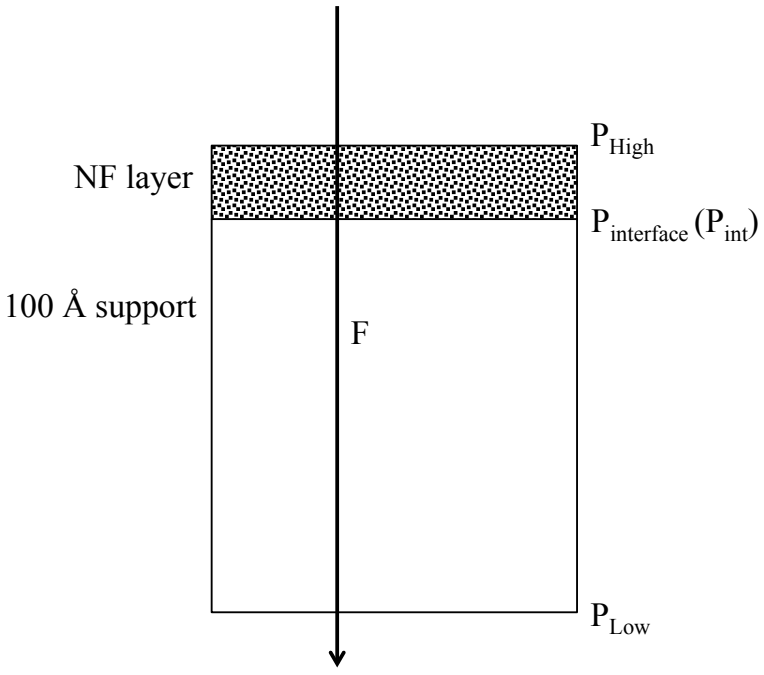

Figure 2.1a: Schematic for gas permeation through single layer membranes.

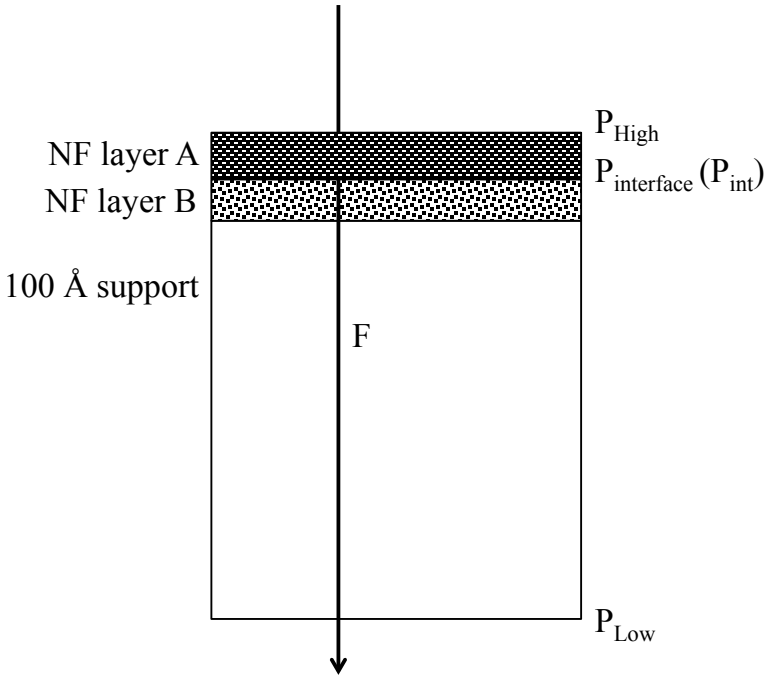

Figure 2.1b: Schematic for gas permeation through bi-layer membranes.

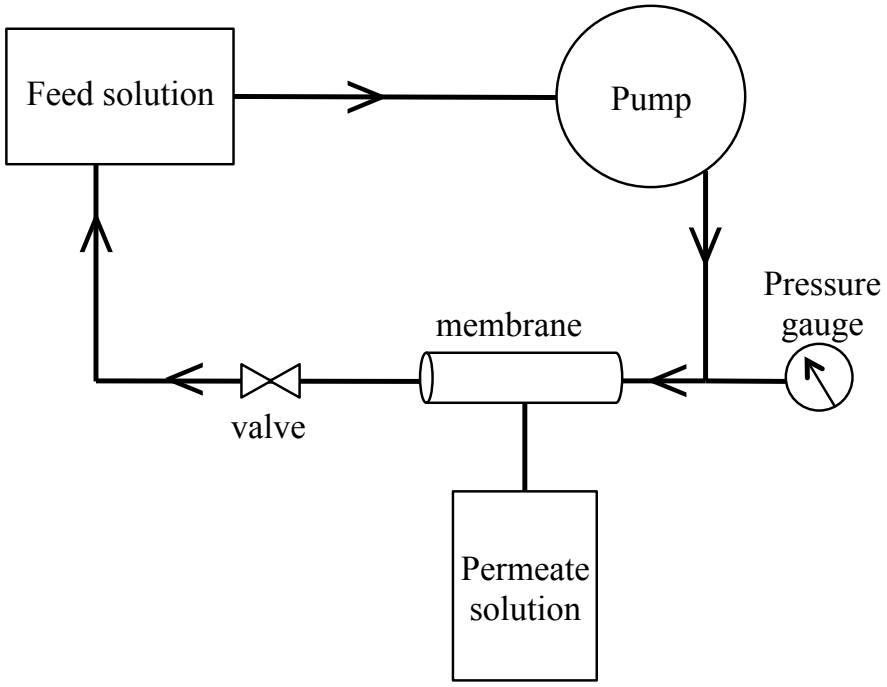

Figure 2.2: Schematic of liquid filtration experimental apparatus

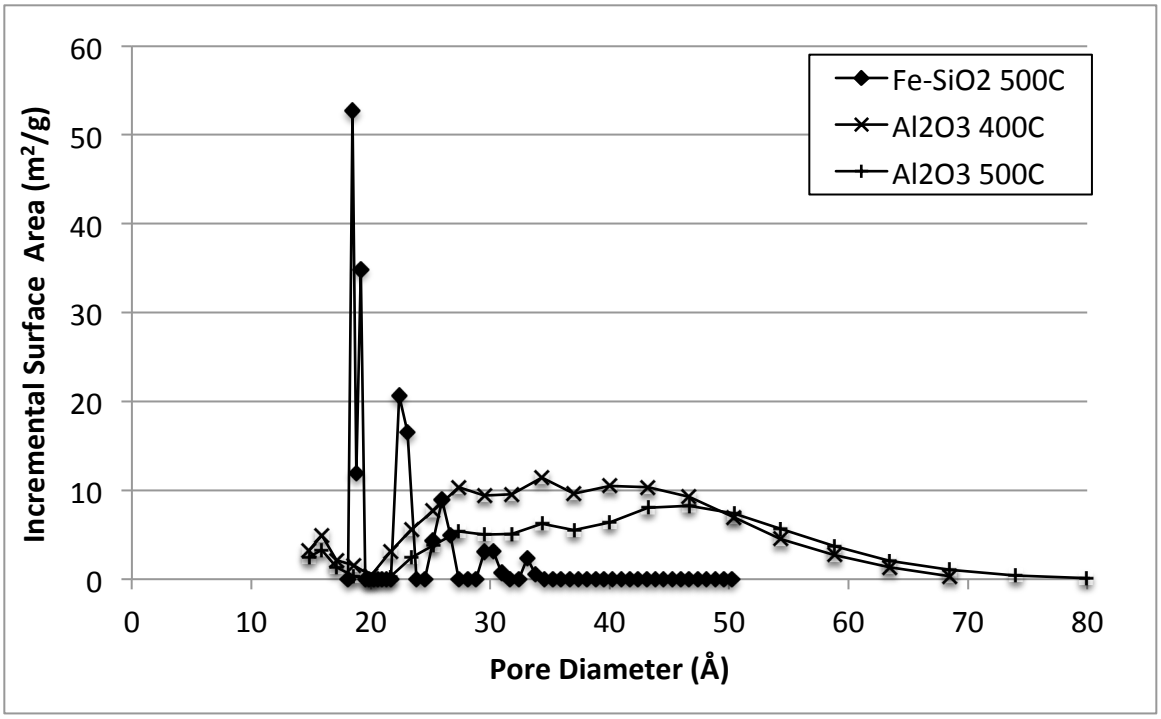

Figure 2.3: Incremental surface area as a function of pore diameter for xerogels of Fe-SiO_2 (500°C) and γ-Al_2O_3 (400°C and 500°C).

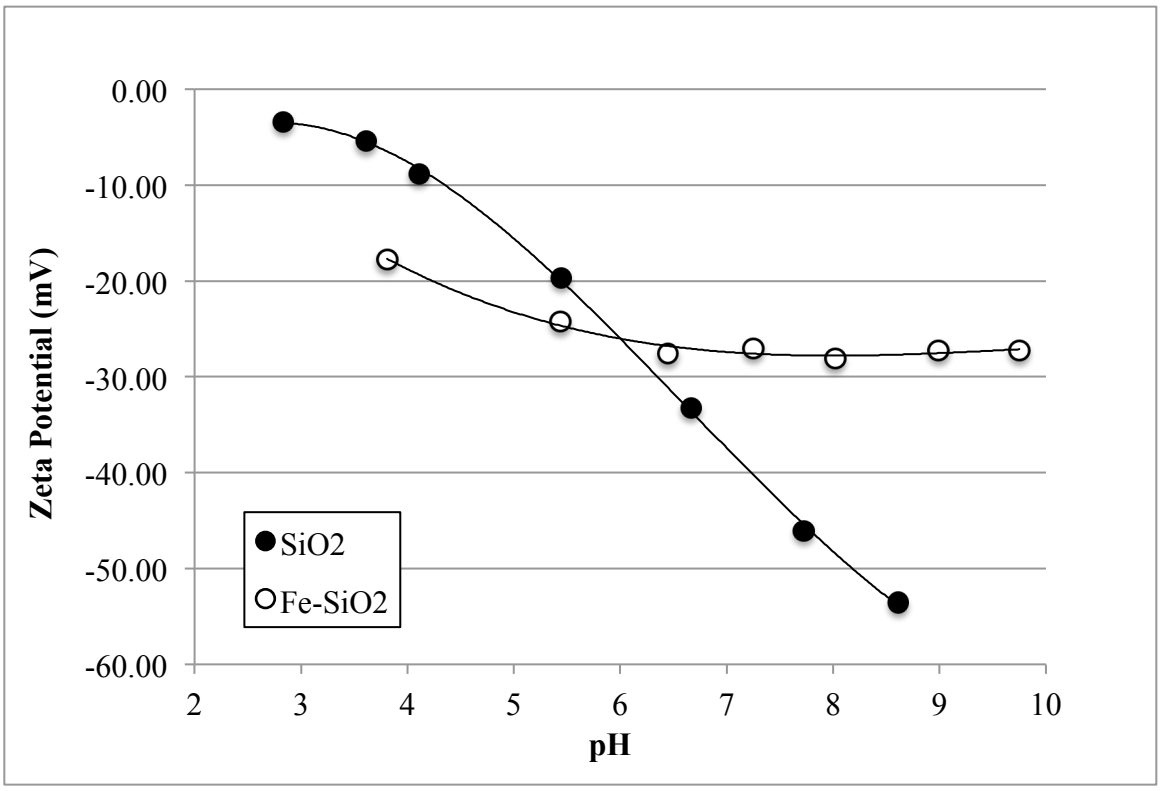

Figure 2.4a: Zeta Potential titration curves for xerogels of SiO_2 and Fe-doped SiO_2 measured in 0.01M NaCl solution.

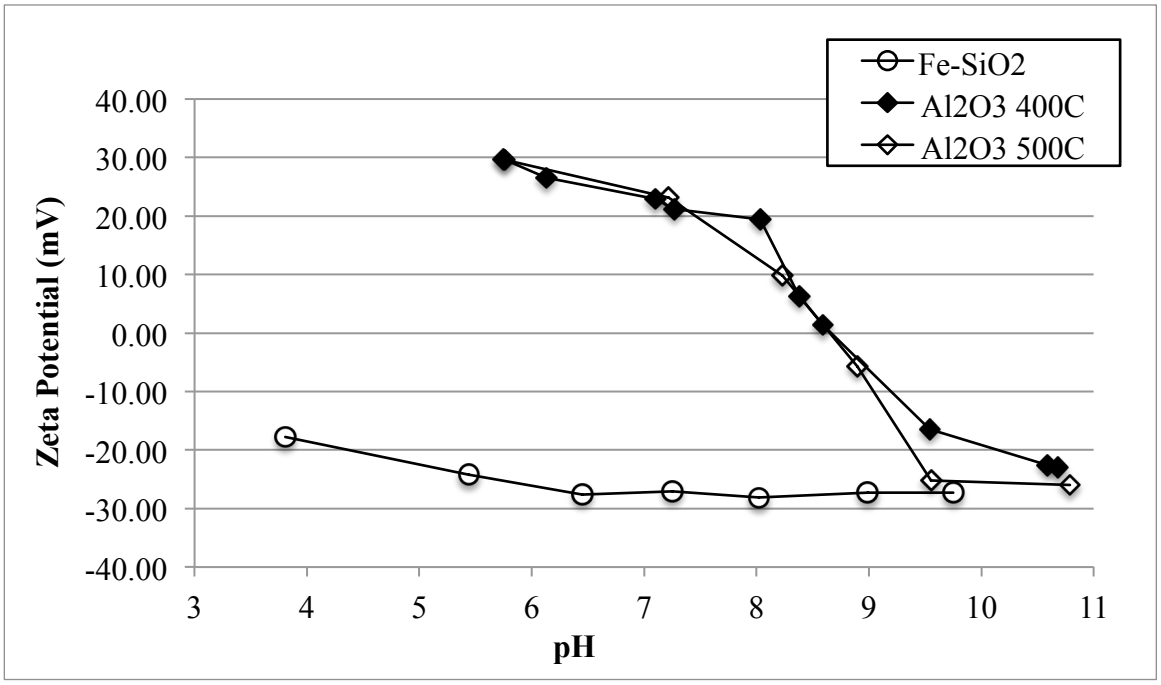

Figure 2.4b: Zeta Potential titration curves for xerogels of Fe-SiO_2 (500°C) and γ-Al_2O_3 (400°C and 500°C) measured in 0.01M NaCl solution.

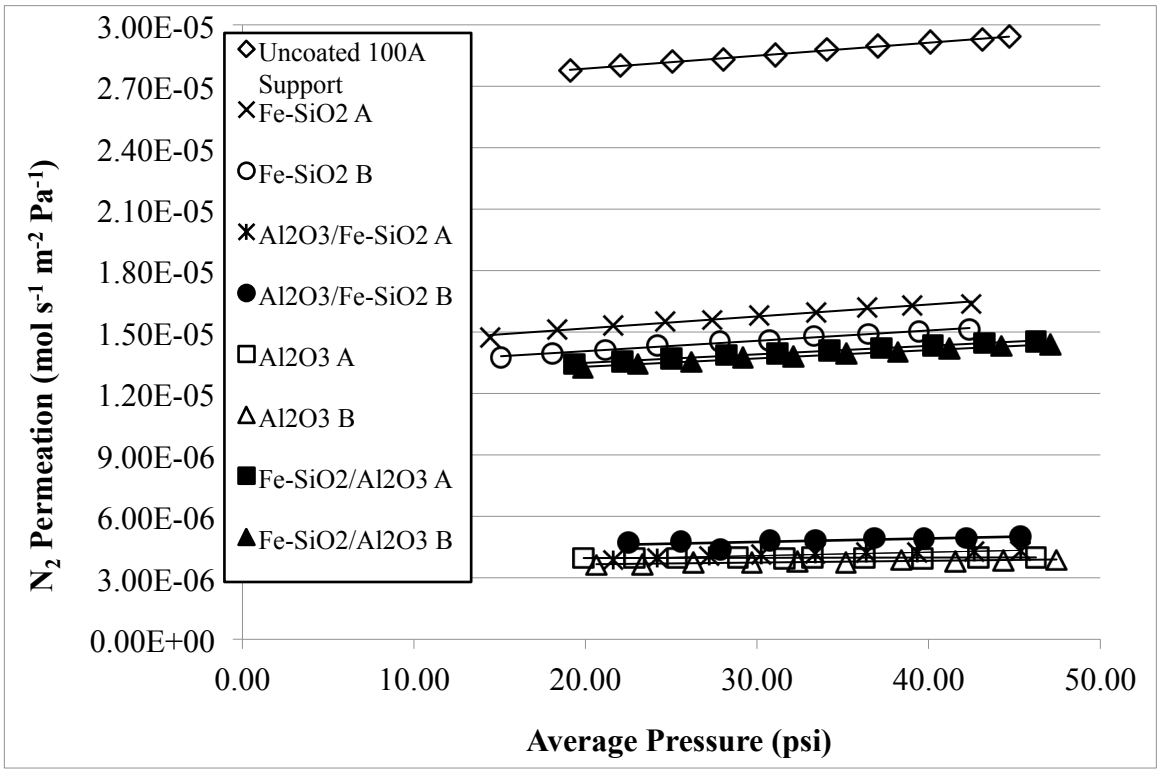

Figure 2.5: Permeation of nitrogen gas through 100Å support and membranes with deposited nanofiltration layers as a function of transmembrane pressure. Values for slope and y-intercept of regression lines are provided in Table 2.2.

Membrane	a_{total}	b_{total}
100 Å support	2.66×10^{-5}	6.33×10^{-8}
Fe-SiO_2 A	1.40×10^{-5}	5.84×10^{-8}
Fe-SiO_2 B	1.31×10^{-5}	5.04×10^{-8}
Al_2O_3 A	3.94×10^{-6}	1.20×10^{-9}
Al_2O_3 B	3.94×10^{-6}	8.58×10^{-9}
Al_2O_3/Fe-SiO_2 A	3.58×10^{-6}	1.69×10^{-8}
Al_2O_3/Fe-SiO_2 B	4.24×10^{-6}	1.71×10^{-8}
Fe-SiO_2/Al_2O_3 A	1.27×10^{-5}	4.14×10^{-8}
Fe-SiO_2/Al_2O_3 B	1.25×10^{-5}	4.05×10^{-8}

Table 2.2: Slope (b_{total}) and y-intercept (a_{total}) values obtained from linear regression of N_2 permeation data through nanofiltration membranes.

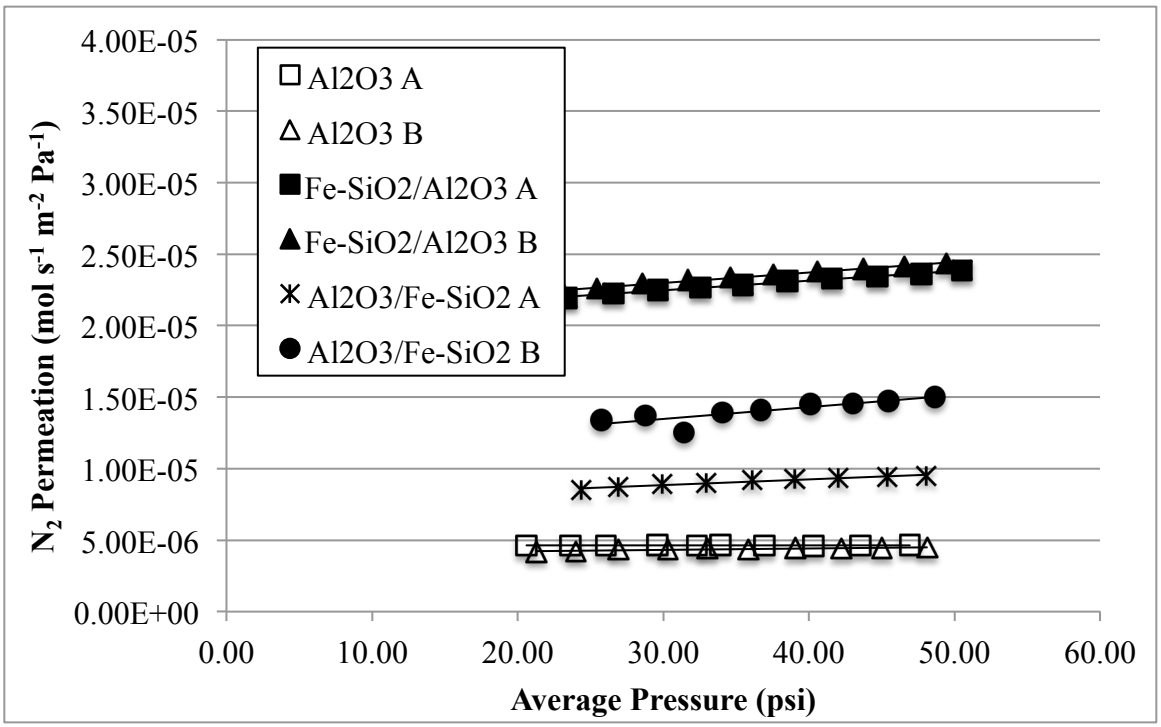

Figure 2.6a: Calculated permeation of N_2 gas through γ-Al_2O_3 nanofiltration layers. Values for slope and y-intercept of regression lines are provided in Table 2.3a.

Membrane	a_{layer}	b_{layer}	L_m *(μm)*	d_p *(nm)*	ε *(%)*	τ
Al_2O_3 A	4.63 x 10^{-6}	-6.37 x 10^{-11}	2.1*	3.9	51	2.7
Al_2O_3 B	4.02 x 10^{-6}	9.93 x 10^{-9}	2.4	3.9	51	2.7
Al_2O_3/Fe-SiO_2 A	7.65 x 10^{-6}	4.00 x 10^{-8}	1.3	3.9	51	2.7
Al_2O_3/Fe-SiO_2 B	1.10 x 10^{-5}	8.26 x 10^{-8}	0.9	3.9	51	2.7
Fe-SiO_2/Al_2O_3 A	2.05 x 10^{-5}	6.73 x 10^{-8}	0.5	4.3	42	2.7
Fe-SiO_2/Al_2O_3 B	2.08 x 10^{-5}	7.30 x 10^{-8}	0.5	4.3	42	2.7

**Indicates value calculated from SEM micrograph; all other L_m values were calculated assuming equal tortuosity.*

Table 2.3a: Summary of membrane parameter values for the γ-Al_2O_3 nanofiltration layer in different membranes. Slope (b_{layer}) and y-intercept (a_{layer}) values obtained from linear regression of calculated N_2 permeation through γ-alumina layers.

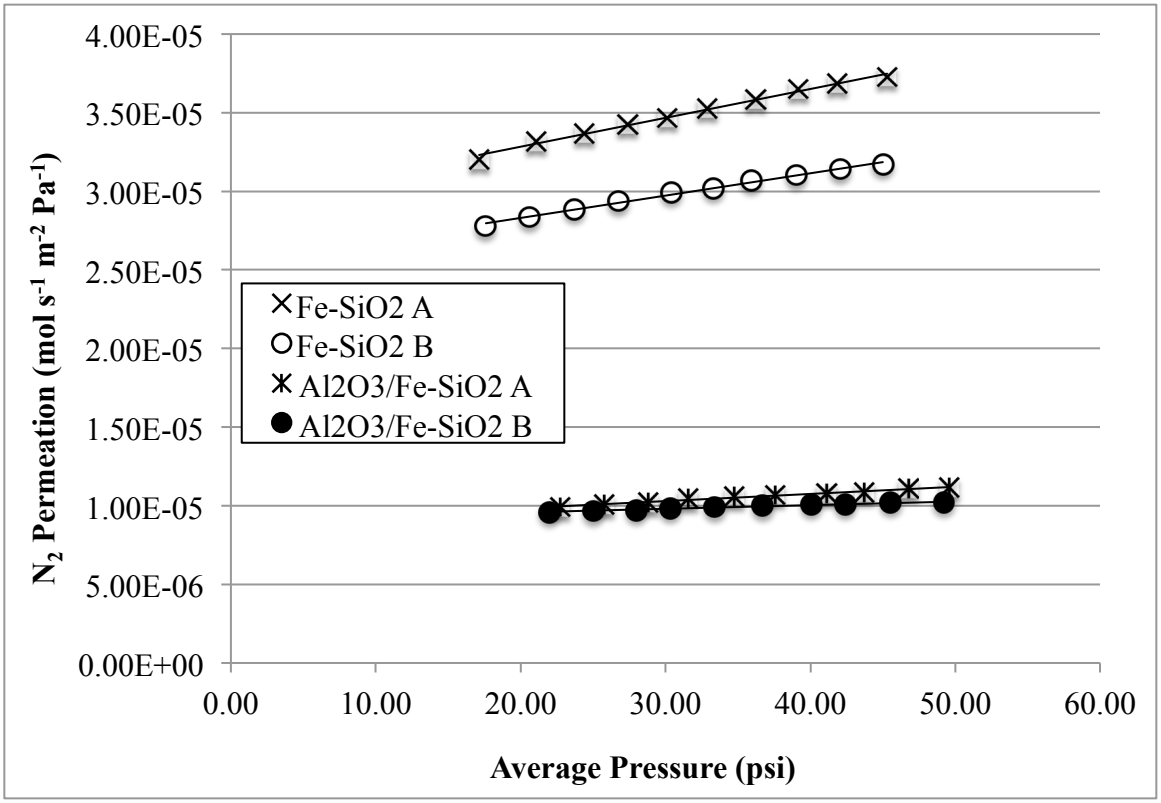

Figure 6b: Calculated permeation of nitrogen gas through Fe-SiO_2 nanofiltration layers. Values for slope and y-intercept of regression lines are provided in Table 2.3b.

Membrane	a_{layer}	b_{layer}	L_m *(μm)*	d_p *(nm)*	ε *(%)*	τ
Fe-SiO_2 A	2.92 x 10^{-5}	1.84 x 10^{-7}	0.4	2.1	31	3.4
Fe-SiO_2 B	2.55 x 10^{-5}	1.42 x 10^{-7}	0.5*	2.1	31	3.4
Al_2O_3/Fe-SiO_2 A	8.93 x 10^{-6}	4.56 x 10^{-8}	1.4	2.1	31	3.4
Al_2O_3/Fe-SiO_2 B	9.11 x 10^{-6}	2.31 x 10^{-8}	1.4	2.1	31	3.4
Fe-SiO_2/Al_2O_3 A	*no data*	*no data*	0.4*	2.1	31	3.4
Fe-SiO_2/Al_2O_3 B	*no data*	*no data*	*no data*	2.1	31	3.4

**Indicates values calculated from SEM micrographs; all other L_m values calculated assuming equal tortuosity*

Table 2.3b: Summary of membrane parameter values for the Fe-SiO_2 nanofiltration layer in different membranes. Slope (b_{layer}) and y-intercept (a_{layer}) values obtained from linear regression of calculated N_2 permeation through iron-doped silica layers.

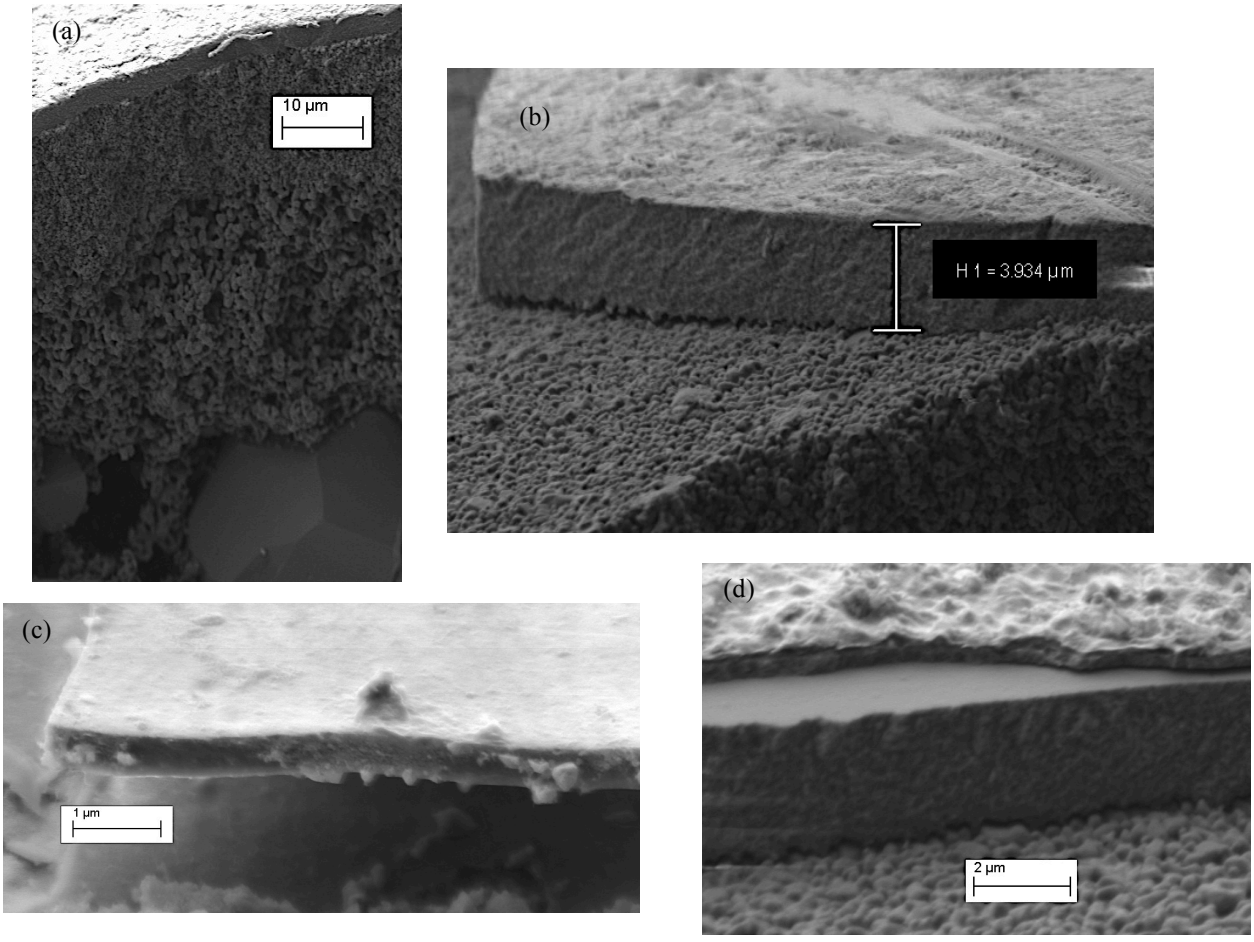

Figure 2.7: Scanning electron micrographs of single layer γ-Al_2O_3 (a,b) and Fe-SiO_2 (c) and bilayer Fe-SiO_2/γ-Al_2O_3 (d) membranes.

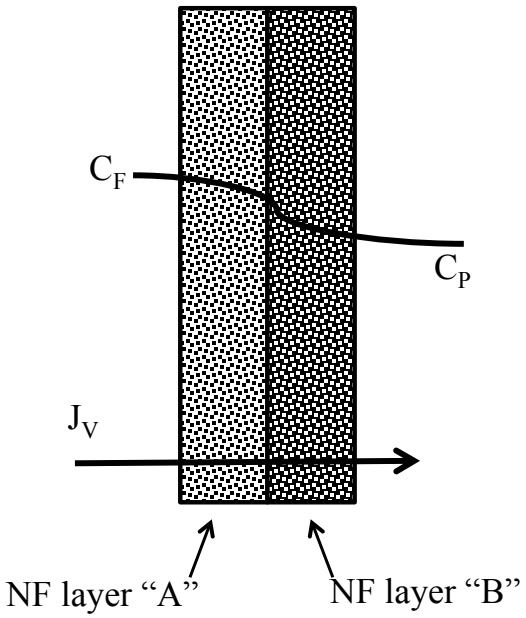

Figure 2.8: Schematic of transport through NF membrane in liquid filtration experiments

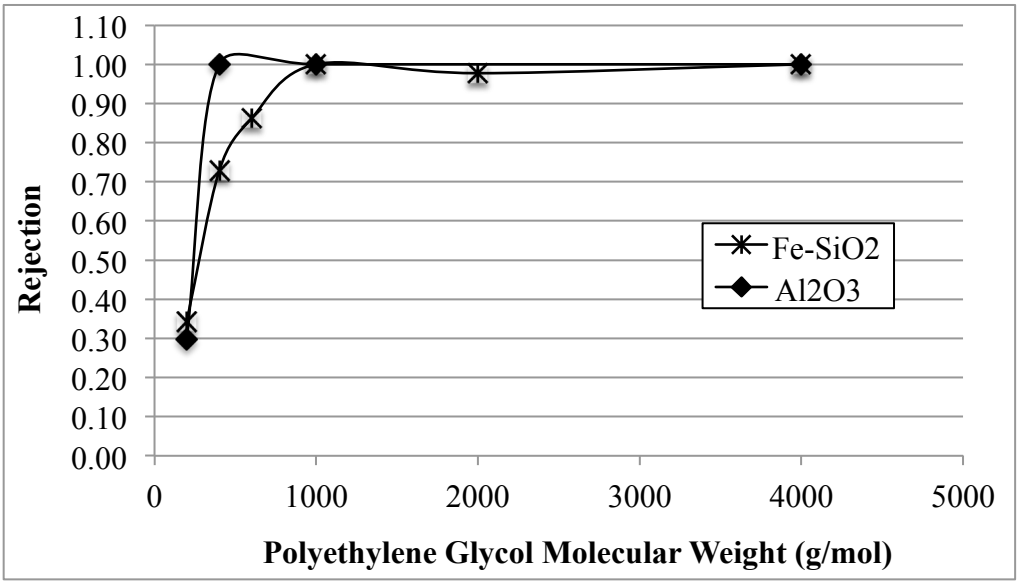

Figure 2.9: Rejection of polyethylene glycol as a function of molecular weight for single layer membranes.

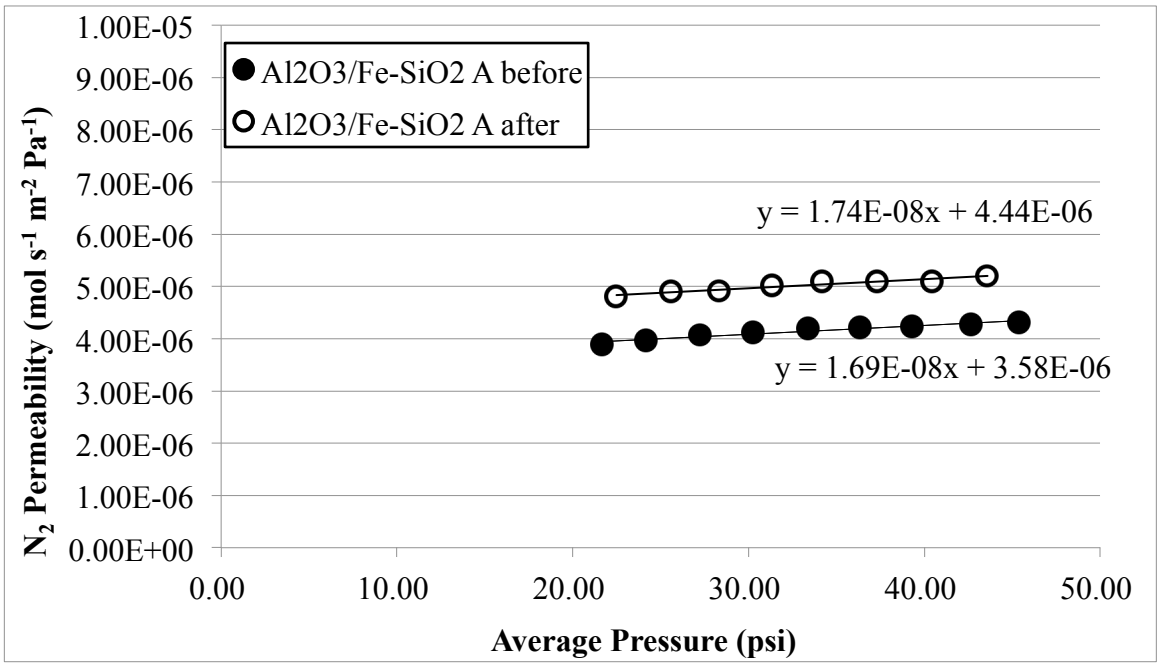

Figure 2.10: Permeation of nitrogen gas through Al_2O_3 A membrane as a function of transmembrane pressure before liquid filtration experiments and after permeation of 2600 L m^{-2} of solution through membrane.

3. Effect of pH on Salt Rejection Performance of Single and Bilayer γ-Al_2O_3 and Fe-SiO_2 Nanofiltration Membranes

3.1. Introduction

In the past 20 years, much of the work in the field of nanofiltration (NF) has focused on understanding and modeling the complex interactions between charged membranes and solutes in order to predict and quantify the removal of charged species from solution. Several modeling efforts have been dedicated to investigating which membrane and solution parameters are most critical in determining salt rejection. There is general agreement in the literature that positively or negatively charged NF membranes separate charged species from aqueous solution predominantly by electrostatic mechanisms. These NF membranes are typically composed of either organic (polymeric) or inorganic (ceramic) materials. In either case, an NF membrane performs best in solution conditions where membrane potential is high.

Ceramic NF membranes, which are the focus of this study, are composed of nanoporous layers of amphoteric metal oxides. These materials are most highly charged at pH values far from the isoelectric pH (pH_{iep}). Under these conditions, the surface charge leads to an electrostatic double layer of ions near the pore wall surface, which results in a decaying electrochemical potential across the pore diameter.[1–3] This potential prevents ions of the same charge (co-ions) from passing through the porous membrane. Ions of opposite charge (counter-ions) are rejected as well in order to maintain electroneutrality in solution. The amount of overlap of electrostatic double layers (EDL) from opposing pore walls is controlled primarily by the ionic strength (I) of the solution for a given pH.[4] Due to the electrochemical potential in pores, Donnan potential differences develop at the membrane/solution interface. This potential acts to hinder the diffusion of ions having the same sign as that of the Donnan potential. Due to electroneutrality requirements, ions of opposite charge to the Donnan potential are also rejected, leading to salt

retention and separation[5,6]. Thus, fabrication of ceramic nanofilters can be tailored to specific applications based on pH and ionic strength of the feed solution. Almost all ceramic NF membranes are composed of a single filtration layer that is either positively or negatively charged for a given solution composition; the sign of membrane charge determines whether the cation or the anion behaves as the co-ion. Ions with higher valence states are more readily rejected than monovalent ions due to increased charge density. Therefore, currently available ceramic NF membranes are best suited for applications where removal of divalent ions is important and pH of feed solution is far from the pH_{iep} of the nanofiltration layer.

In polymeric NF membranes, much of the current research is devoted to the characterization and evaluation of polyelectrolyte multilayer (PEM) membranes, which are composed of oppositely charged layers of polymers prepared by immersion in positively and negatively charged polyelectrolyte solutions[7–9]. The motivation for preparing PEM membranes is to fabricate a NF membrane that is both bilayer and bipolar. Bilayer NF membranes consist of 2 or more nanofiltration layers composed of different materials. Depending on solution composition, bilayer membranes may also behave as bipolar membranes; meaning that for a given solution pH, ionic strength, and salt species, the two NF layers will develop opposite charges when in contact with the solution. Thus, rejection performance of NF membranes should increase as both the cation and anion may act as co-ions. Recently, several modeling efforts have been devoted to understanding the transport of charged solutes in bipolar PEM memranes[10,11].

In the field of ceramic NF membranes, there have been very few studies devoted to developing an inorganic counterpart to the bipolar membrane. In 2006, de Lint et al.[12] published a paper that

models transport through bilayer microporous silica/mesoporous γ-alumina membranes. In addition, their study compared the calculated values for the rejection of NaCl with experimentally determined values. The model provides a good fit to the data at some pH values; however in very acidic or basic conditions the correlation is less strong. Additionally, the authors themselves express some doubts about the microstructure of the silica layer, as it has extremely small pores (0.8 nm) and very low porosity (around 15%). Therefore, they were unable to explain the lack of agreement between predicted and experimental rejection data. It is clear that there is still much work to be done in fabricating, characterizing and evaluating bilayer, bipolar ceramic NF membranes.

3.2. Theory

Our objective in this work is to examine the differences in performance between membranes with a single nanofiltration layer (Fe-SiO_2 or γ-Al_2O_3) and membranes with two nanofiltration layers (Fe-SiO_2 and γ-Al_2O_3). These membranes will be evaluated for rejecting single salt solutions consisting of 1:1, 1:2, or 2:1 strong electrolytes. Furthermore, the scope of the study will include evaluating the performance of these membranes under different surface charge conditions. For this purpose, rejection of the different electrolytes will be measured in feed solutions with pH ranging from 5.0 to 9.0.

3.2.1 Modeling rejection performance of single layer nanofiltration membranes

Our interest in evaluating membrane performance at different pH values is related to the general consensus, from the predictions of several nanofiltration models, that the charge of the pore walls in the membrane is a major factor in determining ion partitioning at the solution/membrane

interface (Donnan exclusion). Size exclusion (steric effects) for these systems can be neglected. As a consequence of Donnan exclusion, a potential develops at the feed/membrane and at the permeate/membrane interfaces, known as Donnan potential. The transport of ions across the membrane is described by the extended Nernst-Planck equation as controlled by convection (pressure gradient), diffusion (concentration gradient) and electromigration (electric potential gradient, mainly due to the difference in the Donna potential at the two interfaces). Which of these mechanisms predominates in the transport of ions depends on properties of the membrane, such as pore radius (r_p), thickness to porosity ratio (L_m/ε) and the normalized effective membrane charge density (X). Moreover, it depends on solution conditions such as the nature of the electrolyte (the relative value of the diffusion coefficients of the anion and cation), and operational parameters such as the applied cross-membrane pressure (ΔP). This pressure determines the permeate volume flux (J_v) for a given membrane and solution composition. The rejection of a membrane for a given salt solution as a function of J_v has a logarithmic relationship; at low values of J_v rejection increases almost linearly until reaches a plateau[13]. This maximum possible value for rejection is known as the reflection coefficient of the membrane (σ_s). For a given 1:1 electrolyte, σ_s can be expressed as:

$$\sigma_s = 1 - \frac{2}{\left[2\left(\frac{D_1}{D_1 + D_2}\right) - 1\right]\xi + (\xi^2 + 4)^{\frac{1}{2}}} \qquad \text{Equation 3.1}$$

where D_1 is the diffusion coefficient of the counter-ion, D_2 is the diffusion coefficient of the co-ion, and $\xi = X/C$ [normalized charge density, given as the ratio of fixed charge density (X) to solution concentration (C)]. This equation shows that the maximum potential for rejection of a

salt (σ_s) increases with increasing normalized charge density of the membrane (ξ). The fixed charge density (X) of the membrane is related to the surface charge density (q_w) by the following equation:

$$X = \frac{2q_w}{Fr_p} \qquad \text{Equation 3.2}$$

with q_w having units C m^2, F is the Faraday constant and r_p is the pore radius in meters. There are several ways to determine the value of q_w; however, a convenient and well-accepted method is by measuring the zeta potential (ψ_ζ) of the powdered nanomembrane material. For obvious reasons, this methodology is only applicable to ceramic nanofiltration membranes. The Grahame equation relates the surface charge density (q_w) with the surface potential through a sinh function; this function can be simplified when the surface potential is < 50mV. Combining this approximation with the fact that ψ_ζ can be used as a surrogate for ψ_0 (surface potential), leads to the following expression for surface charge density:

$$q_w = \frac{\varepsilon\psi_\xi}{\kappa^{-1}} \qquad \text{Equation 3.3}$$

Where ε is the dielectric constant of water and κ^{-1} is the Debye length, given by:

$$\kappa = \left(\frac{2F^2 I \times 10^3}{\varepsilon\varepsilon_0 RT}\right)^{1/2} \qquad \text{Equation 3.4}$$

and is dependent only on ionic strength (I) of the solution; F, ε, ε_0 and R are constants having their usual meaning. For all experimental data collected, T = 20°C and I = 0.01. Thus, through this set of equations, the relationship between rejection and zeta potential is apparent: for a given membrane and electrolyte concentration, a larger zeta potential (ψ_ζ) value is indicative of a larger surface charge density (q_w) and, therefore, a larger effective membrane charge (X). Equation 3.1 shows that the maximum rejection value for a given membrane and electrolyte increases with increasing X.

It is not the aim of this research to model the rejection of electrolytes for varying membranes and solution compositions. Rather, our objective is to determine, in a semi-quantitative manner, the relationship between ψ_ζ and rejection for the different systems evaluated with both single and bilayer Fe-SiO_2 and γ-Al_2O_3 NF membranes. Skluzacek et al.[4] showed that rejection (%R) is related to potential at the center of the pore ($\psi_{dp/2}$) and therefore to ψ_ζ, I and r_p by:

$$\%R = A + B\ ln(2) + B\ ln\left(\psi_\zeta\right) + B(-\kappa)r_p \qquad \text{Equation 3.5}$$

This equation has one dependent variable (%R), two independent variables (κ and ψ_ξ) and two parameters (A and B). Thus, by measuring the rejection of the system for an electrolyte under two different conditions, one should be able to predict the rejection for other solution conditions in the case of membranes with a single nanofiltration layer.

3.2.2 Predicted behavior of bilayer nanofiltration membranes

It is important to note that calculation of the above parameters is relevant for single layer NF membranes. In bilayer and/or bipolar membranes, the effects of the two oppositely charged NF layers are much more complex. The most thorough theoretical analysis of the subject was accomplished by Tsuru et al. in their modeling of ion separation by bipolar membranes.[10] One of the most interesting findings of their study was that rejection of a given electrolyte is affected by which nanofiltration layer faces the feed solution. To this end, we have prepared bilayer membranes in two different configurations, with either the Fe-SiO_2 or γ-Al_2O_3 facing the feed solution. Our goal in this study is to determine how the combination of layers contributes to membrane potential and, therefore, rejection of ions. In this work, we will examine rejection of ions in four salt solutions NaCl, $NaNO_3$, Na_2SO_4 and $MgCl_2$ at pH values from 5.0 to 9.0. In all our experiments, ionic strength is kept constant in order to relate the nature of the ion (valency, diffusion, etc.) to membrane rejection independent of concentration effects. We perform the experiments with both single and bi-layer Fe-SiO_2 and γ-Al_2O_3 nanofiltration membranes to evaluate each layer independently and when combined in our bilayer system. We hope that our experimental data will be a welcome contribution to the body of research on bilayer NF membranes, since so much of the work thus far has been dedicated to models that are not yet corroborated experimentally.

3.3. Experimental Methods

3.3.1 Composition of γ-Al_2O_3 and Fe-SiO_2 nanofiltration membranes

The composition of each membranes type used in this study is described in Table 3.1. For membranes consisting of multiple nanofiltration layers, the material listed first is facing the feed solution (NF layer "A") during liquid filtration experiments. The fabrication, layer composition

and gas permeability properties of these multiple-layer nanofiltration membranes were described in the previous chapter of this thesis.

3.3.2 Charging properties of γ-Al_2O_3 and Fe-SiO_2 nanofiltration membranes

Charging properties of the pore walls in nanofiltration layers were evaluated by measuring the zeta potential of powdered materials identical to the ones that constitute the nanofiltration membranes. The zeta potential measurements were performed using an electrophoretic mobility device, Malvern (3000 HS) ZetaSizer. Gels of membrane materials were generated by drying sols of Fe-silica and alumina to create xerogels, which were then heated at 400 or 500°C to create Fe-SiO_2 and γ-Al_2O_3. Each of these materials was ground to a fine powder and suspended in salt solutions of interest to perform the zeta potential measurements. Zeta potential measurements were conducted in a variety of salt solutions with ionic strength, I=0.01, including: NaCl, $NaNO_3$, Na_2SO_4 and $MgCl_2$. Solutions were prepared from Fisher Scientific (Certified ACS) chemicals. Samples were titrated to different pH values using either acidic or basic solutions (Fisher Certified ACS chemicals) containing cations or anions common to the salt solution. All samples were allowed to equilibrate for 2 h and pH was re-adjusted if necessary. Zeta potential measurements, in combination with previously determined pore diameters for the Fe-SiO_2 and γ-Al_2O_3 membrane materials, were utilized in the calculation of electric potential across the pore. Specifically, the absolute value of the potential at the center of the pore is useful for relating the Donnan contribution to membrane potential to rejection of charged solutes.

3.3.3 Liquid filtration studies

3.3.3.1 The liquid filtration apparatus

A schematic of the apparatus used to test the filtration properties of the membrane is provided in Figure 3.1. The system utilized SS 316 tubing, a LEWA positive displacement pump, and the pressure was adjusted using manual valves and monitored by a pressure gauge just downstream of the membrane compartment. The feed solution was continuously circulated throughout the system while the permeate solution was collected in a glass vessel. Both solutions were at room temperature and atmospheric pressure. The operating pressure for the filtration system was 250 psi, and samples were simultaneously collected from both the feed and permeate solutions after 30 and 45 min of circulation. Between each experiment, ultra-high purity water was flushed through the filtration line and the membrane for 30 min to prevent contamination and to ensure complete removal of any solute remaining in the pores, respectively.

3.3.3.2 Rejection of charged solutes

Salt rejection studies for each of the membranes were performed with the same four salt solutions (NaCl, $NaNO_3$, Na_2SO_4, $MgCl_2$). Feed solutions, I=0.01, of each salt were prepared using chemicals from Fisher Scientific (Certified ACS) and ultra-pure (Milli-Q) water. The salt solutions were then titrated to the desired pH using hydrochloric, sulfuric or nitric acid and sodium or magnesium hydroxide solutions (Fisher Scientific Certified ACS) for consistent electrolyte species. For each salt solution studied, solutions were prepared at nine different pH values: pH 5.0, 5.5, 6.0, 6.5, 7.0, 7.5, 8.0, 8.5, 9.0. This prepared solution is termed the feed solution, and the pH of both the feed and permeate (solution after passing through membrane) solutions was measured using a Mettler Toledo SevenMulti pH meter at the time the sample was taken. For all data, selectivity values are presented as rejection (R) of the solute, as determined by the following equation:

$$R = 1 - \frac{C_P}{C_F}$$ Equation 3.6

where C_P is the solute concentration in the permeate and C_F is the solute concentration in the feed stream. Feed and permeate samples were analyzed for cation concentration (Na or Mg) using inductively coupled plasma-optical emission spectroscopy (ICP-OES, Perkins Elmer) and for anion concentration (chloride, nitrate, or sulfate) using ion chromatography (IC, Dionex ICS 2100).

3.4. Results and Discussion

3.4.1 Zeta potential

The zeta potential titration curves for the γ-Al_2O_3 membrane material in a number of salt solutions with I=0.01 are presented in Figures 3.2a and 3.2b. The data for solutions of $NaNO_3$ and NaCl salts, in which constitute ions are regarded as indifferent electrolytes, clearly show the pH_{iep} of this material to be close to 9.0 (Figure 3.2a). In solutions of $MgCl_2$ the isoelectric point is slightly shifted to higher pH values (9.5), meaning Mg ions are specifically adsorbed on the surface of γ-Al_2O_3. As seen in Figure 3.2b, the magnitude of this shift is dependent on the concentration of magnesium ions in solution. In all salt solutions studied, with the exception of Na_2SO_4, the γ-Al2O3 has the largest zeta potential at pH ≤ 7.5, where the material is positively charged. In the presence of Na_2SO_4, the zeta potential of γ-Al_2O_3 is very small below pH 9 (Figure 3.2b). The depression of the positive branch of the electrokinetic curve of γ-Al_2O_3 in the presence of sulfate ions concurrent with a rather insignificant shift of the pH_{iep} has been reported several times in literature. The overlapping of these almost antagonist effects has been the cause of discussion on the nature of the interaction between sulfate ions and the γ-Al_2O_3 surface[14]. At

present, based on vibrational spectroscopy, most authors believe that sulfate ions form outer-sphere complexes with the surface of the Alumina (electrostatic interaction) rather than inner-sphere complexes (specific adsorption)[15]. However, these authors claim that a small fraction of the sulfates may be coordinated to the surface of alumina. In the case of our material, when the sulfate concentration is increased to 0.01M the amount of sulfate coverage is large enough to cause a large shift (from pH 8.5 to pH 6.2) of the isoelectric point (Figure 3.2b). As noted above, the γ-Al_2O_3 nanofiltration layer should be most active at pH $\leq$ 7.5. Since the material is positively charged at these pH values, rejection occurs through Na^+ or Mg^{2+} as co-ion, regardless of the type of counter-ion with which the cation is paired.

Figure 3a shows zeta potential measurements for the Fe-SiO_2 membrane material in I=0.01 indifferent salt solutions. For this material, the pH_{iep} in NaCl and $NaNO_3$ solutions is at a pH value below the range in which measurements were taken. Previous studies have shown the pH_{iep} of this material to be around pH 2.0. As pH increases, so does the magnitude of the zeta potential of the negatively charged Fe-SiO_2 in NaCl, $NaNO_3$ and Na_2SO_4 (Figures 3.3a and 3.3b). In the case of sulfate ions, this effect is magnified due to the divalent nature of the anion. The presence of divalent magnesium cations causes a depression of the electrokinetic curve of Fe-SiO_2. However, as we do not have an exact value of the pH_{iep} in solutions of monovalent ions versus solutions with Mg^{2+}, the type of interactions of these ions with the surface of the Fe-SiO_2 can be electrostatic or specific, depending on pH and ion concentration. This is shown in the decreased zeta potential of this material in the presence of $MgCl_2$ solution, as well as the almost constant zeta potential across the entire pH range. The effects of sulfate and magnesium concentration on the zeta potential of Fe-SiO_2 are shown in Figure 3.3b. When the concentration of magnesium

ions in solution is increased, there is clearly a charge reversal of the Fe-SiO_2 material at high pH values. Because the Fe-SiO_2 material is negatively charged across the entire pH range studied, rejection with this material occurs through the anion (chloride, nitrate, or sulfate) as a co-ion. In the range of pH 5-10, the zeta potential of Fe-SiO_2 is highly negative in all three sodium salt solutions, so transport of co-ions should be retarded at these pH values.

3.4.2 Rejection of NaCl in replicate membranes

Rejection of 0.01M NaCl solutions (pH 8 ± 0.5) for duplicate membranes of all four types fabricated is reported in Figure 3.4. The data demonstrate that identically prepared membranes show very close salt rejection values. In all future experiments, for efficiency purposes, salt rejection will be measured using one of the two replicate membranes. Furthermore, we can examine the behavior of the four membrane types in NaCl solution so as to compare the single layer and bi-layer nanofiltration membranes. Our Fe-SiO_2 membranes reject approximately 55% of NaCl in solution at this concentration. In the case of the negatively charged Fe-SiO_2 membrane, Cl^- is the co-ion and we see a fairly large rejection due to the solution pH being relatively far from the pH_{iep} of the material. We can compare this single layer membrane with the bi-layer Al_2O_3/Fe-SiO_2 membranes, in which the γ-Al_2O_3 layer faces the feed solution. At pH 8.5, we expect very little contribution to rejection from the γ-Al_2O_3 material, as we are very close to the isoelectric pH (Figure 3.2a). This prediction is confirmed by the data for the γ-Al_2O_3 single layer membrane, which rejects less than 5% of NaCl at this pH. Both zeta potential and rejection for the layer facing the feed solution provide evidence that, theoretically, rejection of NaCl with the bi-layer Al_2O_3/Fe-SiO_2 membrane should be equivalent to rejection with the Fe-SiO_2 single layer membrane. However, there is a decrease in rejection of NaCl (25% in bilayer versus 55%

in single layer). Clearly, the γ-Al_2O_3 nanofiltration layer affects the salt rejection properties of this membrane despite the absence of a bipolar membrane under these solution conditions. In principle, it would be logical to expect little influence from the γ-Al_2O_3 layer on the magnitude of the NaCl rejection, which should be solely associated with the properties of the Fe-SiO_2 layer, since this membrane has a high negative zeta potential under these solution conditions. We note that pore size and membrane thickness are two parameters that may not be totally equal in these two membrane layers compared to the Fe-SiO_2 layer in single membranes. We will deal with the effects of these membrane properties on salt rejection in detail later in this discussion.

We also investigated the effects of depositing the two nano membrane materials in the opposite configuration. We saw little to no rejection of NaCl at pH 8.0 with the γ-Al_2O_3 single layer membrane. We can compare this membrane with a bilayer Fe-SiO_2/Al_2O_3 membrane where the Fe-SiO_2 layer is now facing the feed solution. We can see that in this configuration, the negatively charged Fe-SiO_2 layer restricts the transport of chloride co-ions. Rejection of NaCl with this bilayer membrane is around 15%, three times that of the 5% rejection with the γ-Al_2O_3 single layer membrane. In this case, the Fe-SiO_2 layer is the one that is first encountered by ions in solution and acts to inhibit ion transport through the membrane, for the reasons described above. However, the question remains of why the rejection is much lower than the 55% seen for the Fe-SiO_2 single layer membrane and almost half of the value for the bilayer membrane with the opposite configuration. The initial data clearly show that, with respect to rejecting ions in solution, bilayer membranes composed of different metal oxide materials behave quite differently than their single layer counterparts. Additionally, we can see from Figure 3.4 that the order in which nanofiltration layers are deposited in a bilayer membrane significantly affects the

salt rejection properties of the membrane. It is important to note that in this solution, the magnitude of the zeta potential of γ-Al_2O_3 is very small. Therefore, the bi-layer membranes do not function as bipolar membranes.

To further investigate the salt rejection properties of our membranes, and elucidate the possible mechanisms for ion rejection, we studied rejection of all four of these salt solutions, with all four membrane configurations, in the pH range of 5-9. In these studies, we explore solution conditions for which our bilayer membranes perform as *bipolar membranes*, where both materials are simultaneously oppositely charged. In an environment where the materials behave as a bipolar membrane, rejection may occur through both the cation and the anion as co-ion. This pH range was chosen to represent the span in which many practical applications of salt removal are likely to fall.

3.4.3 Symmetric rejection of cations and anions in γ-Al_2O_3/Fe-SiO_2 bilayer membrane

In aqueous solutions, H^+ and OH^- ions are present in addition to the ions from the salt. Therefore, electro-neutrality in the solution may be reached in more than one way upon the rejection of one of the salt ions. To this end, we have investigated whether or not the removal of ions for a given salt is symmetric under different solution conditions. Figure 3.5a shows rejection of both Na^+ and Cl^- at nine different pH values for a bi-layer Al_2O_3/Fe-SiO_2 membrane. Feed and permeate solutions were analyzed for both anion and cation concentrations, using ICP and IC techniques, respectively. At every pH value, the data show symmetric rejection of both ions. Similarly, Figure 3.5b represents the same experiment with $NaNO_3$ as the salt. Again, we see that rejection is symmetric at every pH value studied. In the interest of efficiency, these results allow for future

feed and permeate samples to be analyzed for cation concentration only, as rejection of co-ions and counter-ions is practically equivalent, regardless of ionic species.

3.4.4 Rejection of I=0.01 NaCl solutions as a function of pH

3.4.4.1 Single Layer NF Membranes

We first examine rejection of 0.01M NaCl solutions of varying pH for all four membrane types (Figure 3.6). For the Fe-SiO_2 single layer membrane, rejection as a function of pH correlates well with what one would expect from the zeta potential titration curve (Figure 3.3a). The same is true for the γ-Al_2O_3 single layer membrane; however, the minimum of rejection seems to be shifted to one pH value lower (Figure 3.2a). If we compare rejection for the two single layer membranes for a given value of ψ_ζ, it is clear that this is measurement alone does not determine rejection. For example, when the ψ_ζ of both materials is approximately 30 mV in magnitude, the corresponding pH values are 8.2 and 6.0 for the Fe-SiO_2 material and the γ-Al_2O_3 material, respectively. The corresponding rejection of NaCl is roughly 60% for the former and roughly 20% for the latter. For the Fe-SiO_2 membrane, the direction of zeta potential is negative, so rejection is through the chloride co-ion. Meanwhile the γ-Al_2O_3 has a positive ψ_ζ; therefore, rejection occurs through the sodium co-ion. Thus, it is not expected that the same value of ψ_ζ will render equivalent rejection, since the positively charged co-ion may not have the same charge density as the negatively charged co-ion. In fact, the cation is expected to have greater charge density as compared to an anion with equivalent charge. Attempts to model rejection in nanofiltration membranes of opposite charge have noted that this difference in charge density will theoretically yield higher rejection when the cation serves as the co-ion.[10] Furthermore, ψ_ζ,

and more accurately the resulting surface charge density of the material, is only one of the parameters that determines membrane potential.

The potential across the pores of the NF materials determines the extent to which Donnan exclusion contributes to total membrane potential. We previously reported the average pore sizes of the Fe-SiO_2 and γ-Al_2O_3 materials to be 21 Å and 43 Å, respectively. Using these values, the absolute value of the central pore potential ($\psi_{dp/2}$) is presented for Fe-SiO_2 in the presence of various salt solutions in Figure 3.7a and for γ-Al_2O_3 in Figure 3.7b. To return to the previous comparison of equivalent values of ψ_ζ yielding differences in rejection of NaCl, we clearly see the advantage of using $\psi_{dp/2}$. Where ψ_ζ was equivalent (30 mV), $\psi_{dp/2}$ is significantly different, with values of approximately 40 mV and 27 mV for Fe-SiO_2 and γ-Al_2O_3, respectively. The reason central pore potential more accurately describes rejection properties of the NF membranes is that in addition to zeta potential and ionic strength, this parameter incorporates pore diameter, a physical property of the membrane, into the calculation. The larger sized pores of the γ-Al_2O_3 membrane would experience a larger drop in potential in the center of the pore due to incomplete overlap of the EDL from pore walls. This allows for ions to be more readily transported through the porous nanofiltration layer and retained in the permeate solution, therefore decreasing rejection. For the remainder of the discussion, rejection data will be considered in relation to Figures 3.7a and 3.7b.

3.4.4.2 Bilayer, Bipolar NF Membranes

One of the major goals of this study was to evaluate whether or not the rejection capabilities of a single layer nanofiltration membrane (either positively or negatively charged throughout the

relevant pH range) are enhanced by adding a top layer of a material that is oppositely charged at the same pH values; hence creating a bilayer membrane that is also bipolar. Several modeling efforts in the literature have reported that bipolar membranes, which have the ability to restrict ion transport by interacting with both cation and anion co-ions, are capable of increased rejection of monovalent, symmetric salts in solution.[10,11] To the best of our knowledge, very few experimental studies have confirmed this theoretical result and only one such work employed ceramic (as opposed to polymeric) membrane materials[12]. If each of the layers were summed to determine rejection in a bilayer membrane, one would expect the rejection curve for the bilayer membranes in Figure 3.6 to be a linear combination of the rejection curves of each of the single layer membranes in this Figure. However, the rejection curve of the bilayer membrane with γ-Al_2O_3 facing the feed solution could not be fit by a linear combination of the rejection curve of the single layer membranes. Therefore, rejection in bilayer membranes is not an additive property, at least for every pH value. Rather, the manner in which these nanofiltration layers interact with each other is more complex.

The comparison for rejection of NaCl between the single layer membranes and the bilayer membrane with the positive layer facing the feed solution (Al_2O_3/Fe-SiO_2) can be accomplished considering membrane potential alone. The thickness of the two NF layers is approximately equivalent when the γ-Al_2O_3 faces the feed solution, so this property of the membrane layers should not affect rejection. In the pH range 5.0 to 7.0 both NF layers have highly charged pores ($\psi_{dp/2}$ is 40 mV for Fe-SiO_2 and around 25 mV for γ-Al_2O_3, Figures 3.7a and 3.7b) so the bilayer membrane is considered bipolar. As the data show, rejection of NaCl in this pH range is controlled by the layer facing the feed solution,. As neutral pH is approached and surpassed,

there is separation between the bilayer and single layer γ-Al_2O_3 membranes' rejection capabilities. The pH at which we start to see very low rejection (less than 15%, Figure 3.6) from the γ-Al_2O_3 single layer membrane corresponds with a drop in the central pore potential of this material to less than 20 mV (Figure 3.7b). Rejection of NaCl continues to be very low as pH increases and $\psi_{dp/2}$ remains below 20 mV. In this pH range (7.0 to 9.0), the bilayer membrane shows improved rejection compared to the positively charged single layer membrane. It appears that although the bilayer membrane is still bipolar in this pH range, there may be a nominal value of central pore potential, near 20 mV, that is necessary to create enough membrane potential for the NF layer to contribute to the rejection of NaCl.

In the basic pH range, with little to no contribution from the positive layer, rejection of NaCl should occur between the Cl^- co-ion and the negatively charged Fe-SiO_2 NF layer. However, Figure 6 clearly demonstrates that rejection of NaCl is not equivalent to that obtained with a single layer Fe-SiO_2 NF membrane. If we consider the γ-Al_2O_3 to be a "neutral" layer in this pH range, having no rejection capability, this experimental result agrees model predictions of bipolar membrane performance.[10,16,17] This is due to the concentration polarization that occurs when the bottom layer has higher rejection than the layer facing the feed solution, increasing the concentration of sodium cations in the Fe-SiO_2 layer. The positively charged cations lower the membrane potential of the negative layer, decreasing the rejection capabilities of the bilayer membrane compared to the negatively charged single layer membrane.

When the negative layer faces the feed solution (Fe-SiO_2/Al_2O_3), the bilayer membrane outperforms the single layer γ-Al_2O_3 membrane and even the single layer Fe-SiO_2 at pH values

lower than 6. However, above this pH value the bilayer membrane shows lower rejection than the negatively charged single layer membrane. Rejection of NaCl still seems to be dictated by the feed-facing layer, which is negatively charged in this configuration. Compared to the bilayer membrane with oppositely ordered layers, rejection is higher in the range pH 5.0 to 7.5 when the negative layer faces the feed (Figure 3.6); this result is expected with a greater contribution from the top layer, as the central pore potential in the Fe-SiO_2 is 30-40 mV compared to 20-30 mV for γ-Al_2O_3. Around pH 7.5, the rejection vs. pH lines cross for the two bilayer membranes and rejection is now larger when the positive layer faces the feed solution. As pH increases, the isoelectric pH of the γ-Al_2O_3 is approached; therefore, the bilayer membrane is no longer bipolar. Above pH 8.0, the bilayer membrane with γ-Al_2O_3 as the layer facing the feed solution shows much higher rejection. It may be that the rejection is affected by the combined thickness of the NF layers; in this membrane total NF layer thickness is three times that of the bilayer membrane with Fe-SiO_2 facing the feed solution.

3.4.5 Rejection of I =0.01 $NaNO_3$ solutions as a function of pH

The trends for rejecting $NaNO_3$ as a function of pH are exactly the same as described above for the NaCl solution. Figure 3.8 shows the data for all four membrane types in $NaNO_3$ solution, which is included here for two purposes. The first is to show repeatability. The rejection experiments performed in this study are time-intensive, and therefore replication is inefficient. However, if we obtain comparable data for identical membranes in two different inert electrolytes, we can use this as a measure of reproducibility. The second purpose is to demonstrate that despite the difference in anionic species between the NaCl and $NaNO_3$ solutions, at equal pH and ionic strength, rejection of salt is equal as well. Since these are both

symmetric, monovalent salts, we would assume that all salts of this type should show similar patterns of rejection with the single and bilayer membranes produced in this research.

3.4.6 Rejection of I =0.01 Na_2SO_4 solutions as a function of pH

3.4.6.1 Single Layer NF Membranes

Figure 3.9 shows the data for rejection of Na_2SO_4 in solution for all four membrane types. As expected, rejection with the single layer Fe-SiO_2 membrane is very high (almost 90%) across the entire pH range studied. This is due to the divalent nature of the anion, the co-ion interacting with the negatively charged Fe-SiO_2 membrane, causing a comparatively larger central pore potential (Figure 3.7a). In contrast, the single layer γ-Al_2O_3 exhibits little to no rejection at most pH values. As previously discussed, this is most likely due to specific adsorption of the divalent sulfate ion to the positively charged γ-Al_2O_3, effectively discharging the material. This can be seen by examining Figure 3.7b. The central pore potential is very low in magnitude, less than 10 mV, and reaches a point of zero potential around pH 8.5. However, as pH increases, $\psi_{dp/2}$ begins to increase as pH becomes more basic. Although Figure 3.7b displays the absolute value of this parameter, $\psi_{dp/2}$ is actually negative at basic pH. It is clear that the interaction between the sulfate ion and the γ-Al_2O_3 surface leads to a charge reversal of this material, the magnitude of which increases with increasingly basic pH.

3.4.6.2 Bilayer, Bipolar NF Membranes

In the bilayer membrane where the positive layer faces the feed solution (Al_2O_3/$FeSiO_2$), we again see the effects of concentration polarization, this time for Na_2SO_4 rejection, when compared to rejection with a negatively charged single layer membrane. When pH < 8.5, the low

magnitude of $\psi_{dp/2}$ for γ-Al_2O_3 restricts the capacity of the bilayer membrane to act as a bipolar membrane. At increasingly basic pH values, the charge reversal of γ-Al_2O_3 leads to a bilayer membrane with both layers having negative charge, and the expected result is that at pH greater than 10 this bilayer membrane may even surpass the single layer Fe-SiO_2 membrane in rejection performance for Na_2SO_4 removal. This result is most likely attributed to the thicker Fe-SiO_2 layer in the bilayer membrane than in the monolayer one (0.4 μm vs. 1.4 μm). When the layers are reversed and the negative layer faces the feed solution, rejection of Na_2SO_4 is greater at pH < 7. For this case, the bilayer membrane is bipolar in this pH range, and the layer facing the feed solution has a greater contribution to rejection. At basic pH values, rejection of Na_2SO_4 is greater when the positive layer faces the feed solution. This result is most likely attributed to the difference in thickness between the NF layers in the two oppositely configured bilayer membranes; the one with γ-Al_2O_3 as the feed-facing layer is almost three times thicker.

3.4.7 Rejection of I=0.01 $MgCl_2$ solutions as a function of pH

The final solution studied in these experiments was $MgCl_2$, another asymmetric salt but with the cation being divalent. Figure 3.10 shows rejection as a function of pH for all four membrane types in I=0.01 $MgCl_2$ solution.

3.4.7.1 Single Layer NF Membranes

With the divalent cation in solution, the γ-Al_2O_3 membrane shows much higher rejection than the Fe-SiO_2 membrane across the entire pH range studied. γ-Al_2O_3 interacts with the divalent co-ion and rejection decreases as pH increases and approaches the pH_{iep} of the positively charged membrane material. With the Fe-SiO_2 membrane, the NF layer is negatively charged, but the

magnitude of central pore potential is less than 20 mV in the pH range studied. This value is much less than in salts with sodium as the cation, due to previously described interactions between magnesium ions and Fe-SiO_2 surface. As described in Figure 3.7a, $\psi_{dp/2}$ is fairly constant at the pH values studied. However, rejection is significantly higher from pH 5 to 6 than at pH 6.5 and greater. This anomolous behavior is almost certainly a result of electrostatic contributions from the 100Å alumina support layer. In fact, Skluzacek et al.[18] evaluated rejection as a function of the porous support, prior to depositing the NF layers, and found a larger value for $MgCl_2$ compared to other solutions studied. It can be seen in Figure 3.7b that at lower pH values, $\psi_{dp/2}$ is very large, near 40 mV. Although the pores are much larger in the support layer than in the NF layer, there is likely a large enough potential across some pores to result in bipolar behavior for the single layer Fe-SiO_2 membrane exposed to $MgCl_2$ solution. This result may be important for future experimental or modeling efforts in ceramic nanofiltration, as the support itself is typically composed of a ceramic material as well.

4.7.2 Bilayer, Bipolar NF Membranes

Magnesium chloride is the only solution studied in which the bilayer membrane is bipolar throughout the entire pH range. In the bilayer membrane where the positively charged layer faces the feed solution, for the divalent cation we see for the first time that rejection is greater for the bilayer membrane compared to it's single layer counterpart. The addition of the positively charged γ-Al_2O_3 top layer allows for a greater rejection through the divalent co-ion. The bipolar membrane with this configuration outperforms the single layer Fe-SiO_2 membrane across the entire pH range for rejection of $MgCl_2$ (Figure 3.10). The data also show that the bipolar membrane with layers in reversed order (Fe-SiO_2 facing the feed solution) produces similar

values for rejection from pH 5 to pH 7. This bilayer membrane outperforms the former at pH values above 7. In this range of pH, the potential at the pore center in γ-Al_2O_3 decreases from +20 mV to below +5mV while the potential of the Fe-SiO_2 is constant at -20 mV. Again, it seems the feed-facing layer (Fe-SiO_2) is the one responsible for the 20 % rejection of this salt.

3.5. Conclusions

Replicate single and bilayer nanofiltration membranes have comparable salt rejection capabilities. Rejection of ions in solution is symmetric (equivalent rejection of cation and anion for a given solution) with our ceramic NF membranes, meaning that hydroxide ions and protons do not participate in the separation process; therefore, changes in pH from the feed to the permeate stream are negligible. Rejection of 1:1 electrolytes (NaCl and $NaNO_3$) was found to be similar with all four membrane types. For these salts, the anionic species does not affect the salt removal properties of our NF membranes.

Depending on solution conditions, and especially solution pH, bilayer membranes may or may not function as bipolar membranes. This is determined mainly by evaluating the charging properties of the membranes, which can be deduced from zeta potential values and subsequent calculation of central pore potential. Whether or not the bilayer membrane behaves as a bipolar one has significant consequences for rejection of salts in solution.

In this study, bilayer membrane rejection values generally fell in between rejection values found with the single layer membranes consisting of the same two NF layers. The results show that the order in which nanofiltration layers are deposited onto the support (whether γ-Al_2O_3 or Fe-SiO_2

faces the feed solution) greatly affects the salt rejection properties of the resulting membrane. Specifically, the data imply that the layer facing the feed solution is more important in determining rejection performance in bilayer membranes. In the case where the bilayer membrane is also bipolar, interactions between the membrane and the solute will be through the feed-facing layer, so the co-ion will be the one with the same sign of charge as the NF layer that faces the feed solution. If the bilayer membrane is not bipolar, or perhaps only slightly so, and the feed-facing NF layer has a smaller value of $\psi_{dp/2}$ compared to the layer facing the permeate solution, the concentration polarization phenomenon enhances solute transport. Under these conditions, rejection for the bilayer membrane is lower than with the single layer counterpart, even though the "A" layer can be considered a neutral layer. These findings confirm model predictions for bilayer NF membrane behavior.

For NaCl and $NaNO_3$ (symmetric monovalent salts), the Fe-SiO_2 single-layer membrane performed best throughout the entire pH range studied. However, in comparing a positively charged γ-Al_2O_3 with a bilayer membrane where the Fe-SiO_2 layer faces the feed solution, rejection of NaCl and $NaNO_3$ is greater with the bilayer membrane.

For $MgCl_2$ and Na_2SO_4 (asymmetric 1:2 or 2:1 salts), a single layer γ-Al_2O_3 or Fe-SiO_2 membrane, respectively, is capable of rejecting more salt in solution than is either configuration of bilayer membrane. However, the data presented in Figures 3.9 and 3.10 clearly show that either bilayer membrane would perform better if we had a mixture of both salts in solution.

In these experiments, we worked at constant ionic strength; in the future, we plan to investigate how changing solute concentration would affect salt rejection properties in our bilayer membranes. In addition, we hope to continue experiments with the bilayer membranes to further elucidate the mechanisms of salt rejection in hopes that we can apply the findings towards practical applications for which the nanofiltration layers act as a bipolar membrane and show excellent salt removal and/or separation capabilities.

3.6 References

1. Farsi, A. *et al.* Modeling water flux and salt rejection of mesoporous γ-alumina and microporous organosilica membranes. *J. Membr. Sci.* **470,** 307–315 (2014).

2. Fievet, P., Szymczyk, A., Aoubiza, B. & Pagetti, J. Evaluation of three methods for the characterisation of the membrane-solution interface: streaming potential, membrane potential and electrolyte conductivity inside pores. *J. Membr. Sci.* **168,** 87–100 (2000).

3. Kukizaki, M. Relation between salt rejection and electrokinetic properties on Shirasu porous glass (SPG) membranes with nano-order uniform pores. *Sep. Purif. Technol.* **69,** 87–96 (2009).

4. Skluzacek, J. M., Tejedor, M. I. & Anderson, M. A. NaCl rejection by an inorganic nanofiltration membrane in relation to its central pore potential. *J. Membr. Sci.* **289,** 32–39 (2007).

5. Schaep, J., Van der Bruggen, B., Vandecasteele, C. & Wilms, D. Influence of ion size and charge in nanofiltration. *Sep. Purif. Technol.* **14,** 155–162 (1998).

6. Schaep, J., Vandecasteele, C., Mohammad, A. W. & Bowen, W. R. Analysis of the salt retention of nanofiltration membranes using the Donnan–Steric partitioning pore model. *Sep. Sci. Technol.* **34,** 3009–3030 (1999).

7. Hadj Lajimi, R., Ferjani, E., Roudesli, M. S. & Deratani, A. Effect of LbL surface modification on characteristics and performances of cellulose acetate nanofiltration membranes. *Desalination* **266,** 78–86 (2011).

8. Ouyang, L., Malaisamy, R. & Bruening, M. L. Multilayer polyelectrolyte films as nanofiltration membranes for separating monovalent and divalent cations. *J. Membr. Sci.* **310,** 76–84 (2008).

9. Sanyal, O., Sommerfeld, A. N. & Lee, I. Design of ultrathin nanostructured polyelectrolyte-based membranes with high perchlorate rejection and high permeability. *Sep. Purif. Technol.* **145,** 113–119 (2015).

10. Tsuru, T., Nakao, S. & Kimura, S. Ion separation by bipolar membranes in reverse osmosis. *J. Membr. Sci.* **108,** 269–278 (1995).

11. Dirir, Y. I., Hanafi, Y., Ghoufi, A. & Szymczyk, A. Theoretical Investigation of the Ionic Selectivity of Polyelectrolyte Multilayer Membranes in Nanofiltration. *Langmuir* **31,** 451–457 (2015).

12. Samuel de Lint, W. B., Zivkovic, T., Benes, N. E., Bouwmeester, H. J. . & Blank, D. H. . Electrolyte retention of supported bi-layered nanofiltration membranes. *J. Membr. Sci.* **277,** 18–27 (2006).

13. Szymczyk, A. *et al.* Contribution of convection, diffusion and migration to electrolyte transport through nanofiltration membranes. *Adv. Colloid Interface Sci.* **103,** 77–94 (2003).

14. Kosmulski, M., Prochniak, P. & Rosenholm, J. B. Electrokinetic potentials of Al2O3 in concentrated solutions of metal sulfates. *J. Colloid Interface Sci.* **338,** 316–318 (2009).

15. Peak, D., Ford, R. G. & Sparks, D. L. An in Situ ATR-FTIR Investigation of Sulfate Bonding Mechanisms on Goethite. *J. Colloid Interface Sci.* **218,** 289–299 (1999).

16. Jagur-Grodzinski, J. & Kedem, O. Transport coefficients and salt rejection in unchanged hyperfiltration membranes. *Desalination* **1,** 327–341 (1966).

17. Jonsson, G. Concentration profiles retention—flux curves for composite membranes in reverse osmosis. *J. Membr. Sci.* **14,** 211–227 (1983).

18. Skluzacek, J. M., Isabel Tejedor, M. & Anderson, M. A. An iron-modified silica nanofiltration membrane: Effect of solution composition on salt rejection. *Microporous Mesoporous Mater.* **94,** 288–294 (2006).

Membrane ID	Composition of "A"	Composition of "B"
Fe-SiO_2	4 layers Fe-doped SiO_2	*N/A*
γ-Al_2O_3	4 layers γ-Al_2O_3	*N/A*
Al_2O_3/Fe-SiO_2	3 layers γ-Al_2O_3	3 layers Fe-doped SiO_2
Fe-SiO_2/Al_2O_3	3 layers Fe-doped SiO_2	3 layers γ-Al_2O_3

Table 3.1: Four types of nanofiltration membranes used in this study. Bilayer membranes are described with layer "A" facing feed solution in liquid filtration experiments and layer "B" facing the permeate solution.

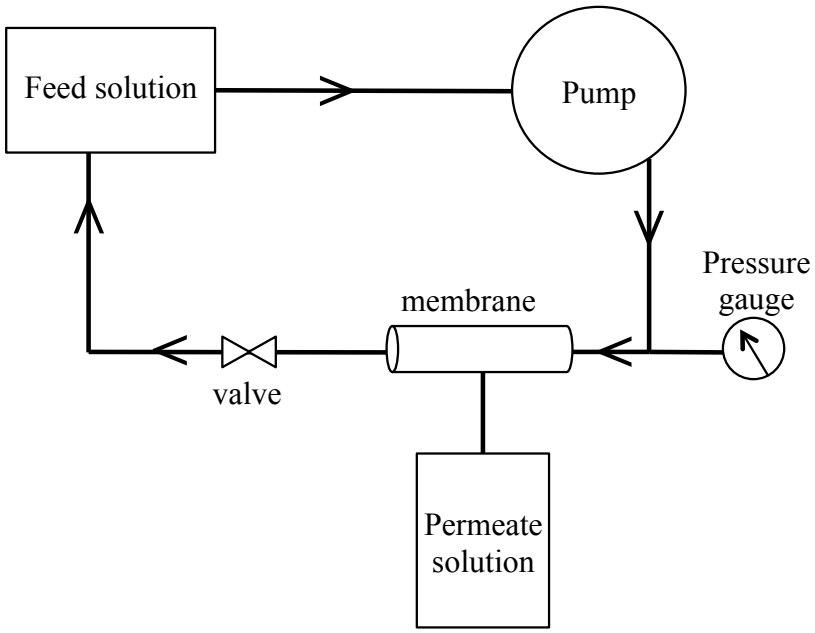

Figure 3.1: Schematic of liquid filtration experimental apparatus.

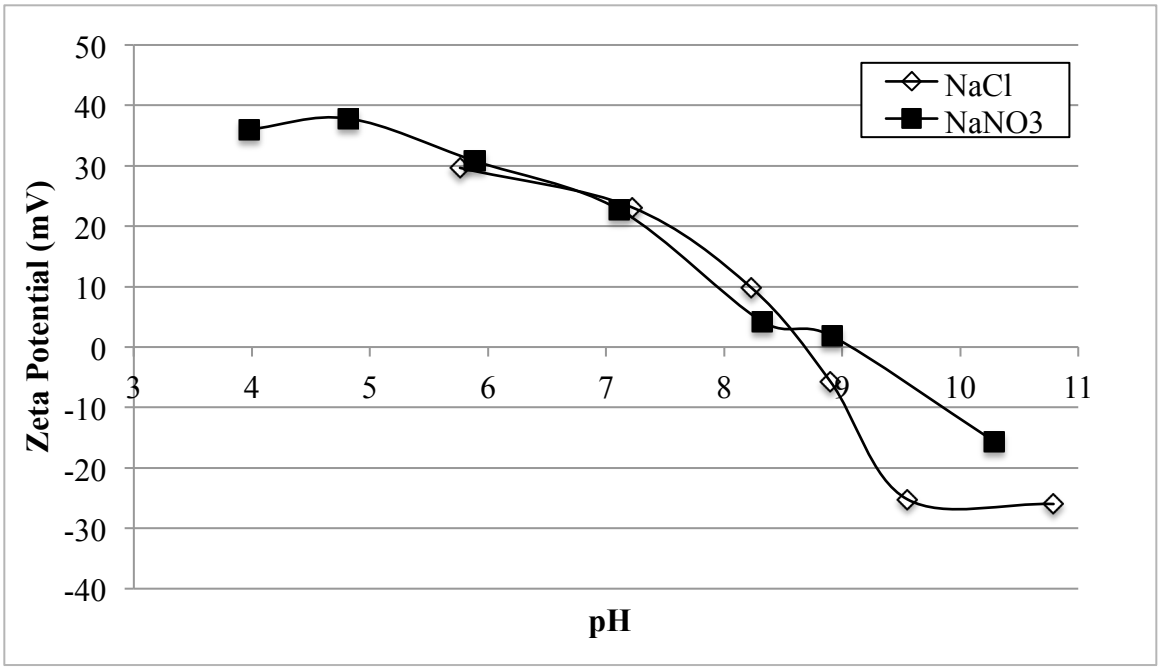

Figure 3.2a: Zeta potential measurements of γ-Al_2O_3 membrane material heated at 500°C, 3h exposed to I=0.01 monovalent, symmetric salt solutions at different pH values.

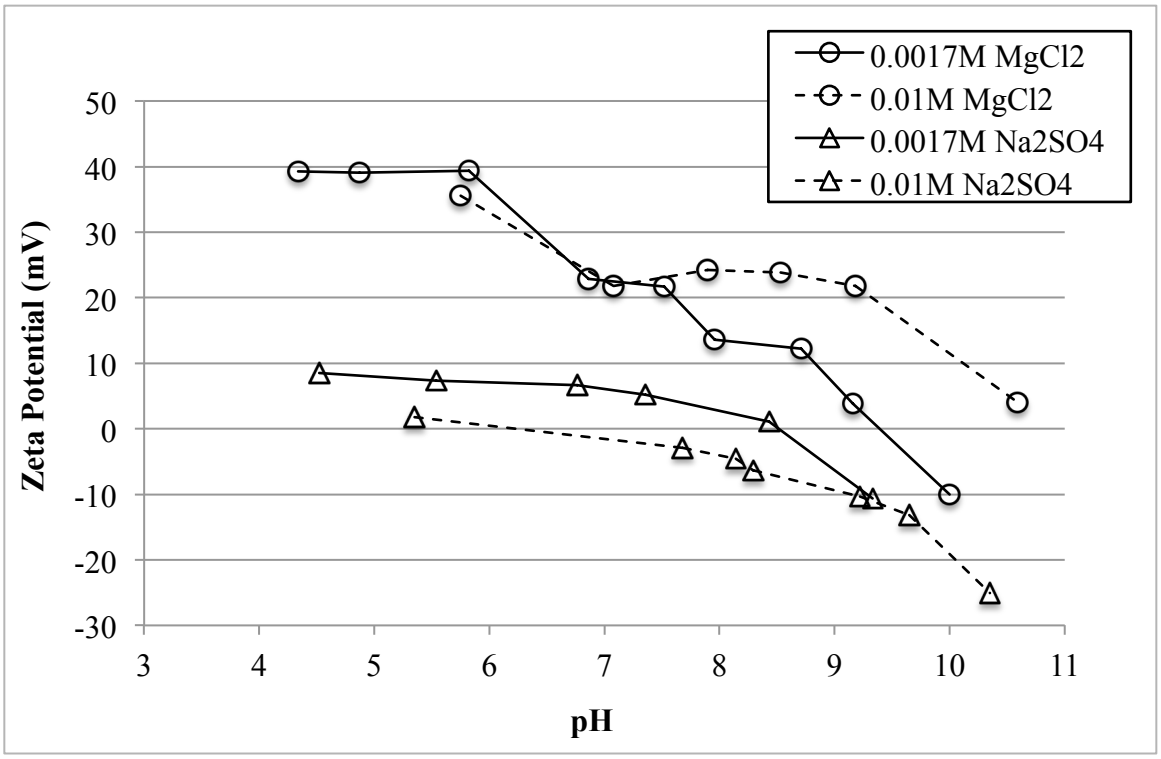

Figure 3.2b: Zeta potential measurements of γ-Al_2O_3 membrane material heated at 500°C, 3h exposed to salt solutions with varying concentrations of Mg^{2+} and SO_4^{2-} ions at different pH values.

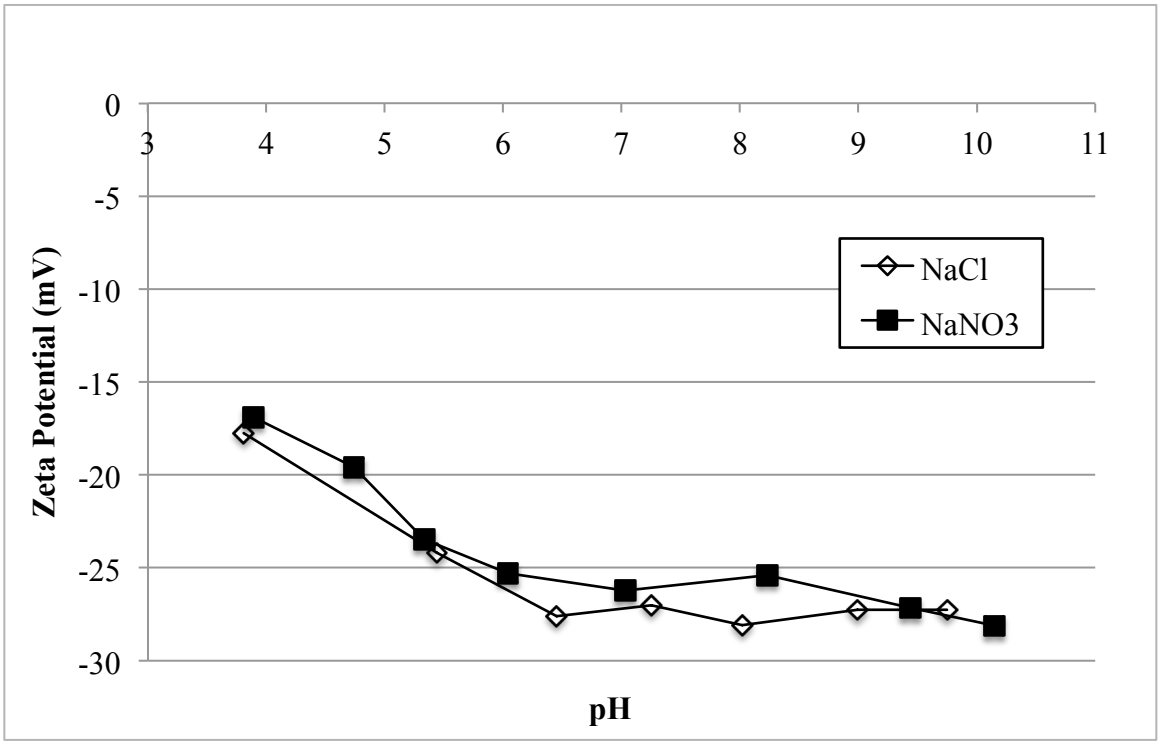

Figure 3.3a: Zeta potential measurements of Fe-SiO_2 membrane material heated at 500°C, 3h exposed to I=0.01 monovalent, symmetric salt solutions at different pH values.

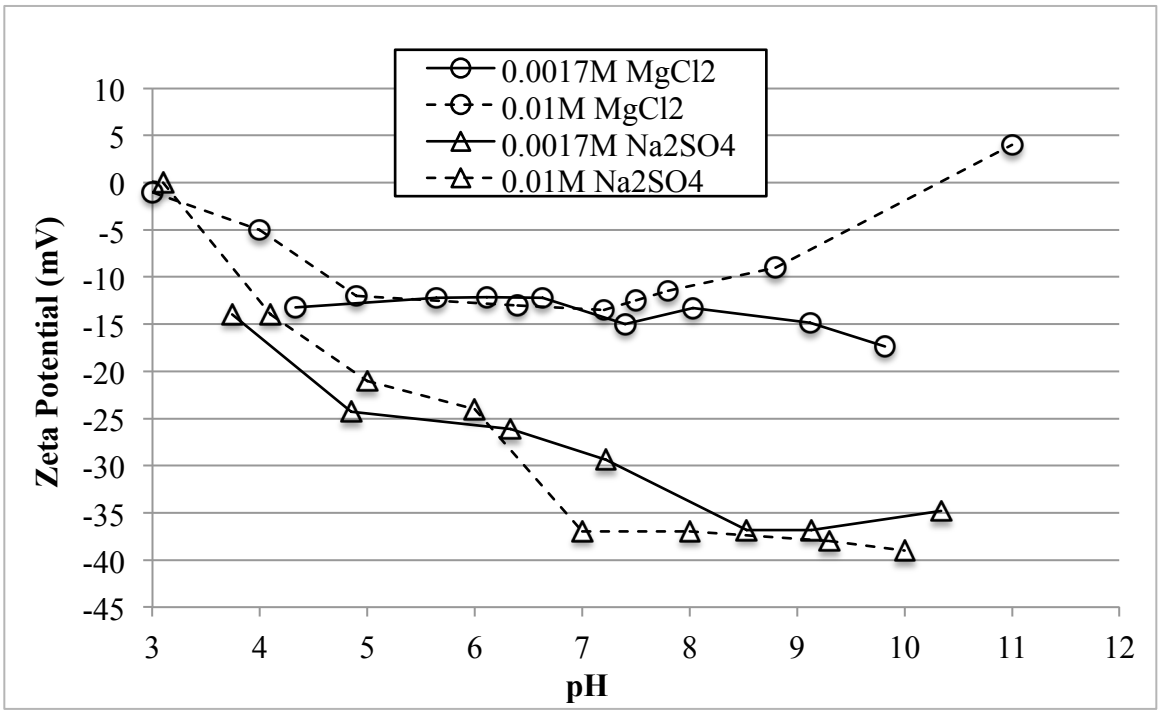

Figure 3.3b: Zeta potential measurements of Fe-SiO_2 membrane material heated at 500°C, 3h exposed to salt solutions with varying concentrations of Mg^{2+} and SO_4^{2-} ions at different pH values.

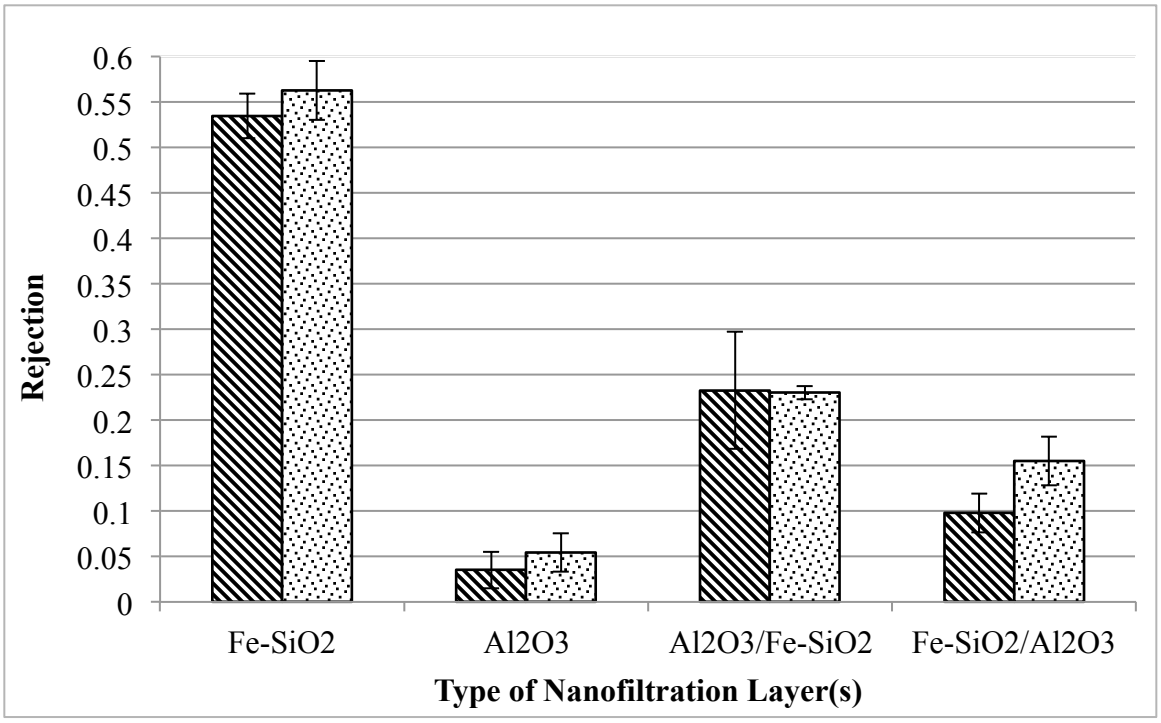

Figure 3.4: Average Rejection for replicate membranes of each type in 0.01M NaCl solution, pH 8 +/-0.5. Error bars indicate standard deviation.

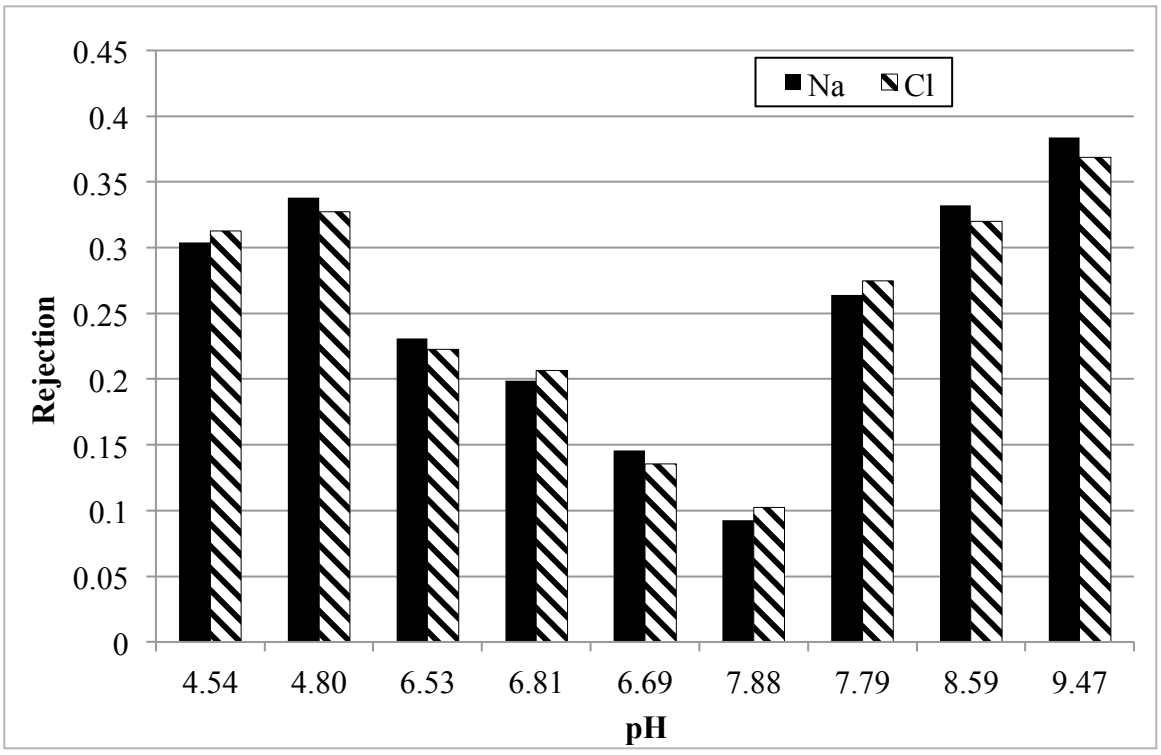

Figure 3.5a: Rejection of Na and Cl^- at various pH values with Al_2O_3/Fe-SiO_2 A membrane.

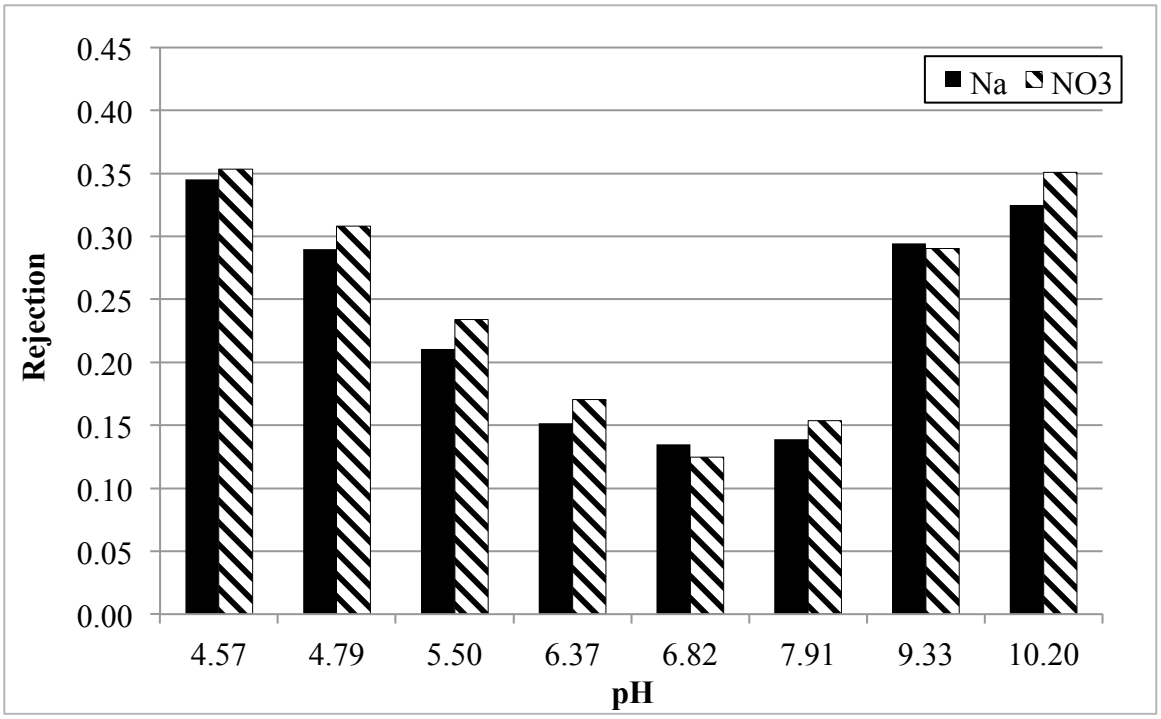

Figure 3.5b: Rejection of Na and NO_3^- at various pH values with Al_2O_3/Fe-SiO_2 A membrane.

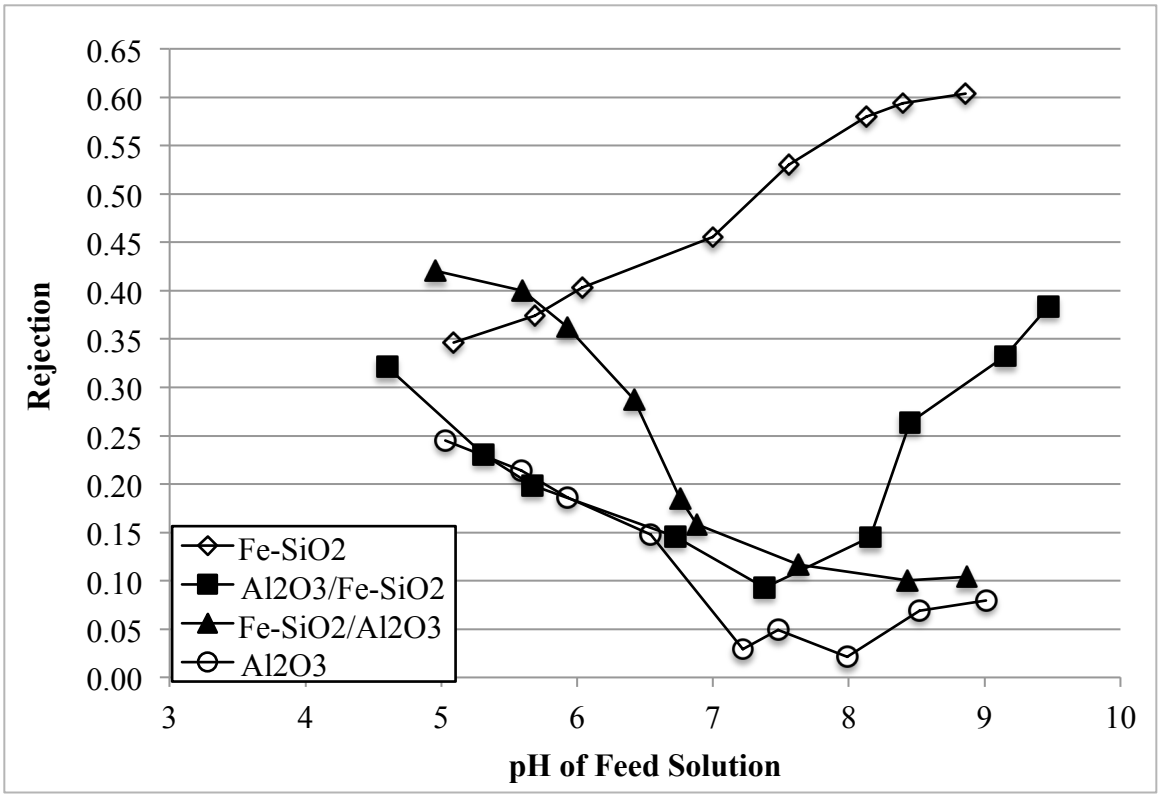

Figure 3.6: Rejection of I=0.01 NaCl as a function of pH for single and bilayer membranes.

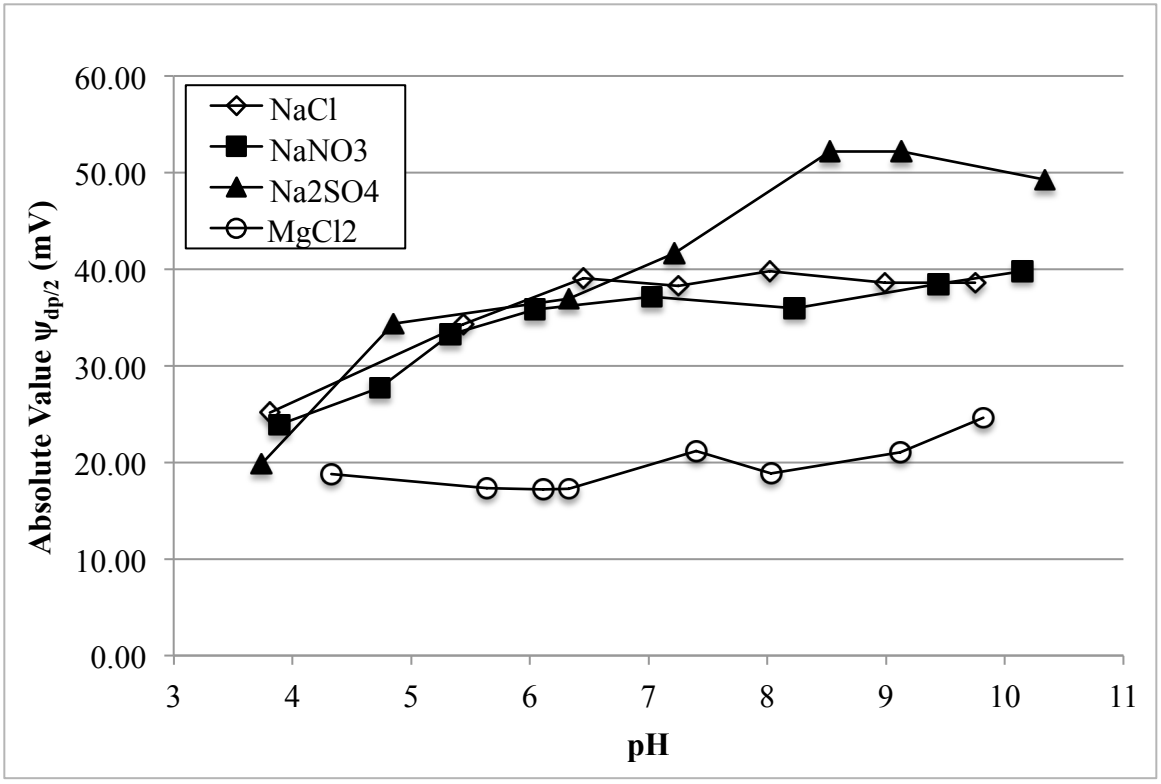

Figure 3.7a: Absolute value of the central pore potential ($\psi_{dp/2}$) as a function of pH for Fe-SiO_2 exposed to various I = 0.01 salt solutions.

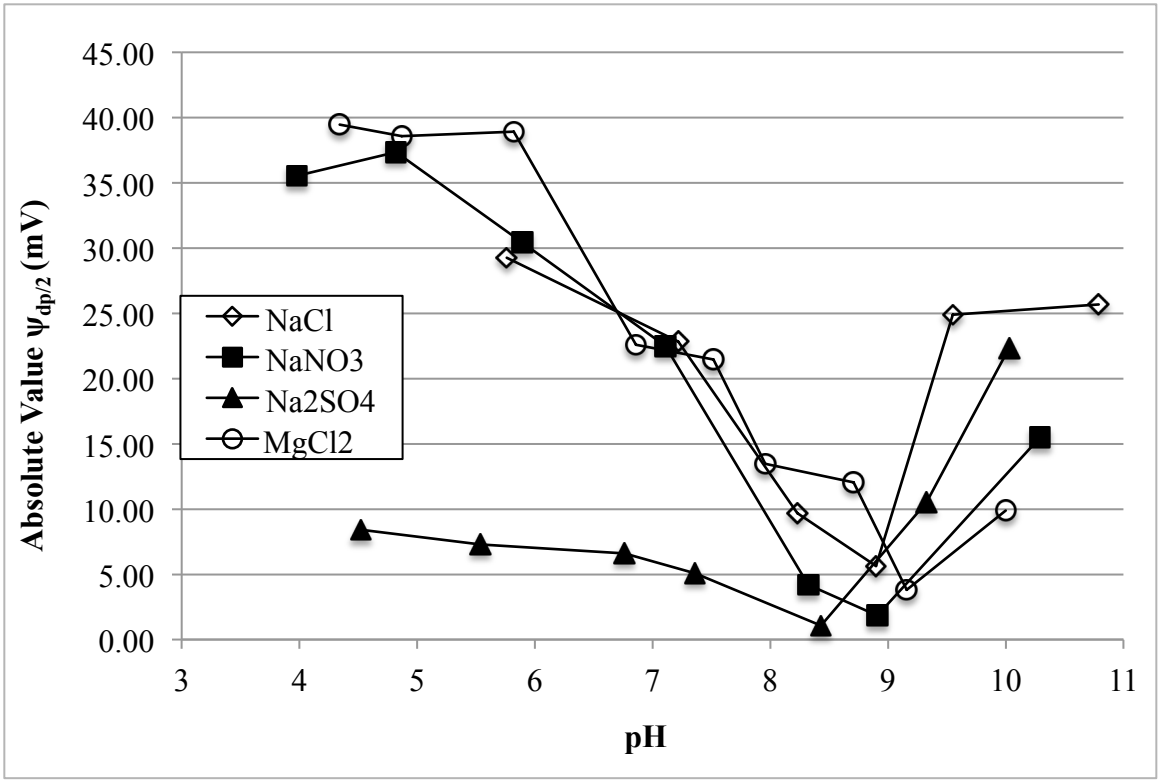

Figure 3.7b: Absolute value of the central pore potential ($\psi_{dp/2}$) as a function of pH for γ-Al_2O_3 exposed to various I = 0.01 salt solutions.

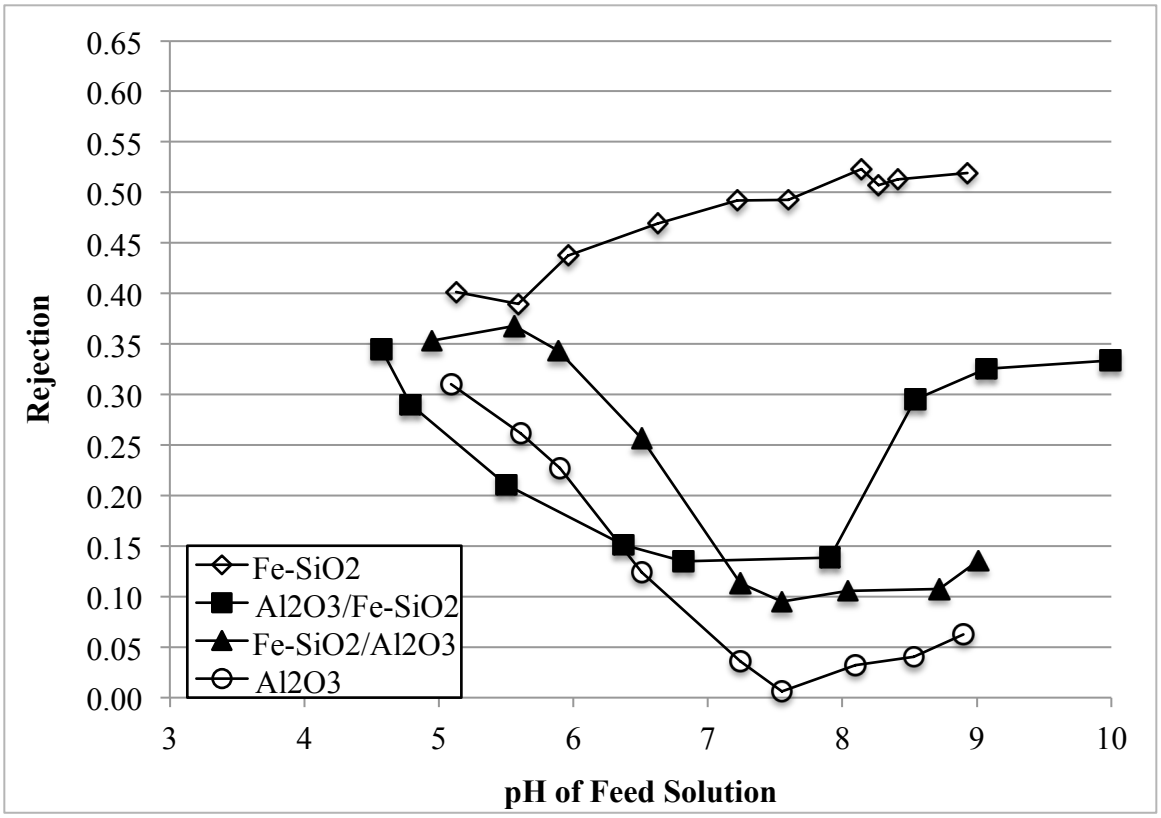

Figure 3.8: Rejection of I=0.01 $NaNO_3$ as a function of pH for single and bilayer membranes.

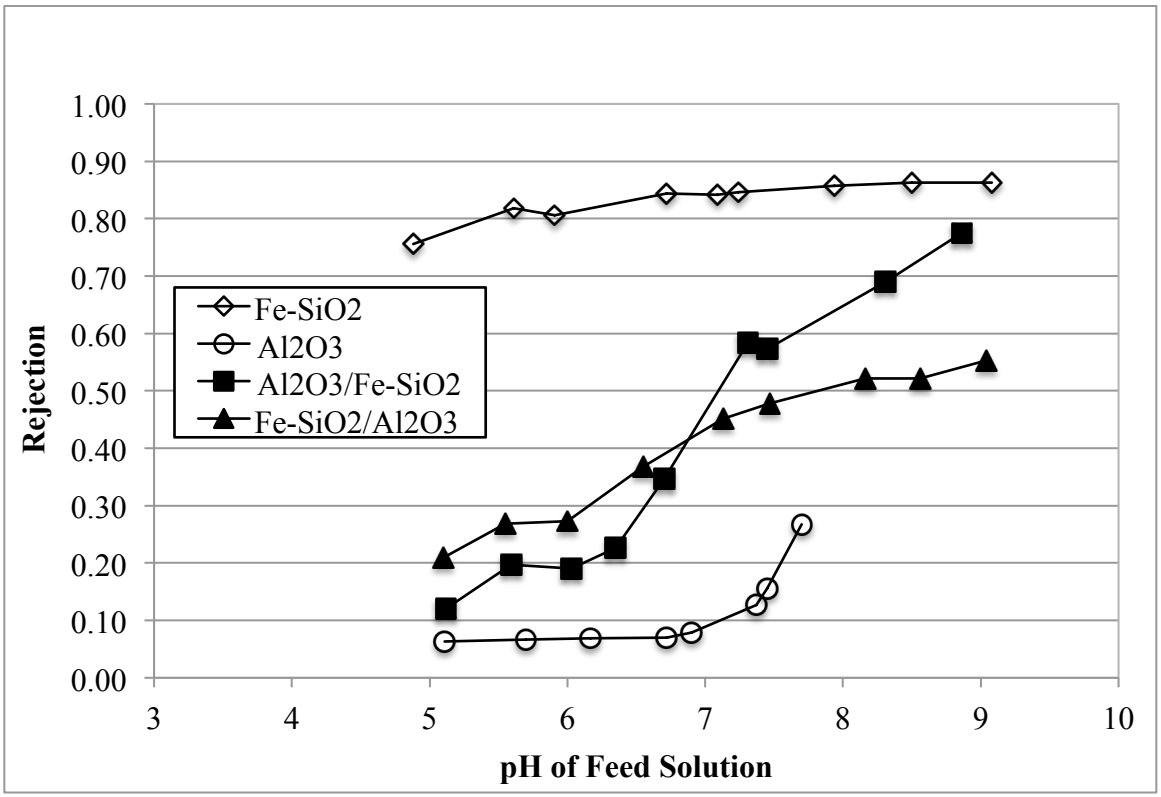

Figure 3.9: Rejection of I=0.01 Na_2SO_4 as a function of pH for single and bilayer membranes.

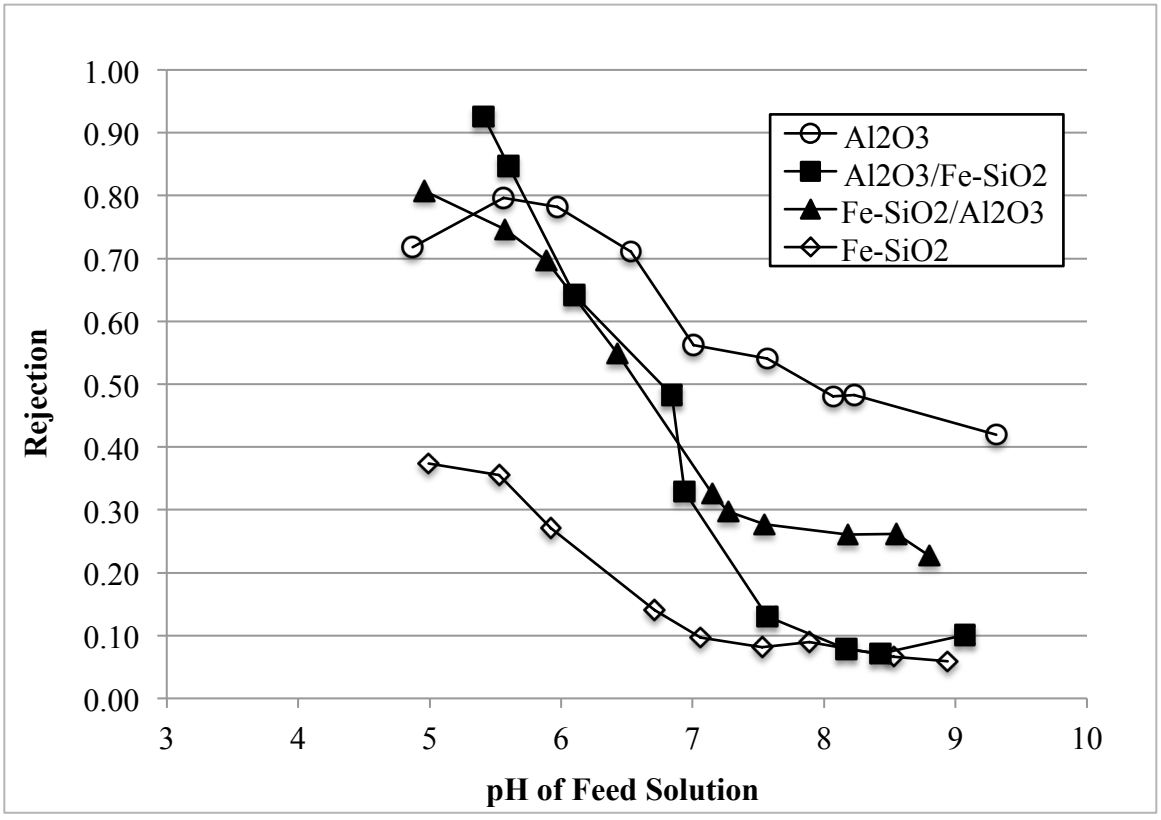

Figure 3.10: Rejection of I=0.01 $MgCl_2$ as a function of pH for single and bilayer membranes

4. Evaluating Bilayer γ-Al_2O_3 and Fe-SiO_2 Nanofiltration Membranes: Nature of the Ion, Concentration Effects, and Salt Separation

4.1. Introduction

Nanofiltration (NF) is currently utilized in niche markets. However, there is interest in more widespread use of the technology in many water treatment processes. One proposed avenue for broadening the implementation of NF membranes is by fabricating bilayer or bipolar membranes[1,2]. Commercially available NF membranes are either positively or negatively charged and, therefore, reject some species while retaining others in the permeate solution. Additionally, many current NF membranes are only effective under specific solution conditions, such where pH and ionic strength are limited to certain values. Multilayer NF membranes consist of 2 or more nanofiltration layers of different materials capable of having opposite charges. Depending on solution composition, bilayer membranes may also behave as bipolar membranes; meaning that for a given solution pH, ionic strength, and salt species, the two NF layers will develop opposite charges when in contact with the solution. Thus, performance of NF membranes with respect to rejecting salts should increase as both the cation and anion may act as co-ions. To date, most of the models and experimental data describing bilayer and/or bipolar NF membranes are centered on membranes composed of polymeric materials.

Previously, we have fabricated and evaluated porous, ceramic single layer and bilayer NF membranes with respect to both physical characteristics of NF layers and membrane rejection of 1:1, 1:2 and 2:1 electrolytes at constant ionic strength and varying pH. For reference, Table 4.1 is provided as a summary of physical characteristics of these membranes. Much of the work was devoted to correlating the rejection of salts with charging properties of the membranes, and especially with the potential in the center of the pore. Experimental results were compared for single and bilayer membranes to determine feed solution conditions under which bilayer

performance exceeded that of conventional NF membranes. The purpose of the present study is to examine how characteristics of the solution affect the rejection of different salts in our ceramic bilayer NF membranes.

Rejection of 1:1 electrolytes of NaCl and $NaNO_3$ was found to be equivalent with our bilayer membranes. In order to confirm this result, we measured rejection of an additional 1:1 electrolyte ($NaClO_4$) and compared rejection values to central pore potential calculations. According to Shang et al., depending on the concentration and composition of the feed stream, diffusion may play a role in hindering ion transport, along with electrostatic interactions[3]. As different ions exhibit different transport diffusivities, rejection in bilayer membranes may be affected by the size and/or geometry of the ion, in addition to its valence state. The particular electrolytes chosen for these studies have relevant applications in water treatment. The chloride ion is ubiquitous in many contaminated water streams, and is of particular interest in the desalination of seawater. Nitrate and perchlorate are groundwater contaminants, and nanofiltration is a promising technique for the removal of these ions from water resources[4–8].

All previous experiments were performed at constant ionic strength. It is well known that ionic strength affects the thickness of the electrical double layer and, therefore, central pore potential, membrane charge, and rejection capabilities of nanofiltration membranes. Our goal has been to study how changes in concentration of a given electrolyte affect rejection, and to relate this to mechanisms of ion transport in NF.

One area in which bilayer NF membranes have been predicted to excel is in separation of salts in solution, and in particular divalent and monovalent ions. In a recent review paper, Van der Bruggen et al. focused on the drawbacks of NF that currently prevent its application on a larger scale[9]. The authors focus on six specific challenges in NF and offer solutions for avoiding or overcoming these issues. One of these six areas for improvement is in the separation ability of NF membranes. It is widely reported that NF membranes selectively transport monovalent ions as compared to divalent or multivalent ones[10–12]; separation of monovalent and divalent ions is especially relevant in considering nanofiltration as a pretreatment for reverse osmosis desalination of seawater. Bipolar membranes, having both positively and negatively charged layers, might improve the separation of multivalent from monovalent ions, due to the ability of these NF membranes to interact with a wider variety of chemical species. In particular, bilayer polymeric NF membrane separation of sulfate and chloride ions has been reported in the literature[13–15]. In the present study, we will compare performance of our ceramic bilayer NF membranes with single layer ones with respect to separating given monovalent and divalent ions.

One of the drawbacks of nanofiltration discussed by Van der Bruggen is related to the generation of a concentrated brine as a liquid residual, which is often referred to as the "concentrate" [9]. This is the water that will need to be disposed of, as the salt concentration is too high for further effective treatment. The treatment or disposal of the concentrated brine stream is an intrinsic problem for all pressure-driven membrane processes, as well as for other water treatment technologies. The goal in water treatment is to reduce the volume of brine discharge in order to (1) recover more clean water and (2) reduce the amount of contaminated wastewater needing disposal. Brine minimization is an active area of research within the water treatment, and

especially desalination, community. The composition of the concentrate should be similar to that of the feed stream, but having increased concentration. The concentration factor (CF) can be calculated as a ratio of the concentration of component *i* in the retentate ($C_{r,i}$) to that in the feed ($C_{r,f}$) according to the equation:

$$CF = \frac{C_{r,i}}{C_{f,i}} \qquad \text{Equation 4.1}$$

The Concentration Factor can be a useful tool for comparing different water treatment technologies with respect to disposal of waste streams. The volume and composition of wastewater generated during the nanofiltration process is a critical parameter from not only an environmental perspective, but may also have legal and/or financial consequences. This study attempts to elucidate which of the solution characteristics affect the rejection of given salts and also to evaluate the findings in light of some of the practical considerations in nanofiltration membrane technology.

4.2. Experimental Methods

The composition of the NF membranes and the experimental apparatus utilized in all liquid filtration studies were previously described in Chapter 2 of this thesis.

4.2.1 Salt rejection with γ-Al_2O_3 and Fe-SiO_2 bilayer membranes

In order to investigate the effects of concentration and the nature of the ion on salt rejection in bilayer NF membranes, liquid filtration experiments were performed with both membrane configurations, i.e. either γ-Al_2O_3 or Fe-SiO_2 facing the feed solution. Feed solutions of NaCl,

$NaNO_3$, and $NaClO_4$ at various concentrations (0.025 M, 0.01 M or 0.005 M) were prepared using chemicals from Fisher Scientific (Certified ACS) and ultra-pure (Milli-Q) water to maintain constant anionic species in all experiments. The salt solutions were then titrated to the desired pH using hydrochloric, sulfuric or nitric acid and sodium or magnesium hydroxide solutions (Fisher Scientific Certified ACS) to maintain consistent electrolyte species in solution. For each salt solution studied, solutions were prepared at nine different pH values: pH 5.0, 5.5, 6.0, 6.5, 7.0, 7.5, 8.0, 8.5, 9.0. The pH of both the feed and permeate solutions was measured using a Mettler Toledo SevenMulti pH meter at the time the sample was taken. For all data, selectivity values are presented as rejection (R) of the solute, as determined by the following equation:

$$R = 1 - \frac{\boldsymbol{C_P}}{\boldsymbol{C_F}} \qquad \text{Equation 4.2}$$

where C_P is the solute concentration in the permeate and C_F is the solute concentration in the feed stream. Feed and permeate samples were analyzed for Na concentration using induced coupled plasma-optical emission spectroscopy (ICP-OES, Perkins Elmer).

4.2.2 Salt separation with γ-Al_2O_3 and Fe-SiO_2 bilayer membranes

Feed solution conditions for all experiments were pH 8.5 ± 0.5, I=0.01 with equal concentrations of NaCl and Na_2SO_4; pH was adjusted by the addition of NaOH. The solution was prepared using chemicals from Fisher Scientific (Certified ACS) and ultra-pure (Milli-Q) water. Feed and permeate samples were again analyzed for Na concentration using induced coupled plasma-optical emission spectroscopy (ICP-OES, Perkins Elmer). Samples were also analyzed for sulfate

and chloride concentration using ion chromatography (IC, Dionex ICS 2100). For comparison, experiments were duplicated with single layer Fe-SiO_2 membranes. In all liquid filtration studies, applied transmembrane pressure is kept constant at 250 psi in order to eliminate any influence of volume flux, J_v, on solute rejection.

4.2.3 Charging properties of γ-Al_2O_3 and Fe-SiO_2 nanofiltration membranes

Charging properties of the pore walls in nanofiltration layers were evaluated by measuring the zeta potential of powdered materials identical to the ones that constitute the nanofiltration membranes. The zeta potential measurements were performed using an electrophoretic mobility device, Malvern (3000 HS) ZetaSizer. Gels of membrane materials were generated by drying sols of Fe-silica and alumina to create xerogels, which were then heated at 400 or 500°C to create Fe-SiO_2 and γ-Al_2O_3. Each of these materials was ground to a fine powder and suspended in salt solutions of interest to perform the zeta potential measurements. Zeta potential measurements were conducted in I=0.01 solutions of NaCl, $NaNO_3$ and $NaClO_4$ prepared from Fisher Scientific (Certified ACS) chemicals. Samples were titrated to different pH values using either acidic or basic solutions (Fisher Scientific Certified ACS chemicals) containing cations or anions common to the salt solution. All samples were allowed to equilibrate for 2 h and pH was re-adjusted if necessary. Zeta potential measurements, in combination with previously determined pore diameters for the Fe-SiO_2 and γ-Al_2O_3 membrane materials, were utilized in the calculation of electric potential across the pore. Specifically, the absolute value of the potential at the center of the pore is useful to predict the strength of the Donna exclusion upon normalizing for pore size (r_p) and ionic strength (I).

4.2.4 Determining concentration factor (CF) for a bilayer γ-Al_2O_3/Fe-SiO_2 membrane

The experiment to determine CF was conducted at ΔP = 250 psi with the previously described liquid filtration apparatus utilizing a bilayer membrane having a γ-Al_2O_3 NF layer facing the feed solution. The feed solution was I = 0.01 NaCl titrated to pH 9.0 using NaOH (Fisher Scientific ACS Certified chemicals.) Solution pH was monitored and adjusted throughout the experiment to keep this variable constant; in an open system, solution pH will decrease from 9.0 due to equilibrium between the aqueous phase and atmospheric carbon dioxide. The feed solution was cycled through the membrane in a continuous circulation loop for 14 h. Initial feed solution volume was measured at 3500 mL and final volume 875 mL; the experiment was terminated at this point as a further reduction in volume was not possible due to system requirements. Samples of the feed and permeate solutions were taken at 30 min intervals and were analyzed for Na concentration using ICP-OES (Perkins-Elmer.)

4.3. Results and Discussion

4.3.1 Influence of anion species on bilayer membrane rejection of salt solutions

4.3.1.1 Bilayer membrane rejection with positive γ-Al_2O_3 NF layer facing feed solution

We have already shown that the maximum rejection obtained in nanofiltration (σ_s, reflection coefficient) depends on membrane charge and diffusion coefficients of the co-ion and counter-ion. The rejection of single salts solutions for three different 1-1 electrolytes having a common cation but differing anions is displayed in Figure 4.1. As previously discussed in Chapter 2 of this thesis, rejection of NaCl and $NaNO_3$ is equivalent for this membrane. The data clearly show that rejection of $NaClO_4$ differs, despite the obvious similarities in the monovalent, symmetric nature among the three salt solutions. Our method for comparing the charging properties of the

membrane is by calculalting central pore potential. The data is provided in Figure 4.2 for all three salt solutions. Clearly, the absolute value of $\psi_{dp/2}$ is similar for chloride, nitrate, and perchlorate throughout the pH range studied. Therefore, differences in rejection cannot be attributed to differences in membrane charge, X. From Figure 4.1, at low pH values, rejection of $NaClO_4$ is greater than rejection of NaCl or $NaNO_3$. In the range of pH 5.0 to pH 7.0, this bilayer membrane behaves as a bipolar membrane and the thicknesses of the individual NF layers are practically equivalent. Membrane potential, and therefore rejection, in this pH range is determined by the positively charged, feed-facing γ-Al_2O_3 layer. This means that the Na^+ is the co-ion. The difference in rejection at acidic pH values should then be related to counter-ion diffusion coefficients (D_i), which is the only other variable that determines σ_s that differs among the solutions. From Table 4.2, the lower diffusivity (1.792×10^{-5} cm^2 s^{-1}) of the perchlorate counter-ion lowers transport through the membrane resulting in higher rejection of this salt as compared to NaCl and $NaNO_3$. Furthermore, this result is in agreement with the findings of Colic et al.[16] regarding counter-ion interactions with a charged surface. These authors saw that smaller counter-ions, having a greater affinity for water, are able to penetrate more deeply into the surface hydration layer than larger ions. In the basic pH region, the opposite effect is observed. The rejection of $NaClO_4$ is less than that of NaCl and $NaNO_3$ (Figure 4.1). In this pH range, the γ-Al_2O_3 can be considered a "neutral" layer resulting in concentration polarization due to the larger magnitude of charge density (X) for the bottom Fe-SiO_2 NF layer. Rejection is controlled by the negatively charged Fe-SiO_2, and now the anion is the co-ion. The lower rejection of perchlorate can be attributed to the decreased charge density of this ion as compared to either chloride or nitrate ions, resulting in decreased electrostatic repulsion between the membrane and the co-ion in these solution conditions.

4.3.1.2 Bilayer membrane rejection with negative Fe-SiO_2 NF layer facing feed solution

Throughout the entire pH range studied and as shown in Figure 4.3, when the negatively charged NF layer faces the feed solution, there is less rejection of $NaClO_4$ than of NaCl and $NaNO_3$. In this bilayer configuration, the membrane is bipolar and rejection is controlled primarily by the Fe-SiO_2 layer. The negative layer has a larger magnitude of central pore potential than γ-Al_2O_3 at all pH values. Additionally, at basic pH values, as the pH_{iep} of γ-Al_2O_3 is approached, the bilayer membrane is no longer bipolar. The data of absolute potential in the center of the pore for Fe-SiO_2 in the three salt solutions is displayed in Figure 4.4, and indicate X cannot account for the comparably decreased rejection of $NaClO_4$. The lower rejection of the perchlorate co-ion supports the discussion of anion charge density provided above.

4.3.2 Influence of concentration on bilayer membrane rejection of salt solutions

4.3.2.1 Bilayer membrane rejection with the positive γ-Al_2O_3 NF layer facing the feed solution

The data presented in Figures 4.1 and 4.3 demonstrates that rejection in bilayer NF membranes can be affected by the type of anion, even when comparing ions of equivalent valence state. In order to further elucidate the mechanism(s) that determine this result, we measured rejection of NaCl and $NaClO_4$ as a function of pH when solute concentration was varied. Rejection of NaCl solutions at two different concentrations is shown in Figure 4.5 for a bilayer membrane having γ-Al_2O_3 layer facing the feed solution. As the concentration of the solute increases from 0.01M to 0.025M, there is very little rejection across the entire pH range (<5%). This result is expected, as the increase in concentration results in a compression of the electrical double layer at the pore walls. This compression lowers the value of central pore potential. Therefore, ions are freely transported through the pores of the NF membrane to the permeate solution. In Figure 4.6,

rejection of $NaClO_4$ at varying concentrations is shown for the same membrane. When the γ-Al_2O_3 NF layer faces the feed solution and solution pH ≤ 6.5, Na^+ is the co-ion and is rejected by the positively charged layer. Therefore, ClO_4^- is the counter-ion. In this pH range, the system is less concentration dependent, as there is less separation among the rejection values for 0.005M, 0.01M and 0.025M $NaClO_4$ solutions as compared to rejection in the basic pH range. Compared to rejecting NaCl for this same membrane, rejection of $NaClO_4$ is much larger at 0.025M. This is unexpected, as rejection of both solutions should be equivalent as they contain the same co-ion. Therefore, this difference can only be attributed to the different species of the counter-ion. When Cl^- is the counter-ion, the spherical shape of this chemical species allows for efficient packing of the negatively charged ion on the EDL at the interface between the positively charged surface and the solution. As previously discussed, this shielding of the EDL by chloride ions explains the lack of rejection at high NaCl concentration. Conversely, the ClO_4^- counter-ion exhibits different geometry (tetrahedral) as well as lower charge density due to its larger size. Therefore, packing in the EDL layer does not provide as complete surface charge shielding compared to Cl^-. This explains why increasing $NaClO_4$ concentration does not have as significant of an effect on rejection. In fact, the difference in rejection between 0.01M and 0.025M sodium perchlorate solutions is less than 5% at most pH values in this range.

With values of solution pH > 7, the bilayer membrane becomes less bipolar as the pH_{iep} of γ-Al_2O_3 is approached. As discussed in Chapter 2 of this thesis, at a basic pH, the γ-Al_2O_3 behaves as a neutral layer, and rejection is controlled by the more highly charged Fe-SiO_2 layer. Perchlorate is now the co-ion and sodium is the counter-ion. Concentration polarization results in enhanced transport of Na^+ through the γ-Al_2O_3 feed-facing layer, which increases the amount of

cation packing within the EDL layer of Fe-SiO_2 pore walls, decreasing central pore potential of this material when it faces the permeate solution in a bilayer membrane. This phenomenon provides an explanation for the larger separation in rejection values between 0.01M and 0.025M solutions of $NaClO_4$ in this pH range. We also measured rejection of a 0.005M sodium perchlorate solution over this same pH range. From Figure 4.6, it is clear that the three different solution concentrations exhibit much more of a dissimilar rejection at higher than at lower pH.

4.3.2.2 Bilayer membrane rejection with the negative Fe-SiO_2 NF layer facing the feed solution For comparison, we studied the concentration effect for rejecting sodium perchlorate with a bilayer membrane having the Fe-SiO_2 layer facing the feed solution. In this configuration of NF layers, rejection is governed by the negatively charged Fe-SiO_2 layer with ClO_4^- being the co-ion. The results for rejecting $NaClO_4$ at different concentrations as a function of pH for the bilayer membrane with Fe-SiO_2 facing the feed solution are given in Figure 4.7. In this type of bilayer membrane, rejection of perchlorate is constant at pH $\geq$ 6, even when concentration is more than doubled. The concentration independent rejection of sodium perchlorate at [$NaClO_4$] > 0.01M has important practical consequences. For this salt at least, rejection is still possible even at very high concentrations. This has practical implications as this bilayer membrane is versatile with respect to effectiveness in concentrated feed solutions. In addition to the commercial and environmental applications of this result, it should also be of value to verifying nanofiltration model predictions concerning the concentration effects on the rejection of salts in solution.

4.3.3 Salt separation with γ-Al_2O_3 and Fe-SiO_2 bilayer membranes

Nanofiltration is a well-known technique for separating divalent ions from monovalent ones. Furthermore, both models and experimental data predict that membrane selectivity towards monovalent ions is increased in bilayer NF. Selectivity values for both single and bilayer membranes are given in Table 4.3, and are reported as the ratio of chloride ions to sulfate ions obtained in the permeate solution. Data is provided for both the results of the experiments in this study with feed solution containing equivalent concentrations of both ions (mixed salt solution). In addition, the selectivity value was calculated for previous experiments with single salt solutions of either NaCl or Na_2SO_4 at the same ionic strength and pH as the mixed salt solution. The data clearly show that γ-Al_2O_3 and Fe-SiO_2 bilayer membranes outperform Fe-SiO_2 single layer membranes in separating sulfate ions from chloride ions. This experimental result is in agreement with predictions and reported data in the literature[13]. Additionally, we can see from the data that the calculation of this selectivity factor from single salt solutions is a fairly accurate predictor of the experimental data obtained when the salts are in solution together for a single layer membrane. Also, this calculation predicts that bilayer membranes will more effectively separate chloride and sulfate as compared to a single layer membrane. At pH 8.5, rejection will be dictated by the anion (Cl^- or SO_4^{2-}) as the co-ion. Sulfate, being divalent, will be strongly repelled by the first NF layer and will therefore be rejected. When a second NF layer is added, the sulfate is diluted prior to approaching the layer, so rejection through the second layer will also be sufficient. This agrees with the data for ClO_4^- showing greater rejection when the solution is more dilute (Figures 4.7 and 4.8) and clarifies the greater separation of sulfate and chloride with a bilayer membrane than a membrane with a single layer.

For the bilayer membrane having γ-Al_2O_3 as the NF layer facing the feed solution, there is a significant increase in the selective transport of Cl^- when the two salts are mixed in one solution. In this case, sulfate and chloride co-ions compete with respect to their interaction with the negatively charged membrane. Repulsion of divalent SO_4^{2-} is still much stronger as compared to the monovalent Cl^-. Due to the Donnan potential that develops from co-ion rejection, Na^+ counter-ions are more readily transported when Cl^- is in solution compared to when the only ions are Na^+ and SO_4^{2-}. This may explain the larger value for selectivity with the bilayer γ-Al_2O_3/Fe-SiO_2 membrane compared to the predicted value from calculations of rejection of single salt solutions. The enhanced separation ability with bilayer membranes has practical applications in both seawater desalination and in the use of nanofiltration as a pretreatment to reduce the large energy requirements associated with reverse osmosis.

4.3.4 Concentration Factor (CF) for NaCl rejection with a bilayer γ-Al_2O_3/Fe-SiO_2 membrane

In order to determine the volume and chemical composition of the brine solution generated in our nanofiltration system, the liquid filtration apparatus was operated continuously until the volume of the feed stream approached the minimum possible to operate the pump (near the dead-end volume of the reactor). The concentration of the feed and permeate solutions as a function of time is given in Figure 4.8; rejection as a function of time is plotted on the secondary y-axis in this Figure. The feed solution volume was decreased by 75% in this experiment; the concentration factor, calculated from Equation 4.1, is CF = 1.25. However, the actual value is predicted to be larger, considering the limitations due to the volume requirements for our filtration. Furthermore, this experiment was performed in NaCl. For other salt solutions, the

value of CF will likely change. This prediction is based on the effects of solute charge density, geometry and concentration in the comparison of chloride and perchlorate anions.

The results of linear regression analysis for the three variables indicate that the concentration of sodium chloride in the permeate remains relatively unchanged even as the feed concentration steadily increases; accordingly, rejection increases throughout the experiment as well. From the data, it is reasonable to assume that if the liquid filtration apparatus required less volume to operate, the brine stream could be reduced further in volume with sustained rejection. Experimental values for brine volume and composition are critical for analyzing the practical feasibility of nanofiltration technologies for specific purposes. These brine wastes need to be further treated or properly disposed; the amount of wastewater and the contaminants present determine the ecological and perhaps legal and financial ramifications of this type of water treatment process.

4.4. Conclusions

In this work, we have investigated the properties of the solute that affect rejection in our ceramic NF membranes. In particular, we found that bilayer membranes do not provide equivalent rejection amongst all strong of the 1:1 electrolytes examined. Although comparable values were found for NaCl and $NaNO_3$, the rejection of $NaClO_4$ was not equivalent. Therefore, the nature of the ion (charge density, diffusivity, geometry) is important to the understanding of solute/membrane interactions in NF membranes, even when comparing ions of the same valency. These interactions are important for corroborating model predictions and have practical applications for the concentration-independent rejection of perchlorate.

Bilayer membranes show excellent selectivity for transport of chloride as compared to sulfate. Our bilayer NF membranes show better separation of mono- and divalent anions than the single layer counterpart. Furthermore, separation with bilayer membranes is greater than predicted based on rejection data with single salt solutions. The bilayer configuration seems to enhance transport of sodium ions when chloride and sulfate are both present in the solution, therefore resulting in greater separation. This finding has practical consequences for seawater desalination and suggests that nanofiltration may be a desirable pretreatment process for reverse osmosis.

Our bilayer γ-Al_2O_3/Fe-SiO_2 showed continuous rejection of NaCl as the feed stream volume decreased by 75%. However, the results of the experiment are somewhat inconclusive, as our ability to calculate concentration factor is limited by the volume requirements of the filtration system employed in this research. Still, this result is promising with respect to evaluating brine water recovery and disposal, which has ecological implications that must be considered when selecting the appropriate technology for a specific water treatment purpose.

4.5 References

1. Jin, W., Toutianoush, A. & Tieke, B. Use of polyelectrolyte layer-by-layer assemblies as nanofiltration and reverse osmosis membranes. *Langmuir* **19,** 2550–2553 (2003).

2. Dirir, Y. I., Hanafi, Y., Ghoufi, A. & Szymczyk, A. Theoretical Investigation of the Ionic Selectivity of Polyelectrolyte Multilayer Membranes in Nanofiltration. *Langmuir* **31,** 451–457 (2015).

3. Shang, W.-J., Wang, X.-L. & Yu, Y.-X. Theoretical calculation on the membrane potential of charged porous membranes in 1-1, 1-2, 2-1 and 2-2 electrolyte solutions. *J. Membr. Sci.* **285,** 362–375 (2006).

4. Van der Bruggen, B. & Vandecasteele, C. Removal of pollutants from surface water and groundwater by nanofiltration: overview of possible applications in the drinking water industry. *Environ. Pollut.* **122,** 435–445 (2003).

5. Bohdziewicz, J., Bodzek, M. & Wąsik, E. The application of reverse osmosis and nanofiltration to the removal of nitrates from groundwater. *Desalination* **121,** 139–147 (1999).

6. Santafé-Moros, A., Gozálvez-Zafrilla, J. M. & Lora-García, J. Performance of commercial nanofiltration membranes in the removal of nitrate ions. *Desalination Environ. Desalination Environ.* **185,** 281–287 (2005).

7. Urbansky, E. Perchlorate as an environmental contaminant. *Environ. Sci. Pollut. Res.* **9,** 187–192 (2002).

8. Yoon, J., Amy, G., Chung, J., Sohn, J. & Yoon, Y. Removal of toxic ions (chromate, arsenate, and perchlorate) using reverse osmosis, nanofiltration, and ultrafiltration membranes. *Chemosphere* **77,** 228–235 (2009).

9. Van der Bruggen, B., Mänttäri, M. & Nyström, M. Drawbacks of applying nanofiltration and how to avoid them: A review. *Sep. Purif. Technol.* **63,** 251–263 (2008).

10. Oumar Anne, C., Trébouet, D., Jaouen, P. & Quéméneur, F. Nanofiltration of seawater: fractionation of mono- and multi-valent cations. *Desalination* **140,** 67–77 (2001).

11. Tanninen, J., Mänttäri, M. & Nyström, M. Effect of salt mixture concentration on fractionation with NF membranes. *J. Membr. Sci.* **283,** 57–64 (2006).

12. Hilal, N., Al-Zoubi, H., Darwish, N. A. & Mohammad, A. W. Performance of Nanofiltration Membranes in the Treatment of Synthetic and Real Seawater. *Sep. Sci. Technol.* **42,** 493–515 (2007).

13. Tsuru, T., Nakao, S. & Kimura, S. Ion separation by bipolar membranes in reverse osmosis. *J. Membr. Sci.* **108,** 269–278 (1995).

14. Hong, S. U., Malaisamy, R. & Bruening, M. L. Optimization of flux and selectivity in Cl−/SO42− separations with multilayer polyelectrolyte membranes. *J. Membr. Sci.* **283,** 366–372 (2006).

15. Ouyang, L., Malaisamy, R. & Bruening, M. L. Multilayer polyelectrolyte films as nanofiltration membranes for separating monovalent and divalent cations. *J. Membr. Sci.* **310,** 76–84 (2008).

16. Colic, M., Franks, G. V., Fisher, M. L. & Lange, F. F. Effect of Counterion Size on Short Range Repulsive Forces at High Ionic Strengths. *Langmuir* **13,** 3129–3135 (1997).

Membrane	L_m Al_2O_3 (μm)	L_m $Fe\text{-}SiO_2$ (μm)	d_p Al_2O_3 (nm)	d_p $Fe\text{-}SiO_2$ (nm)	ε Al_2O_3 ($\%$)	ε $Fe\text{-}SiO_2$ ($\%$)	τ Al_2O_3	τ $Fe\text{-}SiO_2$
Al_2O_3 A	2.1		3.9		50.8		2.7	
Al_2O_3 B	2.4		3.9		50.8		2.7	
Fe-SiO_2 A		0.4		2.1		31.3		3.4
Fe-SiO_2 B		0.5		2.1		31.3		3.4
Al_2O_3/Fe-SiO_2 A	1.3	1.4	3.9	2.1	50.8	31.3	2.7	3.4
Al_2O_3/Fe-SiO_2 B	0.9	1.4	3.9	2.1	50.8	31.3	2.7	3.4
Fe-SiO_2/Al_2O_3 A	0.5	0.4	4.3	2.1	42.2	31.3	2.7	3.4
Fe-SiO_2/Al_2O_3 B	0.5		4.3	2.1	42.2	31.3	2.7	3.4

Table 4.1: Physical properties of single and bilayer NF membranes.

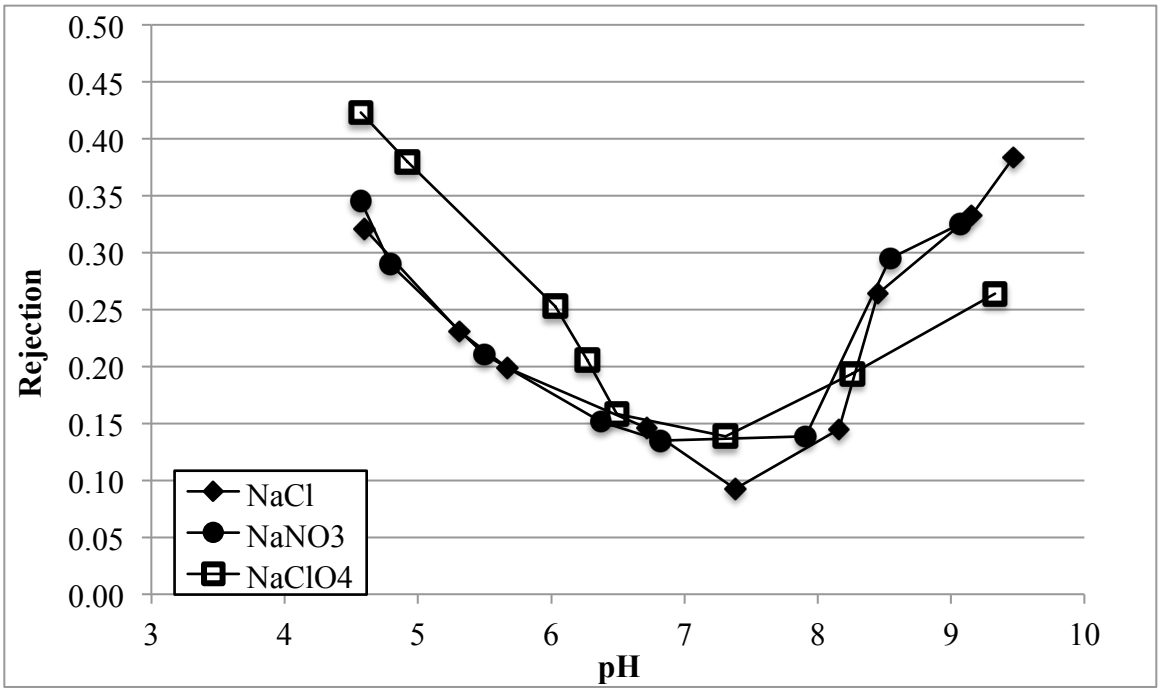

Figure 4.1: Rejection of I=0.01 monovalent symmetric salts as a function of pH with bilayer membrane having γ-Al_2O_3 NF layer facing the feed solution.

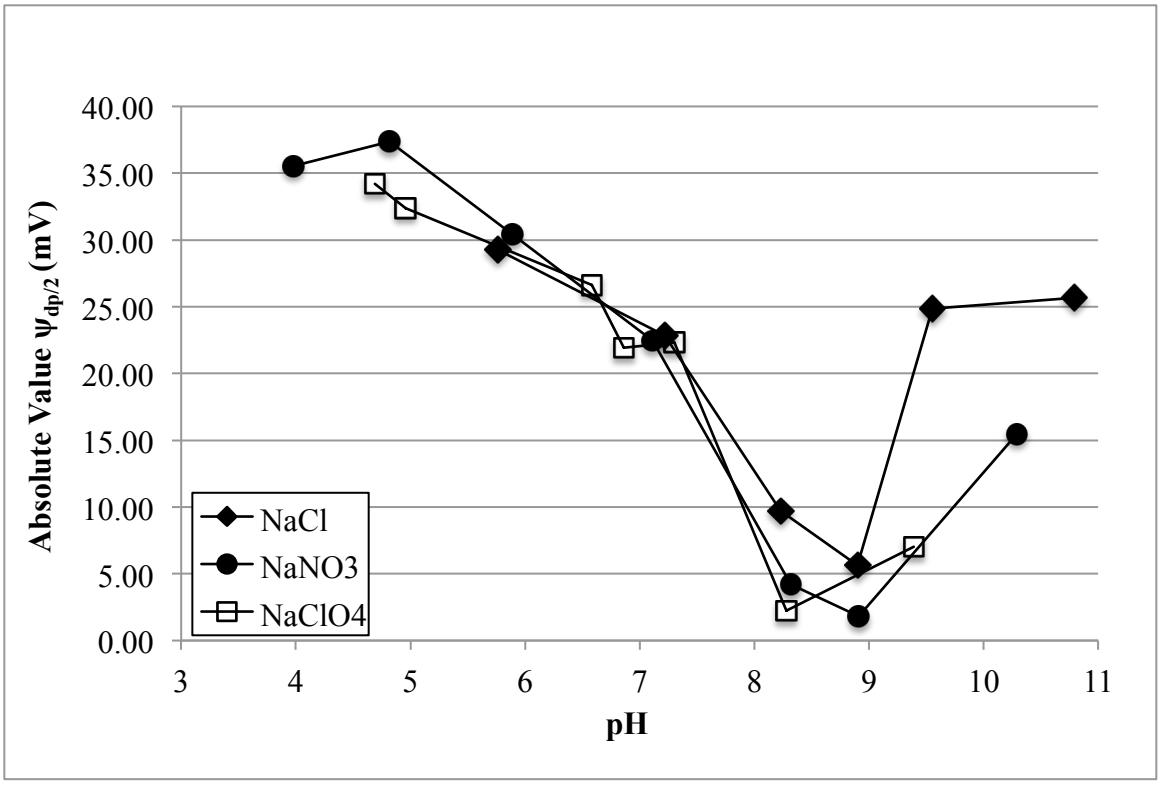

Figure 4.2: Central pore potential ($\psi_{dp/2}$) as a function of pH for γ-Al_2O_3 membrane material exposed to I =0.01 monovalent asymmetric salt solutions with Na cation and varying anion.

Ionic Species	*Ion Size[t] (nm)*	*Diffusion coefficient* ($x10^{-5}$ cm^2 s^{-1})*
Na^+	0.097 - 0.47	1.334
Cl^-	0.164 - 0.39	2.032
NO_3^-	0.177 - 0.335	1.902
ClO_4^-	0.241 - 0.35	1.792

**CRC Handbook of Chemistry and Physics. 85th ed. CRC Press: Boca Raton, FL, 2004-2005.*
[t] Values compiled from several sources. See footnote.

Table 4.2: Size range (in nm) and diffusion coefficients (in cm^2 s^{-1}) for ions in this study.

Kielland, J. Individual activity coefficients of ions in aqueous solutions. *J. Am. Chem. Soc.* **59,** 1675–1678 (1937).
Nightingale Jr, E. R. Phenomenological theory of ion solvation. Effective radii of hydrated ions. *J. Phys. Chem.* **63,** 1381–1387 (1959).
Marcus, Y. Ionic radii in aqueous solutions. *Chem. Rev.* **88,** 1475–1498 (1988).
Marcus, Y. Thermodynamics of solvation of ions. Part 5.-Gibbs free energy of hydration at 298.15 K. *J. Chem. Soc. Faraday Trans.* **87,** 2995–2999 (1991).
Volkov, A. G., Paula, S. & Deamer, D. W. Two mechanisms of permeation of small neutral molecules and hydrated ions across phospholipid bilayers. *Bioelectrochem. Bioenerg.* **42,** 153–160 (1997).

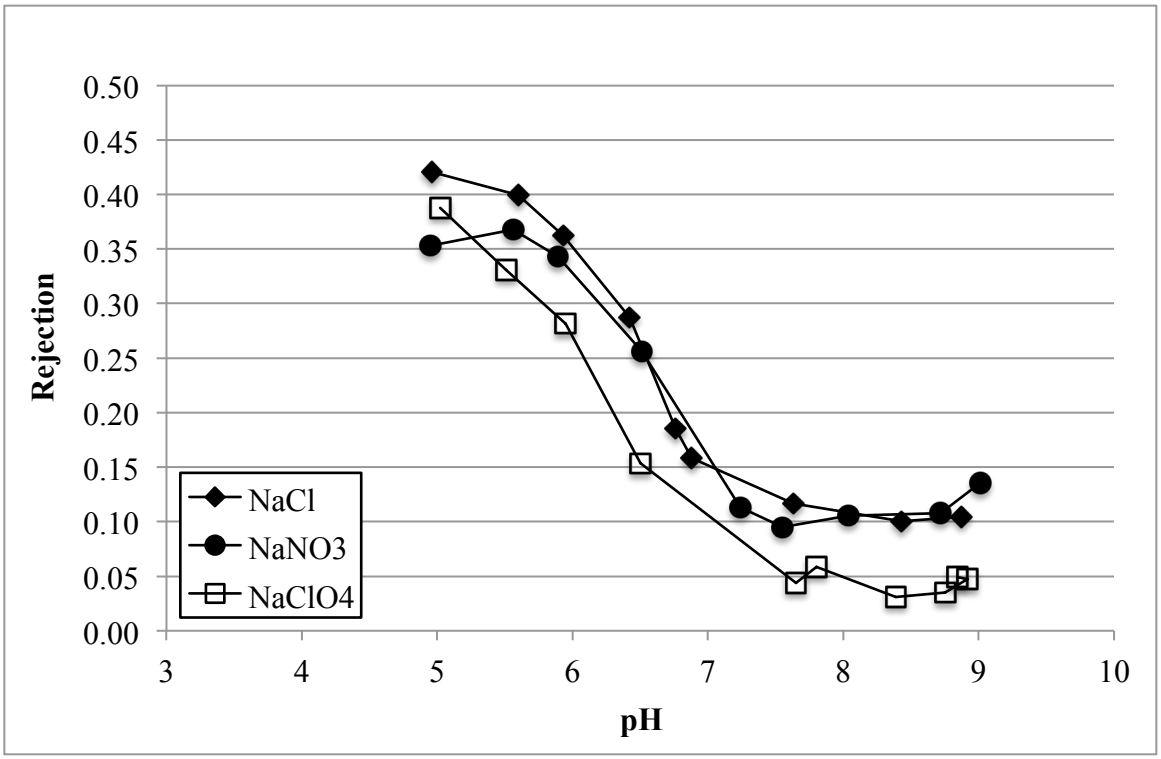

Figure 4.3: Rejection of I=0.01 monovalent symmetric salts as a function of pH with bilayer membrane having Fe-SiO_2 NF layer facing the feed solution.

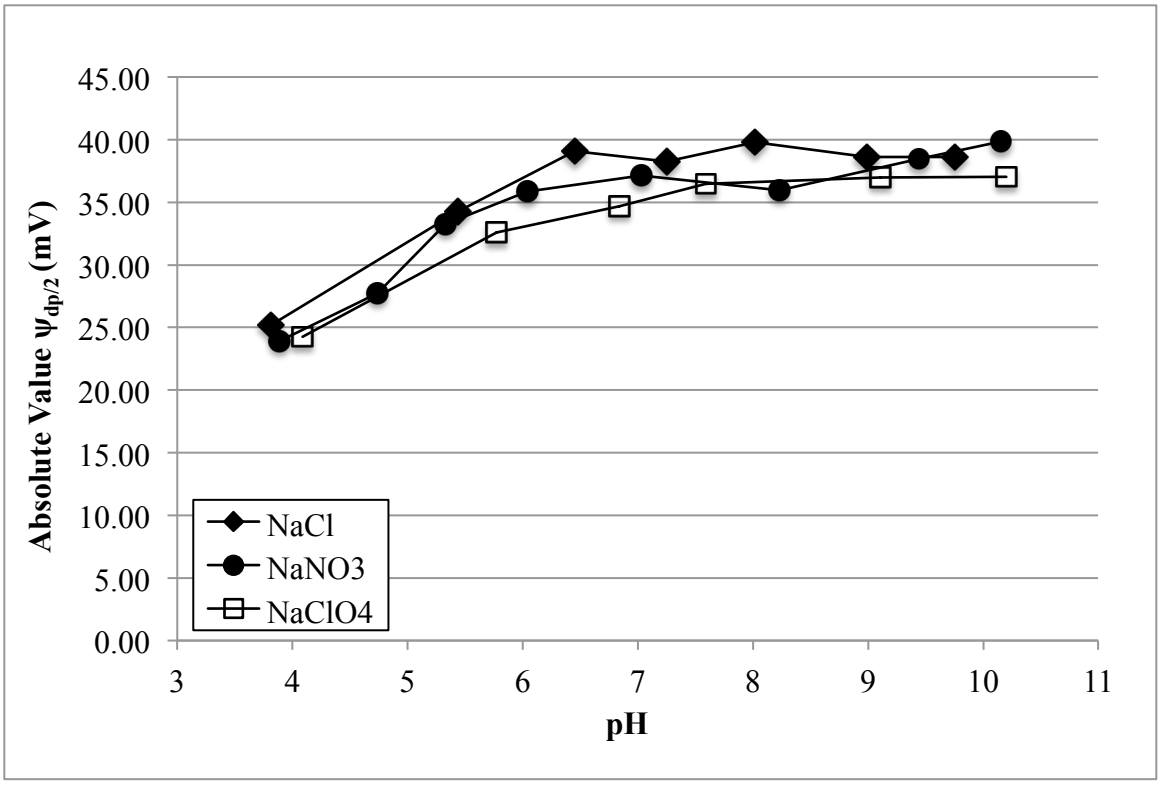

Figure 4.4: Central pore potential ($\psi_{dp/2}$) as a function of pH for Fe-SiO_2 membrane material exposed to I =0.01 monovalent asymmetric salt solutions with Na cation and varying anion.

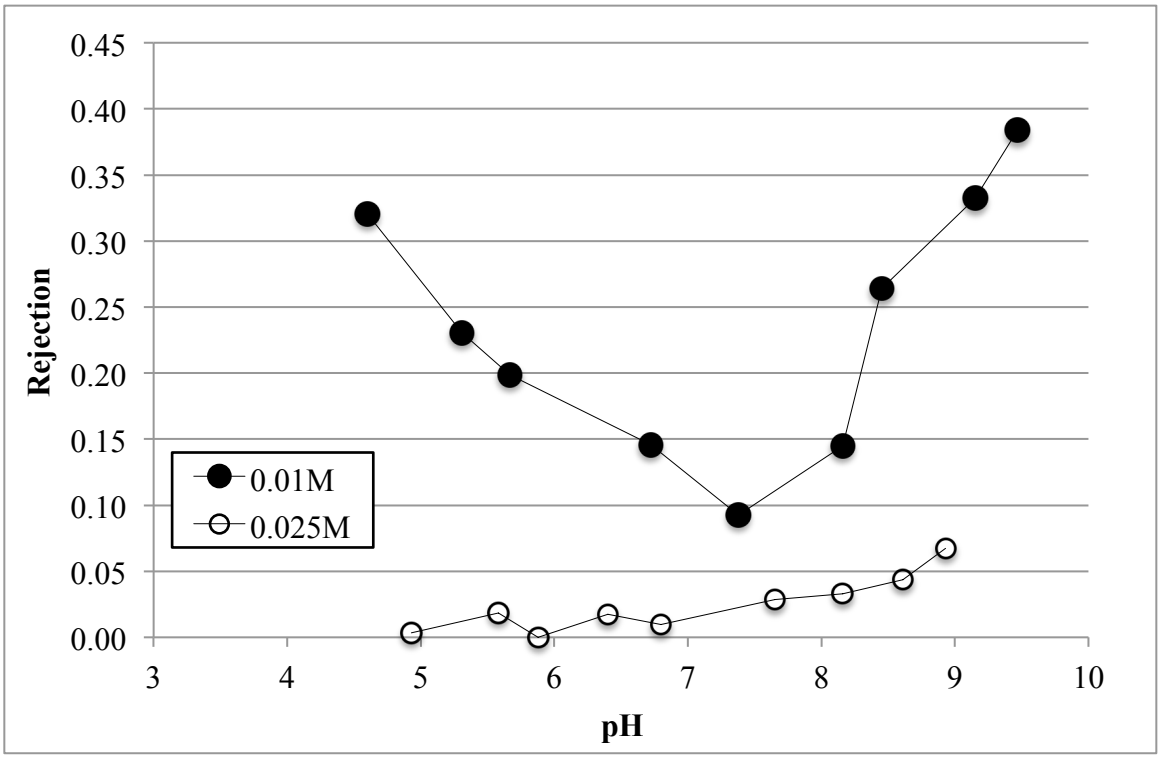

Figure 4.5: Rejection of NaCl solutions at varying concentration as a function of pH with bilayer membrane having γ-Al_2O_3 NF layer facing the feed solution.

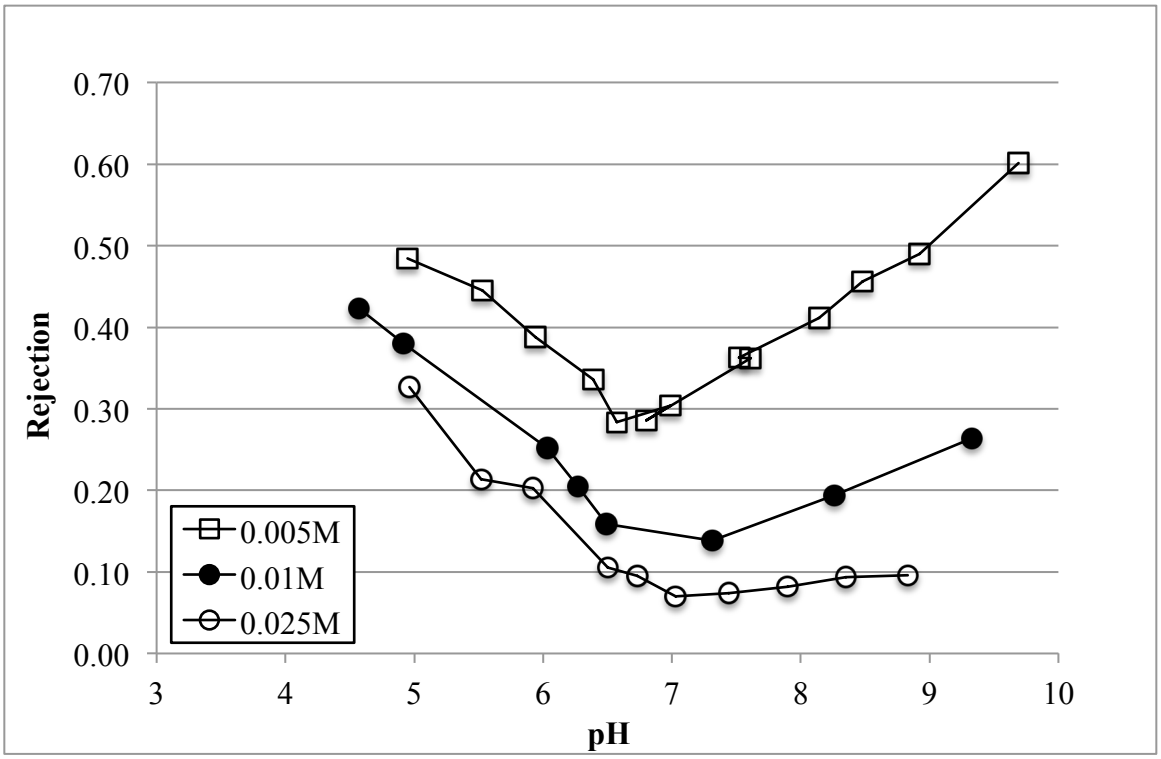

Figure 4.6: Rejection of $NaClO_4$ solutions at varying concentration as a function of pH with bilayer membrane having γ-Al_2O_3 NF layer facing the feed solution.

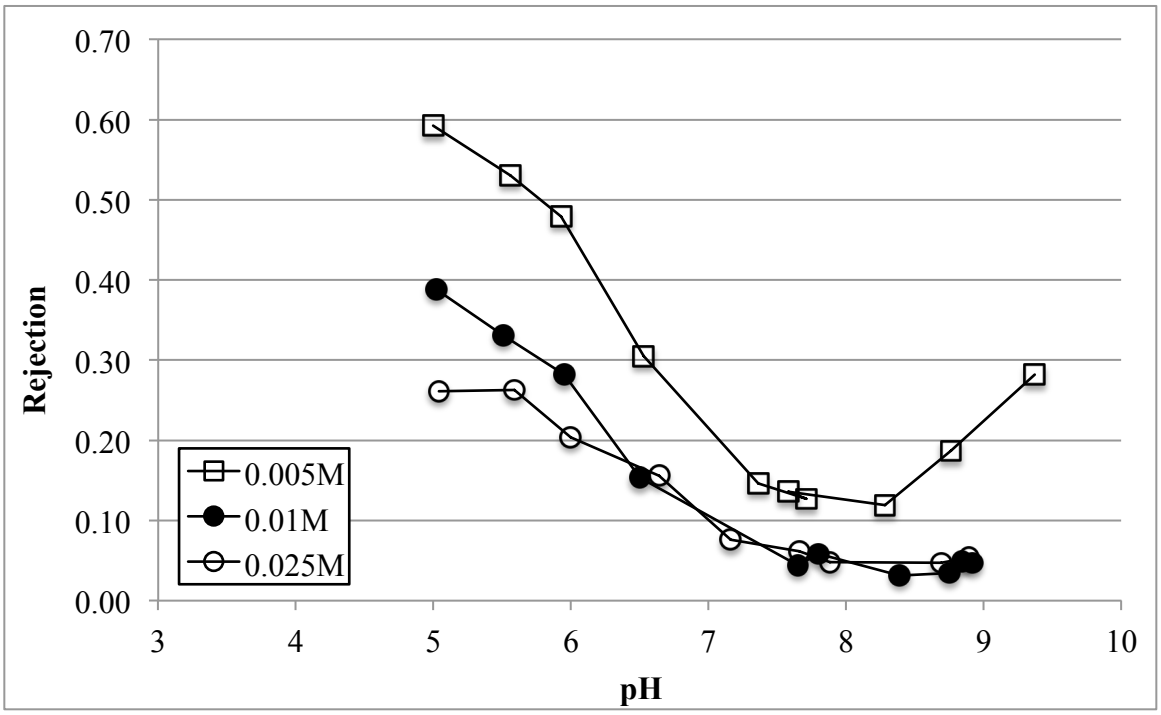

Figure 4.7: Rejection of $NaClO_4$ solutions at varying concentration as a function of pH with bilayer membrane having Fe-SiO_2 NF layer facing the feed solution.

Membrane	*Selectivity Cl^-/SO_4^{2-} in single salt solutions*	*Selectivity Cl^-/SO_4^{2-} in mixed salt solutions*
Fe-SiO_2	1.43	1.36
γ-Al_2O_3/Fe-SiO_2	2.60	5.81
Fe-SiO_2/γ-Al_2O_3	5.50	5.88

Table 4.3: Transport selectivity for mono- and divalent anions in bilayer membranes; Fe-SiO_2 single layer membrane data shown for comparison. Feed solution conditions for all experiments were pH 8.5 ± 0.5, I=0.01.

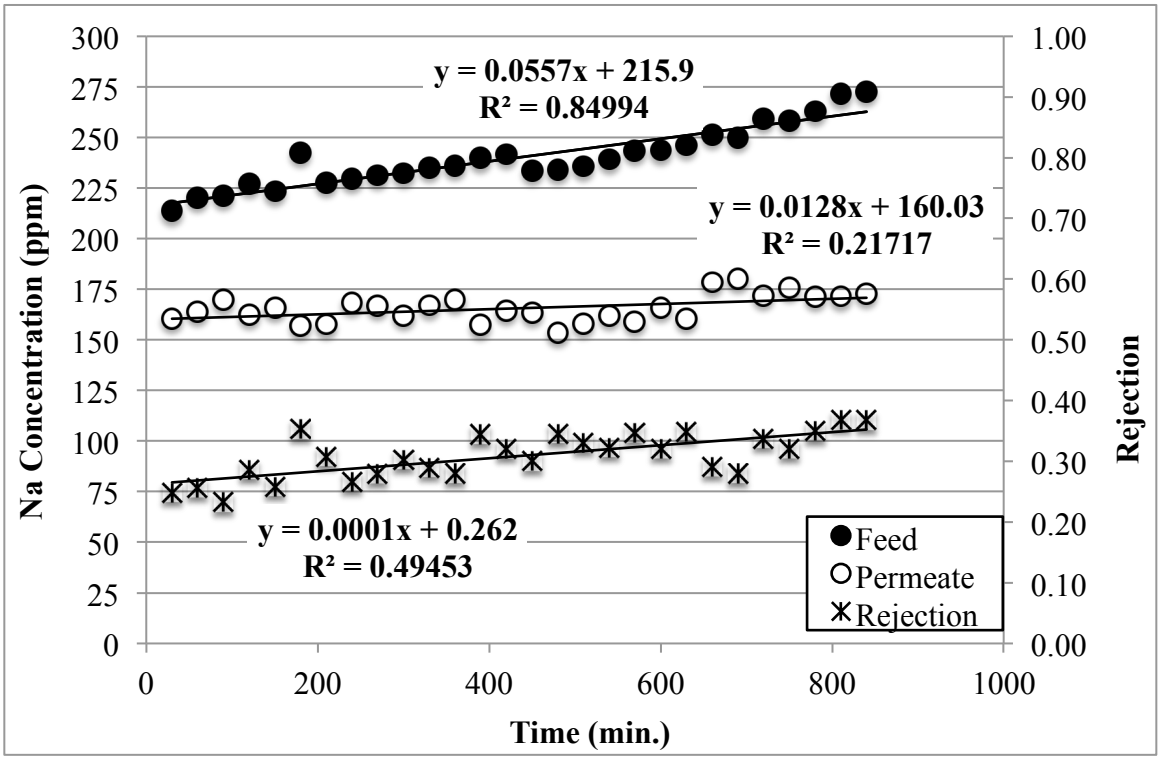

Figure 4.8: Rejection (secondary y-axis) of I =0.01, pH 9.0 NaCl solution as a function of time with bilayer membrane having γ-Al_2O_3 NF layer facing the feed solution. On the primary y-axis, the time-dependent solute concentrations in the feed and permeate solution are displayed.

5. Conclusions and Future Directions

5.1 Introduction

Almost all ceramic NF membranes are composed of a single filtration layer that is either positively or negatively charged for a given solution composition; the sign of membrane charge determines whether the cation or the anion behaves as the co-ion. Ions with higher valence states are more readily rejected than monovalent ions due to increased charge density. Therefore, currently available ceramic NF membranes are best suited for applications where removal of divalent ions is important and pH of feed solution is far from the pH_{iep} of the nanofiltration layer. In this work, we fabricated, characterized, and evaluated the performance of bilayer ceramic membranes composed of γ-Al_2O_3 and Fe-SiO_2 nanofiltration layers. Our ceramic membranes are an alternative to commercially available NF membranes, almost all of which are made from polymeric materials. Specifically, state-of-the art NF membrane research and development is centered around polyelectrolyte multilayer (PEM) membranes. The concept behind a PEM membrane is comparable to our bilayer ceramic membranes; the use of multiple materials during fabrication results in a membrane that may contain oppositely charged NF layers in certain solution conditions. However, it is widely accepted that ceramic materials have greater thermal, mechanical, and chemical stability, making NF membranes derived from these materials desirable for many water treatment applications. Furthermore, much of the published work towards researching PEM membranes focuses on modeling their performance. Our wealth of experimental data obtained in these studies should be a welcome contribution to the field of multilayer membranes for comparison purposes.

5.2 Major Conclusions

5.2.1 Physical properties of membranes

The sol-gel method provides a useful technique for preparing ceramic membranes. Bilayer γ-Al_2O_3 and Fe-SiO_2 nanofiltration membranes were fabricated and characterized to determine the parameters of the membrane that contribute to ion transport. For comparison, single layer membranes were prepared from the same materials. These physical properties of our γ-Al_2O_3 and Fe-SiO_2, such as pore size, porosity and NF layer thickness, helped contribute to our understanding of the mechanisms for salt rejection with our bilayer ceramic membranes. Furthermore, while there is generally good reproducibility in the data for similarly prepared membranes, our findings indicate that a controlled relative humidity environment is necessary for fabricating membranes that are exactly identical in every detail. For example, the thickness of a NF layer of γ-Al_2O_3 or Fe-SiO_2 is affected by the method of deposition. A layer cannot be perfectly slipcast onto the support unless the conditions ensure that the pores of the support are completely free of water. This discovery will be important for future work in ceramic nanofiltration, as improvements in the methodology for fabricating membranes will result in more effective, and therefore more competitive, membranes for water treatment applications.

5.2.2 Salt rejection performance of bilayer membranes

Our hypothesis was that by preparing membranes made of layers having two different nanoparticulate metal oxide materials, with distinct charging properties as a function of pH, we will be able to "reject" ions in a wider range of solution conditions than has been otherwise impossible with current ceramic NF membrane technology. In comparison to single layer membranes made of the same materials, our bilayer γ-Al_2O_3 and Fe-SiO_2 membranes showed intermediate rejection capabilities for 1:1 electrolytes, with values falling between those for the two single layer membranes. However, the data shows that the bilayer membranes can show

superior performance for rejecting 1:2 or 2:1 electrolytes, and especially when the cation is the divalent ion. We measured rejection for several electrolytes throughout the pH range of 5.0 to 9.0. This data proved to be valuable for determining whether or not the bilayer membrane behaved as a bipolar membrane. While pH has been predicted to affect membrane charging properties, very few experimental studies have explicitly evaluated these pH effects.

In addition to pH and ionic strength of the solution, we found that the nature of the ion affects rejection as well. When comparing rejection of symmetric, monovalent salts with our bilayer NF membranes, we discovered differences that were contributed by the nature of the ion itself. Ion charge density, diffusivity, and concentration are important parameters when modeling the interaction between a nanofiltration membrane and a salt solution. Furthermore, these ion effects have practical applications for concentration-independent rejection.

5.2.3 Salt separation performance of bilayer membranes

Our bilayer membranes excelled in the area of salt separation in solutions containing both sodium sulfate and sodium chloride. The results were compared with the separation ability of a single layer membrane, and bilayer membranes were found to be four times more selective towards chloride transport as compared to that of sulfate. This is an area of great practical importance, as sulfate and chloride are the major ions present in seawater. Desalination of seawater using membrane technology, such as reverse osmosis, is a much more efficient process when the feed stream can be treated to first separate these two anions. The use of these ceramic nanofiltration membranes as a pretreatment for seawater desalination may be a possible market

for these membranes. Separation of salts is relevant to many wastewater feed streams in both industrial and naturally occurring systems.

5.3 Recommendations for Future Work

The results of these studies provide a better understanding of the properties of both the membrane and solution that determine rejection in ceramic membrane bilayer nanofiltration. Specifically, a comprehensive set of experimental data was generated and analyzed that will be useful for future modeling efforts to validate theoretical predictions. Our goal is to collaborate with other researchers to make these predictions, as the experimental techniques in nanofiltration are labor and time-intensive. Increased accuracy in model predictions will enable one to evaluate performance of NF membranes in a more cost-effective manner that would allow for a more rapid advancement in research and development.

From a practical standpoint, the logical next step would be to compare our bilayer NF membranes with competing technologies. The comparison would be based on selectivity (rejection or separation of salts), productivity (rate at which “clean” water can be produced), stability and efficiency (amount of energy required for operation), as well as brine water volume and composition. Treatment of wastewater streams is often accomplished with multiple technologies tied together as unit operations in series in an effort to maximize the above parameters. The global supply of freshwater is limited and increased demand for this resource warrants the pursuit of creative solutions to address water stress and scarcity. As many industrial processes generate a wastewater stream during production of goods, this is one sector where water reclamation would support the conservation and preservation of our freshwater resources.

Nanofiltration membrane technology is currently being used for this type of water treatment, as the production of potable, purified water is not necessary. Rather, this industrial water needs to be treated only to a certain accepted standard in order for sustained use of a constant volume, thereby reducing the water footprint of the process and the goods produced. Further improvements in performance, with respect to removal of ions and other contaminants, would allow for the more widespread implementation of nanofiltration technology for this application.

Recently, nanofiltration has also been proposed as an excellent technology for the removal of organic contaminants, such as bisphenyl-A[1,2], personal care products[3,4] and other pharmaceuticals[5] and emerging trace organic contaminants[6]. Although this is a very new application for nanofiltration (within the last year or two), it is an exciting potential market for this technology, as these substances are often found in very low concentrations and are difficult to remove with traditional water treatment methods.

Lastly, in order for ceramic membranes to penetrate this nanofiltration market, they will first have to operate in niche target areas as they are almost 100 times more costly than their polymeric counterparts. Efforts should be made to reduce these costs, which largely lie in the expense of producing the microporous ceramic support. If one could reduce the cost of preparing these supports by a factor of 10, these ceramic nanofiltration membranes would be able to find many more applications, where their superior performance would justify a 10-fold cost increase.

5.4 References

1. Escalona, I., de Grooth, J., Font, J. & Nijmeijer, K. Removal of BPA by enzyme polymerization using NF membranes. *J. Membr. Sci.* **468,** 192–201 (2014).

2. Escalona, I. *et al.* Fenton coupled with nanofiltration for elimination of Bisphenol A. *Desalination* **345,** 77–84 (2014).

3. Cincinelli, A., Martellini, T., Coppini, E., Fibbi, D. & Katsoyiannis, A. Nanotechnologies for Removal of Pharmaceuticals and Personal Care Products from Water and Wastewater. A Review. *J. Nanosci. Nanotechnol.* **15,** 3333–3347 (2015).

4. Yang, H. & Wang, X. Mechanism of removal of pharmaceuticals and personal care products by nanofiltration membranes. *Desalination Water Treat.* **53,** 2816–2824 (2014).

5. Vona, A. *et al.* Comparison of different removal techniques for selected pharmaceuticals. *J. Water Process Eng.* **5,** 48–57 (2015).

6. Nguyen, L. N., Hai, F. I., Kang, J., Price, W. E. & Nghiem, L. D. Removal of emerging trace organic contaminants by MBR-based hybrid treatment processes. *Int. Biodeterior. Biodegrad.* **85,** 474–482 (2013).